Effect of Surface Processing Variables on Hydrogen Embrittlement of Steel Fasteners

by

Salim Brahimi

Department of Metals and Materials Engineering

McGill University
Montreal, Quebec, Canada

November 2007

A thesis submitted to McGill University in partial fulfilment of the requirements of the degree of Master of Engineering

© Brahimi 2007

Library and Archives Canada

Published Heritage Branch

395 Wellington Street
Ottawa ON K1A 0N4
Canada

Bibliothèque et Archives Canada

Direction du Patrimoine de l'édition

395, rue Wellington
Ottawa ON K1A 0N4
Canada

Your file Votre référence
ISBN: 978-0-494-51450-4
Our file Notre référence
ISBN: 978-0-494-51450-4

NOTICE:
The author has granted a non-exclusive license allowing Library and Archives Canada to reproduce, publish, archive, preserve, conserve, communicate to the public by telecommunication or on the Internet, loan, distribute and sell theses worldwide, for commercial or non-commercial purposes, in microform, paper, electronic and/or any other formats.

The author retains copyright ownership and moral rights in this thesis. Neither the thesis nor substantial extracts from it may be printed or otherwise reproduced without the author's permission.

AVIS:
L'auteur a accordé une licence non exclusive permettant à la Bibliothèque et Archives Canada de reproduire, publier, archiver, sauvegarder, conserver, transmettre au public par télécommunication ou par l'Internet, prêter, distribuer et vendre des thèses partout dans le monde, à des fins commerciales ou autres, sur support microforme, papier, électronique et/ou autres formats.

L'auteur conserve la propriété du droit d'auteur et des droits moraux qui protège cette thèse. Ni la thèse ni des extraits substantiels de celle-ci ne doivent être imprimés ou autrement reproduits sans son autorisation.

In compliance with the Canadian Privacy Act some supporting forms may have been removed from this thesis.

While these forms may be included in the document page count, their removal does not represent any loss of content from the thesis.

Conformément à la loi canadienne sur la protection de la vie privée, quelques formulaires secondaires ont été enlevés de cette thèse.

Bien que ces formulaires aient inclus dans la pagination, il n'y aura aucun contenu manquant.

Canada

ABSTRACT

Incremental step load testing was used in accordance with ASTM F1940 to rank a number coating processes used in the fastener industry for their propensity to cause internal hydrogen embrittlement. The results showed that coating permeability has a first order effect, while the quantity of hydrogen introduced by the process has a second order effect. Pure zinc electroplating processes, alkaline and acid, were found to be the most embrittling, owing to the low permeability of zinc. The least embrittling processes were zinc-nickel, alkaline and acid, owing to the high permeability of Zn-Ni coatings. Non-electrolytic processes, namely phosphating, mechanical galvanising, Dacromet® and Magni 555® were found to be non-embrittling. Hot dip galvanising was found to be highly embrittling, evidently due to trapped hydrogen being released by the thermal shock of up-quenching upon immersion in molten zinc. The full effect of up-quenching on the metallurgical and mechanical properties of high strength steel requires further investigation.

RÉSUMÉ

La méthode de chargement par accroissement d'étape a été employée selon ASTM F1940 afin d'examiner des processus de revêtement industriels, utilisés dans le domaine des éléments de fixation. Le but était de quantifier la propension de causer la fragilisation par hydrogène interne. Les résultats ont démontré que la perméabilité du revêtement a un effet du premier degré, tandis que la quantité d'hydrogène introduite par le processus a un effet du second degré. Des processus de galvanoplastie de zinc pur, alcalin et acide, étaient les plus fragilisant, dû à la basse perméabilité du zinc. Les processus zinc-nickel, alcalin et acide, étaient les moins fragilisant en raison de la perméabilité élevée des revêtements Zn-Ni. Les processus non-électrolytiques, à savoir la phosphatation, la galvanisation mécanique, le Dacromet® et le Magni 555® se sont avéré non-fragilisant. La galvanisation à chaud s'est avérée fortement fragilisant, apparemment due à l'hydrogène emprisonné qui se libère par le choc thermique lors de la trempe dans le bain de zinc en fusion. Le plein effet de la trempe sur les propriétés métallurgiques et mécaniques de l'acier de haute résistance exige davantage de recherche.

ACKNOWLEDGEMENTS

I would like to thank my supervisor Professor Stephen Yue for his guidance, support, and for allowing me the leverage to make this project a reality. I would also like to express my appreciation to the individuals and organisations in the fastener community who have sponsored this research. I am grateful for their invaluable support, and especially for their belief in my vision. I hope that the results of this research will have a profound impact on the manner in which the fastener industry deals with the problem of hydrogen embrittlement from coating processes.

Ben Urbanietz – (Canadian Fasteners Institute)
Charlie Wilson – (Industrial Fasteners Institute)
David McCrindle – (Canadian Fasteners Institute)
Don Snyder – (American Electroplaters and Surface Finishers)
Ed Babcock – (Boeing)
James Jennings – (US Navy)
Jean-Claude Legault – (Infasco/Galvano)
Joe Greenslade – (Industrial Fasteners Institute)
Joseph Bahadrian – (Infasco/Galvano)
Ray Tide – (Research Council on Structural Connections)
Roger Hamilton – (Research Council on Structural Connections/Nucor)

Several important people who also deserve much credit for helping to bring this project to fruition are Professor Jerzy Szpunar, Professor George Demopoulos, Edwin Fernandez, Marc Crankshaw, Fred Hunt, Dean Higdon and Bruce Meade. Also, I wish express my admiration for Dr. Louis Raymond who has devoted so much of his life's work to researching and developing accelerated methods for measuring threshold stress. His work is the source of my inspiration. Finally and most importantly, I am grateful to my wife for her boundless support and unconditional love. She is the source of my strength and perseverance.

TABLE OF CONTENTS

ABSTRACT i

RÉSUMÉ ii

AKNOWLEDGEMENTS iii

TABLE OF CONTENTS iv

LIST OF FIGURES viii

LIST OF TABLES x

CHAPTER 1: INTRODUCTION 1

CHAPTER 2: LITERATURE REVIEW 5

2.1 HIGH STRENGTH FASTENERS: PROPERTIES AND MATERIALS 5

2.1.1 Fastener terminology 5

2.1.2 Fastener materials and applications 7

2.2 DEFINING HYDROGEN EMBRITTLEMENT 8

2.2.1 Types of hydrogen embrittlement 8

2.2.2 Damage mechanism 10

2.2.3 Threshold stress 10

2.3 HYDROGEN GENERATION MECHANISMS 12

2.3.1 Mechanism of corrosion 13

2.3.2 Mechanism of electroplating 14

2.4 ELECTROCHEMISTRY OF HYDROGEN GENERATION 17

2.4.1 Cathodic hydrogen generation by galvanic protection 22

2.4.2 Electrochemical conditions at crack tips 24

2.5 EFFECTS OF COATINGS AND SURFACE CHARACTERISTICS 25

2.5.1 Surface preparation 26
2.5.2 Surface characteristics 26
2.5.3 Coating processes 28
2.5.4 Baking 36
2.6 INCREMENTAL STEP LOADING TEST METHOD 37
CHAPTER 3: EXPERIMENTAL PROCEDURE 41
3.1 EXPERIMENTAL PROCEDURES 41
3.2 ISL TEST METHOD 42
3.3 TEST SPECIMENS 45
3.3.1 Dimensional, physical and metallurgical specifications 45
3.3.2 Supplier certification and properties 48
3.4 COATING PROCESS SAMPLING 50
3.4.1 Electroplating processes 50
3.4.2 Non electrolytic processes 53
3.4.3 Hot dip zinc (galvanising) 58
3.5 ANALYTICAL TECHNIQUES 60
3.5.1 Coating thickness measurement 60
3.5.2 Rockwell hardness testing (C scale) 61
3.5.3 Vickers macro and micro-hardness testing 61
3.5.4 Microstructure 61
3.5.5 Fractography 61
CHAPTER 4: RESULTS 63
4.1 ELECTROPLATING PROCESSES 64
4.1.1 Zinc – acid chloride 64
4.1.2 Zinc – alkaline non cyanide 68

4.1.3 Zinc nickel – acid chloride 69

4.1.4 Zinc nickel – alkaline non cyanide 70

4.1.5 Zinc iron – alkaline non cyanide – rack 73

4.1.6 Cadmium – cyanide 74

4.1.7 Acid dip – laboratory 75

4.1.8 Fractography 77

4.2 NON ELECTROLYTIC PROCESSES 78

4.2.1 Mechanical zinc – bulk drum 78

4.2.2 Zinc phosphate – barrel 79

4.2.3 Dacromet® – bulk dip spin 79

4.2.4 Magni 555® – bulk dip spin 81

4.2.5 Fractography 81

4.3 THERMAL DIFFUSION PROCESS – HOT DIP GALVANIZING 82

4.3.1 Group 1 82

4.3.2 Group 2 90

4.3.3 Group 3 92

4.3.4 Group 4 94

CHAPTER 5: DISCUSSION 97

5.1 GENERAL OBSERVATIONS 97

5.2 ELECTROPLATING PROCESSES 100

5.3 BAKING 104

5.4 NON ELECTROLYTIC PROCESSES 106

5.5 THERMAL DIFFUSION PROCESS – HOT DIP GALVANIZING 106

CHAPTER 6: CONCLUSION 111

CHAPTER 7: FUTURE WORK 115

7.1 PHASE TWO INVESTIGATION 115

7.1.1 Coating material characterisation 115

7.1.2 Electrochemical permeation 115

7.1.3 Thermal desorption spectroscopy (TDS) 116

7.2 OTHER TOPICS OF INTEREST 116

7.2.1 Electroplating processes 117

7.2.2 Hot dip zinc 117

REFERENCES 119

APPENDIX A 124

LIST OF FIGURES

Figure 2.1. Threshold stress $K_{I(HE)}$ in relation to fracture toughness K_{IC} 11

Figure 2.2. Generic example of combined activation and concentration polarisation at cathode 21

Figure 2.3. Microstructure of hot-dip zinc coating illustrating successive Zn/Fe phases..... 35

Figure 3.1. Schematic of RSL® loading frame illustrating the bending motion being applied to a test specimen..... 43

Figure 3.2. RSL® loading frame..... 43

Figure 3.3. Example of typical ISL loading profile..... 45

Figure 3.4. Dimensional specifications of ASTM F519 (type 1e) single notch bend square bar. 47

Figure 3.5. ASTM F519 (type 1e) single notch bend square bar. Right hand image shows the specimen mounted in the test fixtures..... 47

Figure 3.6. Generic electroplating processing steps – barrel 53

Figure 3.7. Mechanical galvanising processing steps – tumbler system 55

Figure 3.8. Zinc phosphate processing steps – barrel 56

Figure 3.9. DACROMET® processing steps – applied by dip-spin in two basecoats plus one topcoat..... 57

Figure 3.10. Magni 555® processing steps - applied by dip-spin in two coats..... 58

Figure 3.11. Hot-dip zinc processing steps – applied by dip spin 60

Figure 4.1. Zinc – acid chloride, $NFS_{\%}$ by process condition 65

Figure 4.2. Zinc – alkaline non cyanide, $NFS_{\%}$ by process condition..... 68

Figure 4.3. Zinc nickel – acid chloride, $NFS_{\%}$ by process condition..... 70

Figure 4.4. Zinc nickel – alkaline non cyanide, $NFS_{\%}$ by process condition 71

Figure 4.5. Zinc iron – alkaline non cyanide, $NFS_{\%}$ by process condition..... 73

Figure 4.6. Cadmium – bright cyanide, $NFS_{\%}$ by process condition..... 75

Figure 4.7. Acip dip, $NFS_{\%}$ by process condition..... 76

Figure 4.8. Non electrolytic processes, $NFS_{\%}$ by process 78

Figure 4.9. Dacromet ®, considering material modification by using the fast fracture strength of a Dacromet ® coated specimen as the baseline 80

Figure 4.10. Hot dip zinc Group 1, $NFS_{\%}$ values obtained from initial tests verifying the effects of acid and heat 83

Figure 4.11. Surface and core hardness of hot dip galvanised specimens compared to the pristine condition and to other coating processes sampled 84

Figure 4.12. Hardness profile of pristine specimens as compared to hot dip galvanised specimens. 85

Figure 4.13. Metallurgical structure of pristine specimen consisting of tempered martensite 86

Figure 4.14. Metallurgical structure of galvanised specimen from P1009 composed of martensite with modified appearance 87

Figure 4.15. Metallurgical structure of heat exposed specimen 87

Figure 4.16. Fracture surface overview with schematic of specimen orientation 89

Figure 4.17. Fracture surface of hot dip galvanised sample – intergranular morphology 90

Figure 4.18. Fracture surface of pristine sample – ductile morphology 90

Figure 4.19. Hot dip zinc Group 2, comparing the effects of pre-baking and post baking 91

Figure 4.20. Hot dip zinc Group 3, considering material modification by using the bare fast fracture strength as the baseline 93

Figure 4.21. Hot dip zinc Group 4, galvanising of specimens re-tempered to 36.5 HRC 95

Figure 5.1. Relationship between specimen hardness and fast fracture strength 98

Figure 5.2. ASTM F1940 threshold chart 99

LIST OF TABLES

Table 2.1. Standard oxidation potentials of metals at 25°C 24

Table 3.2. Chemical composition of lot S2 test specimens. 48

Table 3.3. Fast fracture baseline – specimen lot S2 49

Table 3.4. ISL baseline – specimen lot S2 50

Table 3.5. List of sampled electroplating processes 51

Table 3.6. List of sampled non electrolytic processes 54

CHAPTER 1: INTRODUCTION

High strength and ultrahigh strength threaded mechanical fasteners are broadly characterised by tensile strengths ranging from 1,000 to 2,000 MPa. They are often used in critical components, typically comprising load bearing joints in aircraft structures, ships, ground vehicles, bridges, tunnels and buildings. Mechanical fasteners and bolted joints are deceivingly simple components. Damage resulting in loss of integrity or failure can occur by a complex interaction of material characteristics, processing conditions, environmental conditions, manufacturing flaws, installation conditions, and joint design. From a cynical perspective, a bolt is simply a smooth round bar with notches, tantamount to a series of built in "defects" that inevitably lead to failure. The consequences of failures can range from minimal to catastrophic, even resulting in loss of life. One of the most unpredictable failure modes is hydrogen embrittlement (HE). High strength threaded steel fasteners are known for their susceptibility to HE. The prevention of HE failure is therefore a fundamental preoccupation for structural designers, fastener manufacturers and application engineers. An important consideration in the prevention of HE deals with the selection, processing, and application of metallic coatings, particularly electroplated coatings. These coatings are designed to extend the corrosion life of the fastener. However, the introduction of hydrogen during processes such as electroplating or surface preparation steps such as pickling can cause or precipitate delayed HE failure.

Fastener industry standards have not adequately addressed the prevention of hydrogen embrittlement from coating processes. There has also been a lack of consistency in preventive approaches. These preventives measures can range from specifications that prohibit the application of high risk coatings, such as electroplating or hot dip galvanising, to mandatory processing requirements, such as the use of inhibited acids for pickling or baking parts after processing, to the requirement for HE testing as a final inspection of coated parts. The inadequacy of industry-mandated preventive measures is epitomised by specified bake conditions that do not have the desired effect, and test methods that lack the necessary sensitivity to effectively detect embrittled parts. This situation has been slowly changing with the introduction of a new ASTM test method in 1999. ASTM F1940 prescribes a standardised methodology for using the incremental step load (ISL) method for monitoring fastener coating processes for the risk of HE. The test method was introduced as a powerful tool for process control purposes. It is also proving to be a suitable metric to be used for research purposes to investigate ways to optimise coating and baking processes.

The primary objective of this research is to quantify the risk of embrittlement from residual hydrogen from coating processes commonly utilised to coat high strength mechanical fasteners. More specifically, the effects of coating process variables and certain coating characteristics, such as thickness and permeability are investigated. The principal investigative technique used is incremental step loading (ISL) in accordance with test method ASTM F1940. In brief, this approach consists of performing a mechanical test on standardised notched specimens that have been coated along with actual fasteners as "witness" samples. The test is designed to measure the HE fracture

threshold by subjecting the specimen to an incrementally increasing loading sequence that allows for the time dependant nature of hydrogen embrittlement to evolve. Under standardised test conditions, the measured fracture threshold of the specimen is a function of the amount of residual hydrogen from the coating process.

This methodology is used to rank a number of industrial coating processes and processing steps for their propensity to cause internal hydrogen embrittlement (IHE) by: (i) the amount of hydrogen they introduced into the test specimens, and (ii) the ability of each coating to act as a barrier to hydrogen absorption or effusion, also characterised as its hydrogen permeability. It should be noted that a complete analysis of the effect of permeability requires in-depth characterisation of the coating materials which can then be correlated with ISL test results. Detailed coating characterisation will comprise the next phase of this research. However, initial postulations on the primary factors influencing permeability are proposed.

One particular topic of focus in this investigation is the suitability of the ASTM F1940 test method for the hot-dip zinc (galvanising) process. Heat exposure during galvanising invariably changes the metallurgical and mechanical properties of the *standard* test specimen, such that it no longer conforms to any standard. Yet the test method can answer a number of important questions about the effects of hot-dip galvanising on high strength steels. This work is particularly relevant to industry's concerns because hot-dip galvanising is prohibited on high strength fasteners by standards such as ASTM A490.

The long term objective of this research is to serve as a basis for developing guidelines to optimise coating processes and practices. Close industrial collaboration will

ensure that these guidelines are incorporated into fastener industry standards, with the goal of minimising the risk of HE failure of high strength steel fasteners in-service.

CHAPTER 2: LITERATURE REVIEW

In this review the topic of metallic coatings and their "unintended" role in promoting hydrogen embrittlement in fasteners will be expanded. The topic is divided into sub components, beginning with a brief description of mechanical fasteners and the materials used for manufacturing mechanical fasteners. Hydrogen embrittlement is defined, followed by a description of the electrochemistry of hydrogen generation and absorption in metals. The effect of surface properties of coating materials on hydrogen absorption and effusion is discussed. The most prevalent coating processes in the fastener industry are described in detail. The parameters influencing the effectiveness of post exposure *baking* are defined. Finally, the incremental step load test method and its benefits are presented.

2.1 HIGH STRENGTH FASTENERS: PROPERTIES AND MATERIALS

2.1.1 Fastener terminology

The following is a list of terms that broadly categorise different types of mechanical fasteners:

Bolt – an externally threaded fastener designed for insertion through holes in assembled parts, and tightened or released by torquing a *nut*.[1]

Screw – an externally threaded fastener that can in some cases be similar or nearly identical in appearance to a bolt, but is primarily distinguished by how it is used. It is an externally threaded fastener capable of being *screwed* into holes in assembled parts. It is tightened or released by torquing the head.[1] The mating internal threads are previously tapped, or are either formed or tapped by the screw itself.

Stud – a *headless* external threaded fastener that can be designed either as a bolt or a screw.[2]

Rivet – a headed fastener whose shank is inserted through a hole of assembled plies. The un-headed end is then upset to form a second head while pulling the joint plies together. Rivets may be solid, tubular, or split. Rivets are no longer predominant in most structural applications, although one notable exception is in the aerospace industry where they are used for aircraft assembly, but not in critical load bearing structures.[2,3]

Blind fastener – a fastener that is accessed from only one side of the workpiece during installation. It is typically comprised of a threaded screw or pin, assembled with a sliding collar.[3]

Nut – an internally threaded fastener intended for use on external screw threads such as a bolt or a stud for the purpose of tightening or assembling two or more components.[2]

Washer – a metallic ring or a perforated circular plate used to form a seat for the head of a bolt or a nut. Washers can be flat or spring loaded. Washers are an integral part of fastening systems and joint assemblies and fall under the jurisdiction of fastener specifications.[2]

High strength fasteners and ***ultrahigh strength fasteners*** – are characterised by tensile strengths ranging from 1,000 to 2,000 MPa, (i.e., >35 Rockwell C) and are the fastener classes most susceptible to HE failure. These are typically externally threaded fasteners such as bolts and screws.

2.1.2 Fastener materials and applications

The choice of fastener material is governed by industry standards that specify the allowable material grades for each fastener type and strength class. The selection of a specific material with which to manufacture a given part is initially based on the material characteristics of maximum strength, ductility, and notch strength. However, the fabrication and engineering performance requirements of the fastener govern the ultimate material choice made by the fastener manufacturer and his customer. Other selection considerations are based on: (i) service temperature, (ii) corrosiveness of service conditions, (iii) the properties of joining materials, and (iv) the choice and compatibility of coating to the substrate material.[4]

Steel fasteners offer the most sought after combination of high strength at low cost. Protective coatings, such as electrodeposited zinc and cadmium, or organic aluminium based coatings have also provided steel fasteners with effective and low cost corrosion protection. For this reason, fasteners made of carbon and alloy steel constitute the majority of fasteners in use today, with the exception of the aerospace industry. Aerospace applications are more demanding than most other applications. New engine designs require increasing high-temperature resistance in hot zones to improve thrust. Airframe and structural designs are prioritising weight reduction to improve fuel efficiency. These advances have dictated the development and increasing use of other

materials, such as high performance stainless steels, iron-based alloys, aluminium alloys, titanium alloys, nickel-based and cobalt-based alloys.[4]

2.2 DEFINING HYDROGEN EMBRITTLEMENT

A typical definition of hydrogen embrittlement found in literature is as follows: "*a permanent loss of ductility in a metal or alloy caused by hydrogen in combination with stress - either an external or internal residual stress.*"[5]

The loss of mechanical properties in iron and steel due to the embrittling effect of nascent hydrogen was first documented in 1874 by Johnson[6] who observed a significant loss of ductility of steel wire caused by immersion in strong acids. Hydrogen in steel can cause a time-delayed or slow strain rate fracture at applied stresses below the yield strength of the material. In other words, the ductility of the material is degraded over a period of time. In order for this to occur, three elements must be present in sufficient quantities: (i) hydrogen, (ii) stress, and (iii) material susceptibility. There are three possible sources of hydrogen – steelmaking, processing, and the service environment. There are also three sources of stress – applied stress, residual stress from plastic deformation (e.g., cold heading or welding), and residual stress from heat treatment.

2.2.1 Types of hydrogen embrittlement

Raymond[7] and most of the literature classify hydrogen embrittlement into two broad categories based on the source of hydrogen: ***internal hydrogen embrittlement*** (IHE) and ***environmental hydrogen embrittlement*** (EHE).

Internal hydrogen embrittlement, also known as slow strain rate embrittlement or delayed failure, is caused by residual hydrogen from steelmaking or from processing steps such as pickling and electroplating. This is a particular concern with the coating of high strength steel components, especially fasteners. Consequently, a great deal of attention has been paid to IHE phenomena. The delayed nature of this type of hydrogen embrittlement suggests that it is controlled by the rate of diffusion of hydrogen or its entrapment within the matrix. Internal hydrogen embrittlement is usually reversible, meaning that ductility can be restored provided microcracks have not been initiated, and the traps are not characterised by a high bonding energy.[7]

Environmental hydrogen embrittlement is caused by hydrogen introduced into the metal from external sources while it is under stress. Most forms of EHE are not reversible because the presence of stress results in the initiation of microcracks.[8] A number of different mechanisms fall under the EHE classification. The term ***stress corrosion cracking*** (SCC) is applied when hydrogen is produced as a by-product of surface corrosion and is absorbed into the lattice. ***Cathodic hydrogen absorption*** (CHA) is a subset of SCC and occurs when a metallic coating such as zinc, which is sacrificial with respect to steel, is damaged or consumed, leaving the underlying steel exposed. Under these conditions, as the zinc oxidises, a simultaneous reduction process results in the evolution of hydrogen. ***Hydrogen reaction embrittlement*** (HRE), prevalent among titanium alloy fasteners is quite distinct from SCC, even though the source of hydrogen can be the same. Once hydrogen is absorbed, it can react near the surface or it may diffuse substantial distances before it reacts, forming a hydride.

2.2.2 Damage mechanism

Craig[8] identifies two distinct processes for hydrogen damage based on predominantly accepted models. These are hydrogen stress cracking, and loss in tensile ductility. He defines hydrogen stress cracking as the *delayed* brittle fracture of a normally ductile alloy under a sustained load that is below the yield strength in the presence of hydrogen. The time delayed nature of the process reveals that it is transport dependant, meaning that hydrogen must diffuse into areas of high triaxial stress, typically located at the tip of a crack or notch. Loss in tensile ductility is defined as a process by which steels and nickel based alloys lose their ductility in the presence of hydrogen. The process is pronounced at higher hydrogen contents and increasing strain rates, resulting in void nucleation and eventually microcracks.[8]

2.2.3 Threshold stress

The susceptibility of a material to hydrogen embrittlement is characterised by its ***threshold stress***, $K_{I(HE)}$, which is defined by Troiano[9] as being the stress below which no time dependant failure will occur. From an HE perspective, the threshold stress separates finite life from infinite life. It is an intrinsic material characteristic that can be measured as is illustrated in Figure 2.1.

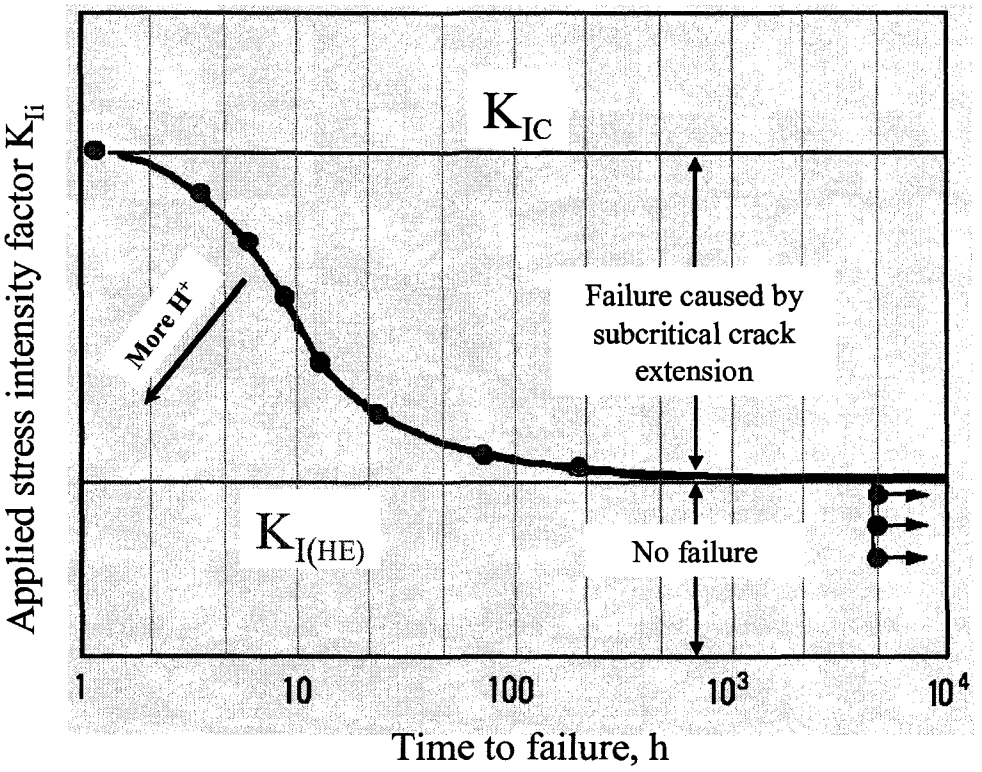

Figure 2.1. Threshold stress $K_{I(HE)}$ in relation to fracture toughness K_{Ic}. In this example the threshold stress was measured by conducting a series of tests at gradually decreasing stress intensities until the point below which no time dependant failure occurred. Above the threshold stress, time to failure decreases with increasing applied stress intensity K_{Ii}. Increasing hydrogen concentration also decreases time to failure, and is illustrated by the curve being shifted to the lower left hand corner.[10]

Above the threshold stress, time to failure decreases with increasing (i) *stress intensity* and/or (ii) *hydrogen concentration*. The stress intensity developed by a material is related to its mechanical properties. Therefore, threshold stress is also affected by mechanical properties. Threshold stress decreases with increasing *strength*; conversely it increases with increasing *ductility* and *toughness*.

Local hydrogen concentration is related to the transport kinetics of the hydrogen ion (H^+) within a material. Transport kinetics is affected by the chemical composition and microstructure of a material. This relationship is significantly more complex than the

previous one because the factors that influence hydrogen transport within a material are not fully understood. The literature points to diffusion as being the primary mode of transport. Factors such as increased dislocation density have been shown to improve transport kinetics. Studies have also shown that martensitic structures enhance hydrogen transport kinetics. Hydrogen trapping has also been extensively studied and is broadly considered to be the binding of hydrogen atoms to impurities or structural defects in the material. Finally, temperature also has an influence on hydrogen transport kinetics. Craig[8] reports that hydrogen embrittlement in steel is most severe near room temperature, but is significantly less severe at lower or higher temperatures. Lower temperatures reduce the diffusion rate, while higher temperatures promote hydrogen effusion or escape.

2.3 HYDROGEN GENERATION MECHANISMS

The discussion that follows focuses on the electrochemical sources of hydrogen. From an electrochemical perspective there are two broad hydrogen generation mechanisms for steel fasteners: (i) hydrogen generated as a result of corrosion, and (ii) hydrogen generated during electroplating. Corrosion of the metal can occur either during surface cleaning and pickling of the fastener prior to coating (internal), or in-service from contact with an electrolyte such as salt water or acidic media (environmental). An additional source of corrosion generated hydrogen is cathodic hydrogen absorption, defined in section 2.1.

Internal hydrogen absorbed during electroplating or cleaning can be removed or relocated by a post-electroplate heat treatment known as *baking*, sometimes mistakenly referred to as *de-embrittlement*. Hydrogen damage occurs in the presence of stress that

exceeds the HE threshold of a given material (once the fastener is under load). Baking does not reverse such damage; however under certain conditions, it can render hydrogen that is in the metal lattice less harmful by either causing it to migrate to internal trap sites, or by expelling it from the lattice altogether.

2.3.1 Mechanism of corrosion

Corrosion will cause the oxidation and dissolution of a metal into a corrosive solution. A corrosive solution can either be present locally, as is typical in environmental corrosion, or can immerse the metal as with acid pickling. The same corrosion mechanism applies to a coated fastener or an uncoated fastener; the difference being the metal that is oxidised. For example, the overall reactions with a hydrochloric acid solution are

$$\mathbf{Zn + 2\,HCl \rightarrow ZnCl_2 + H_2} \qquad (1)$$

or

$$\mathbf{Fe + 2\,HCl \rightarrow Fe_2Cl_3 + H_2} \qquad (2)$$

These reactions can be simplified and expressed as half cell reactions. The anodic reaction is

$$\mathbf{M\ (metal) \rightarrow M^{n+} + ne^-} \qquad (3)$$

while two cathodic reactions are prevalent, the reduction of dissolved oxygen to produce hydroxyl ions,

$$\mathbf{O_2 + 2H_2O + 4e^- \rightarrow 4OH^-} \qquad (4)$$

and once the dissolved oxygen is depleted, the reduction of hydrogen ions to produce first atomic hydrogen which can diffuse into the metal, and then molecular hydrogen.[11]

$$2H^+ + 2e^- \rightarrow 2H \rightarrow H_2 \qquad (5)$$

2.3.2 Mechanism of electroplating

Electroplating is a cathodic deposition process. The plating solution contains metallic chlorides and other salts, rendering it conductive and rich with the metal to be plated. The fasteners serve as cathode (negative terminal) and the metal to be coated serves as anode (positive terminal). For example, in the case of zinc electroplating, when the electric circuit is closed, the cathode becomes negatively charged and zinc ions in solution migrate toward it. The zinc ions diffuse through the cathode film, and plate out as a zinc coating.[12]

$$Zn^{2+} + 2e^- \rightarrow Zn \text{ (deposited zinc)} \qquad (6)$$

Meanwhile at the anode, zinc atoms oxidise by giving up electrons and dissolve into the electrolyte as zinc ions. This essentially maintains the zinc concentration in the electrolyte. Electrons given up by the zinc atoms will flow to the cathode via the power supply.

$$Zn \rightarrow Zn^{2+} + 2e^- \qquad (7)$$

If zinc ions are not readily available for the electrons at the cathode, water is reduced to produce hydrogen ions and hydroxyl ions. Hydrogen ions can in turn be reduced to form atomic hydrogen which can diffuse into the coating and base metal, and molecular hydrogen which bubbles into the plating bath.[12]

$$H_2O + e^- \rightarrow H^+ + OH^- \quad (8)$$

$$2H^+ + 2e^- \rightarrow 2H \rightarrow H_2 \quad (9)$$

Faraday's Law of electrolysis relates the mass of coating substance produced at an electrode during electrolysis to the number of moles of electrons (the quantity of electricity) transferred at that electrode.[12]

$$m = \frac{Q}{qn} \cdot \frac{M}{N_A} = \frac{1}{qN_A} \cdot \frac{QM}{n} = \frac{1}{F} \cdot \frac{QM}{n} \quad (10)$$

Where

m = mass of the coating substance produced at the electrode, g,

Q = total electric charge that passed through the solution, C,

q = electron charge = 1.602×10^{-19} C per electron,

n = valence number of the coating substance as an ion in solution (2 for zinc),

F = Faraday's constant, 96,485 C · mol^{-1},

M= molar mass of the coating substance, g per mole (65.38 for zinc), and

N_A = Avogadro's number = 6.022×10^{23} ions per mole.

In practice, the total charge Q is calculated by integrating the electric current I(t) over time t:

$$Q = \int_0^T I(t) \cdot dt \quad (11)$$

where T is the total amount of time of the electrolysis. In the simple case of constant current electrolysis:

$$Q = I \cdot t \qquad \textbf{(12)}$$

The "cathode efficiency" of a plating bath is a measure of the percentage of the applied current being utilised for depositing the coating substance. For example, cathode efficiency for an acid-chloride zinc bath is roughly 90%.[12] When using Faraday's law to determine the theoretical coating weight of zinc, 90% of the applied current must be taken for I in equation 12. Conversely, current not being used for plating generates hydrogen by equations 7 and 8. Therefore as a general rule, high efficiency baths generate less hydrogen than low efficiency baths, which means that they are also better for minimising the risk of IHE.

The "current distribution" is the ratio of current density at a point X to the average current density on a workpiece as it is being plated. Geometry of the workpiece is the principle factor affecting current distribution. For example, the current density at the centre of a *long* bolt can be several times lower than at the ends. This effect becomes more pronounced as bolt length increases and diameter decreases. The result is what is known as the "dog bone effect", where the coating thickness at the centre is proportionally lower than at the ends. The dog bone effect can cause severe problems with thread fit when plating long bolts, because meeting the minimum required coating thickness at the centre invariably results in excessive coating thickness at the threaded end. Another example of the effect of geometry on current distribution is with a *recess* such as the socket of an *internal drive* screw. Low current density inside the recess as compared to the rest of the screw makes it notoriously difficult to coat adequately. Aside from the geometric effect, the difference between high and low current density locations is increased with increasing plating current. One important consequence of this is that

more efficient plating processes such as acid-chloride zinc baths also exhibit poorer current distribution than a lower efficiency alkaline zinc bath.

The "throwing power" of a plating bath is a measure of the bath's ability to overcome the effect of poor distribution by delivering more uniform coating thickness between the high and low current density areas of the workpiece. Because it is a function of current distribution, throwing power deteriorates with more efficient baths. However, in today's world of surface finishing, many proprietary bath formulations have been developed to improve throwing power for each type of plating process by influencing the localised conductivity of the solution.

2.4 ELECTROCHEMISTRY OF HYDROGEN GENERATION

Consider the following reaction on a platinum electrode.

$$2H^+ + 2e^- \leftrightarrow H_2 \qquad E\text{ (volts)} = 0 \qquad (10)$$

This reaction has an electrode potential E^o (oxidation potential) of zero. When this reaction is at equilibrium, the rate of oxidation equals the rate of reduction, resulting in zero net current. The magnitude of the current generated by the electron flow in either direction is called the exchange current density, i_o. It is defined as the electrochemical equilibrium rate constant and is a function of the conductivity of a particular electrode material. It follows that the electrode potential E for reaction 10 is equal to the equilibrium potential E^o.[13]

A net surface reaction rate can cause a potential change from the equilibrium resulting in a net current flow. This is called polarisation (or overpotential) and is defined by

$$E - E^{o} = \eta \text{ (overpotential).} \qquad (11)$$

For cathodic reactions, the electron-rich electrode moves the surface potential to the negative direction; hence η is negative by definition. For anodic reactions, for which electrons are removed from the electrode surface, η is positive. There are two types of polarisation: activation polarisation and concentration polarisation. Together they determine the reaction rate.[13] Activation polarisation η_{act} is the overpotential corresponding to the transfer of charges at the electrode. It is a function of current density i and is given by

$$\eta_{act} = \beta \log \frac{i}{i_o} \qquad (12)$$

where β is the constant of proportionality, and is known as the Tafel constant for the half cell reaction. When transfer of charges determines the reaction rate, the reaction is said to be under activation control.[13]

Concentration polarisation η_{conc} is a change in potential caused by the depletion of the layer of ionic species next to the electrode (diffusion layer) and is a function of mass transfer. In reaction 4, if dissolved oxygen in the solution adjacent to the electrode surface is depleted, the reaction rate is determined by the rate of diffusion of dissolved oxygen from the bulk solution to the surface of the electrode. In this situation, a concentration

gradient of oxygen exists in the solution and the potential change is referred as concentration polarisation which can be calculated by

$$\eta_{conc} = \frac{-(2.3)\cdot RT}{nF}\log\frac{P_{H_2}}{\left[H^+\right]^2} \qquad \textbf{(13)}$$

where

R = gas constant, 8.31 J/mol · °K,

T = temperature, °K,

n = number of equivalents exchanged (2 for oxygen),

F = Faraday's constant, 96,485 C · mol^{-1},

P_H^2 = hydrogen gas partial pressure, atm,

$[H^+]$ = concentration of hydrogen ions, mol.

The limiting current density i_L occurs when the diffusion rate of the reactive ions (oxygen in this case) to the diffusion layer has reached its limit.

$$\mathbf{i_L = n\,F\,D\,C_b\,\delta} \qquad \textbf{(14)}$$

where

D = diffusivity of reacting species (oxygen),

C_b = bulk concentration of reactive species (oxygen), mol/m^3,

δ = diffusion layer thickness, m.

i_L can be increased by higher solution temperature, which accelerates diffusion and reduces δ. No increase in overpotential can change this condition.[13]

Total cathodic polarisation is the sum of activation and concentration polarisation. For the anodic reaction, in which the metal electrode provides *unlimited* reactant to be dissolved, concentration polarisation is usually minor.[13] Figure 2.2 schematically shows the sum η_{act} and η_{conc} contributions to total cathodic polarisation. When i_o approaches i_L, diffusion takes over from activation to control reaction speed. Therefore the total corrosion rate is limited by the diffusion of the oxidiser from the bulk solution. For iron and steel in dilute aerated salt solution, oxygen reduction (reaction 4) is the major cathodic reaction.[13]

The concentration of hydrogen in solution is represented by the pH value. Therefore, the equilibrium potential for hydrogen reduction, reaction 5, can be calculated by

$$\mathbf{E^{o}_{H+/H} = -0.0591\ pH\ (@298°K\ vs.\ standard\ hydrogen\ electrode\ (SHE))\ (15)}$$

In a neutral solution (pH 7) versus saturated calomel electrode (SCE), 0.241V vs. SHE, $E^{o}_{H+/H}$ is -0.655 V_{SCE}. For this reaction to proceed at a given rate an overvoltage or polarisation, η, is required:

$$\mathbf{E^{o}_{H+/H} = -0.0591\ pH - 0.241 + \eta\ (@298°K\ vs.\ SHE)} \qquad \mathbf{(16)}$$

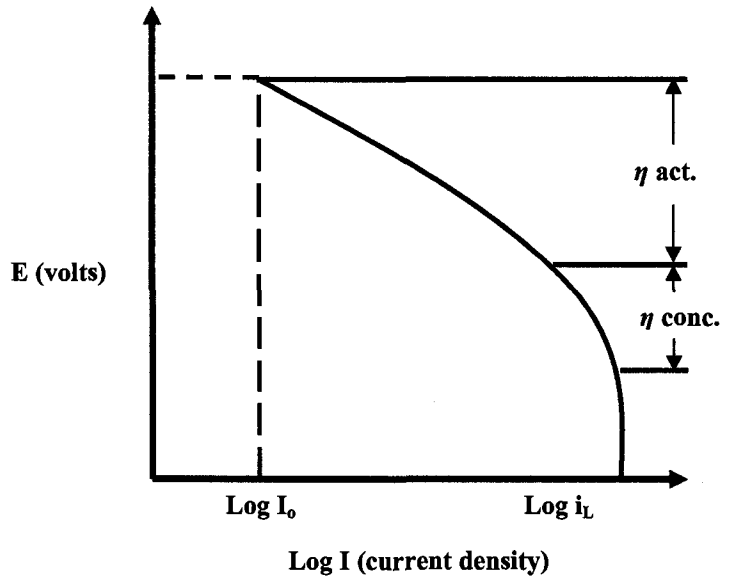

Figure 2.2. Generic example of combined activation and concentration polarisation at cathode.[13]

For hydrogen reduction in NaCl solution with a moderate reaction rate, concentration polarisation can be ignored. Thus the activation polarisation or overvoltage for hydrogen evolution can be estimated by equation 12. The Tafel constant β is given as -0.1V for this calculation.[14] The hydrogen exchange current density, i_o, controls the value of overvoltage. Generally, the value of i_o on Fe is one to five magnitudes larger than those on the coating metals such as Cd, Zn, Sn, and Al. Therefore, the overvoltage for hydrogen evolution on those metals is much higher than that on iron. Consequently, it is more favourable for hydrogen to be generated on iron (and steel) surfaces.[15]

In reaction 5, atomic hydrogen results from the donation of an electron to a proton to form a hydrogen atom on the surface of electrode (e.g., steel). These hydrogen atoms may recombine to form molecular hydrogen that can accumulate and bubble off of the surface. However, before the hydrogen molecule is formed, there is a considerable

residence time during which the nascent hydrogen atoms can ***ad***sorb onto the metal surface and ***ab***sorb into the lattice of steel. The rapidity of forming molecular hydrogen is affected by the catalytic properties of the electrode surface. A good catalyst (e.g., Pt or Fe) has a lower hydrogen overvoltage, whereas a poor catalyst (e.g., Hg) leads to a higher overvoltage. When hydrogen recombination inhibitors or catalyst poisons (e.g., sulphur, arsenic, phosphorus, tin, and cyanide) are present in the environment, hydrogen recombination is retarded, which promotes the ability of atomic hydrogen to enter the steel. On the other hand, poisons do increase the hydrogen overvoltage and may reduce the total reaction rate for the hydrogen evolution reaction 5.[15]

2.4.1 Cathodic hydrogen generation by galvanic protection

For a coated steel fastener, the expected anodic reaction is the dissolution of the coating metal to produce ions in local solution, reaction 1. At the cathode, reactions 4 and 5 apply. The two half-cell potentials from the anodic reaction and the cathodic reaction are different and they are not allowed to coexist on the electrically conductive surface. Each of them has to polarise to a common intermediate oxidation potential E^o.[11]

Metallic coatings such as zinc based coatings are used because their oxidation potential is more negative than that of steel; meaning they have a higher propensity for corrosion. Zn and Fe will develop their own corrosion potentials when immersed separately in dilute acid solution. Zinc, which has a more negative E^o, tends to generate electrons which are transferred to the more positive iron. In this galvanic couple, zinc becomes the anode and the dissolution rate of zinc is increased. On the contrary, the more noble iron has the rate of its dissolution decreased due to the excess of electrons drawn from zinc. Therefore, iron is the cathode of the cell. Decreasing the corrosion rate of one

metal (iron) by coupling it to a sacrificial anode (zinc) is the basis of cathodic (galvanic) protection.[16]

For a coated steel fastener, the anodic activity of the coating is responsible for galvanic protection. This sacrificial nature makes zinc based coatings very effective for protecting steel fasteners against corrosion. Yet this very characteristic can be an additional source of hydrogen that is cathodically generated at the base metal in a corrosive environment, and can precipitate the onset of hydrogen assisted cracking.

For cathodic hydrogen absorption (CHA) to occur, the coating must be either damaged or consumed as a result of corrosion. Townsend[17] and others have demonstrated the occurrence of CHA with fatigue pre-cracked test specimens immersed in conductive solutions while being loaded. In a variation of this theme, Pollack and Grey[18] observed the impact of CHA on high strength 4340 steel that was coated with a porous cadmium coating and subsequently immersed in paint strippers (organic solvent). In this case it was the porosity of the coating, not mechanical damage or corrosion, that provided access to the base metal for creating a galvanic cell.

It follows that by using a less active metal, alloy or multiphase system as protective coating, it is possible to avoid or reduce cathodic hydrogen generation in the corrosive environment. Table 2.1 shows the standard oxidation potentials of a number of common metals.

Table 2.1. Standard oxidation potentials of metals at 25°C.[19]

Oxidation (corrosion) reaction)	Electrode potential* ($E°$)	
$Au \rightarrow Au^{3+} + 3e^-$	+ 1.498	More cathodic: (less likely to corrode)
$2H_2O \rightarrow O_2 + 4H^+ + 4e^-$	+ 1.229	
$Pt \rightarrow Pt^{2+} + 2e^-$	+ 1.200	
$Ag \rightarrow Ag^+ + e^-$	+ 0.799	
$4(OH-) \rightarrow O_2 + 2H_2O + 4e^-$	+ 0.401	
$Cu \rightarrow Cu^{2+} + 2e^-$	+ 0.337	
$H_2 \rightarrow 2H^+ + 2e^-$	0.000	
$Pb \rightarrow Pb^{2+} + 2e^-$	- 0.126	More anodic: (more likely to corrode)
$Sn \rightarrow Sn^{2+} + 2e^-$	- 0.136	
$Ni \rightarrow Ni^{2+} + 2e^-$	- 0.250	
$Co \rightarrow Co^{2+} + 2e^-$	- 0.277	
$Cd \rightarrow Cd^{2+} + 2e^-$	- 0.403	
$Fe \rightarrow Fe^{2+} + 2e^-$	- 0.440	
$Cr \rightarrow Cr^{3+} + 3e^-$	- 0.744	
$Zn \rightarrow Zn^{2+} + 2e^-$	- 0.763	
$Al \rightarrow Al^{3+} + 3e^-$	- 1.662	
$Mg \rightarrow Mg^{2+} + 2e^-$	- 2.363	
$Na \rightarrow Na^+ + e^-$	- 2.714	

*Relative to standard hydrogen electrode

2.4.2 Electrochemical conditions at crack tips

Studies into the electrochemical reactions that occur in occluded areas, such as crevices and pits have revealed that localised conditions can differ substantially from those in the bulk solution. The geometrical constraints posed by localised topography of a pit or crevice prevent mixing with the bulk solution. Therefore, it cannot be assumed that the production of nascent hydrogen cannot occur in neutral or alkaline environments. In fact, there is a tendency for lowering of pH in these areas.[13,15] In one of a number of studies on this topic, Smith, Peterson and Brown[20] conducted experiments in bulk 3.5% sodium chloride (NaCl) with varying acidity ranging from pH 2 to pH 10. They observed

that the pH at the advancing crack tip remained constant in the range of 3.5 to 3.9. They proposed that the anodic reaction

$$\mathbf{Fe \rightarrow Fe^{2+} + 2e^{-}} \qquad \mathbf{(17)}$$

is followed by the hydrolysis of water as it becomes thermodynamically unstable.

$$\mathbf{Fe^{2+} + H_2O \leftrightarrow Fe(OH)^{+} + H_3O^{+}} \qquad \mathbf{(18)}$$

To maintain electroneutrality, Cl^- ions rush to the crack tip. The result is the formation of stable hydrochloric acid.

$$\mathbf{Fe(OH)^{+} + H_3O^{+} \rightarrow Fe(OH)_2 + [2Cl^{-} + 2H^{+}]} \qquad \mathbf{(19)}$$

The continued crack growth observed during these experiments is an indication that nascent hydrogen is able to diffuse into the metal lattice from the crack tip.

2.5 EFFECTS OF COATINGS AND SURFACE CHARACTERISTICS

A large number of studies have been conducted to determine the impact of various coatings on internal hydrogen embrittlement (IHE) of steel and fasteners. This section addresses this topic from the perspective of hydrogen availability, not withstanding stress and susceptibility, the other two ingredients for hydrogen assisted cracking. The topic is divided into four broad categories: (i) the impact of the surface preparation method on hydrogen absorption prior to coating, (ii) surface characteristics as barrier to hydrogen absorption and effusion, (iii) the impact of the coating process itself, and (iv) the effectiveness of baking as a process for hydrogen embrittlement relief following coating

application. These four categories are often closely interrelated. However for the sake of distinguishing the phenomena related to coatings, they are discussed separately.

2.5.1 Surface preparation

Surface preparation is an important prerequisite for coating. Most industrial processes use chemical media for surface preparation, such as alkaline degreasing, and acid pickling. This can be an important source of hydrogen resulting from the oxidation of the metal surface. A great deal has been done to minimise the hydrogen contribution from cleaning processes, starting with tight control of process parameters such as time, temperature, concentration and the type of acid (or alkali) used. Another important development was the use of inhibitors that can limit the oxidation activity in an acid pickling bath, and also reduce hydrogen penetration. In a study on the prevention of HE by surface films, Murray[21] observed that inhibitors added to liquid media (e.g., acids), or to gas media, can occupy the surface area of the metal with a thin strongly bonded layer. This layer alters the surface adsorption characteristics in a manner that effectively prevents hydrogen entering the metal.

An alternative to chemical cleaning has been the use of mechanical abrasion and descaling methods. This approach eliminates any contact with hydrogen altogether, but is sometimes problematic due to material handling issues.

2.5.2 Surface characteristics

Surface properties and a coating's physical characteristics have an immense impact on the rate of hydrogen penetration. Pollack[22] conducted a detailed study on 4340 high strength specimens with a variety of electroplated coatings such as porous Cd,

nonporous Cd, Brush Cd, Cd-Ti, and electroless Ni. Although the study did not isolate individual processing steps, such as surface preparation, plating and baking, one key conclusion was that the degree of embrittlement was a function of the porosity of the specific coating. This finding was illustrated by the lack of baking effectiveness with less porous coatings that tend to prevent hydrogen effusion. Another conclusion in this study was that the addition of brighteners in the plating bath appeared to lower the coating porosity.

In another study, Pollock and Grey[18] applied porous cadmium plating to high strength 4340 steel specimens. They observed embrittlement following immersion of the specimens in paint strippers (e.g., organic solvent). In this case, the porosity of the coating provided access to the base metal to create a galvanic cell and cathodic hydrogen absorption (CHA).

In his study on surface films, Murray[21] also demonstrated that the application of tungsten and non-metallic TiO_2 and Al_2O_3 thin films, in the order of 50 nm, is very effective in preventing hydrogen entry at the metal surface, due to very low hydrogen permeability of the film. It is interesting to note that in 1970 a Canadian patent was issued to Bednar, Dingley and Rogers that prescribed the application of an electroless thin copper layer (flash) before electroplating as a means of minimising hydrogen contact with the base steel.[23] No information regarding the technical or commercial viability of this process for bulk fastener coating was found. The patent expired in 1987.

Surface properties of the metal also have an important role in hydrogen permeability. Murray[21] observed that thermally grown (at 1000 °C) adherent oxide films on stainless steel in the order of 100 nm can also have a barrier effect to hydrogen

penetration. McCarty, Wetzel & Kloberdanz[24] observed that carbonitriding of 1022 steel fasteners significantly lowered hydrogen permeability. These surface properties can block hydrogen absorption, but they can also reduce the effectiveness of baking.

2.5.3 Coating processes

Most studies reviewed do not distinguish between the coating process and the hydrogen contribution of surface preparation. Acid pickling in particular can be a source of hydrogen that remains trapped during and after the subsequent coating step. With this caution in mind, some of the most prevalent coating processes are reviewed.

2.5.3.1 Electroplating

Many studies have found that plating is a high risk process with respect to IHE. As was discussed earlier, electrochemical reactions that occur in the process promote the **ad**sorption and **ab**sorption of hydrogen. Hydrogen charging is most elevated before the build-up of the coating layer, which acts as a barrier that slows down hydrogen absorption, but can also trap hydrogen in the metal. There are a great many formulations for plating processes, each with its own bath chemistry, brightness, efficiency, coating permeability etc. Therefore, specific conditions will vary depending on the plating bath itself.

Zinc, zinc alloys, nickel, chromium, and cadmium are the most common electroplated metals on fasteners. Note that despite the elimination of cadmium coatings in commercial applications due the environmental concerns, these coatings are still widely used in military and aerospace applications. Efforts have been long underway to find suitable alternatives. Zinc-nickel (Zn-Ni) alloys are being given particular attention

by researchers due to advantages such as a good corrosion resistance and high plating rates. Electroplated coating standards for fasteners are specified in ASTM F1941 and F1941M.[25]

2.5.3.2 Non electrolytic processes

<u>*Zinc phosphate*</u>

Zinc phosphate $Zn_3(PO_4)_2$ is an inorganic compound that is chemically deposited on the surface of steel. It is characterised by a porous crystalline structure that can act as a carrier or primer for corrosion protective media such as paints and oil. The phosphating solution is comprised of dilute phosphoric acid that contains zinc phosphate, iron, and chemical accelerators that are oxidants (e.g., nitrites and hydrogen peroxide). Because the coating contains both zinc and iron, it is technically classified as a zinc-iron phosphate. However, it is generally referred to in industry simply as "zinc phosphate," one of a series of phosphate coatings commonly used. Others include (pure) zinc phosphate, iron phosphate, and manganese-iron phosphate.[26]

In some cases grit blasting is used instead of acid pickling for surface preparation. Grit blasting creates a rough surface that accelerates coating formation, producing fine crystalline coatings. Phosphate coating thickness is measured by mass per surface area. Zinc-iron phosphate coatings can range from 100 to 3000 mg/cm^2.

From the perspective of IHE avoidance, this process offers a number of advantages. First, because it does not involve electroplating, there is no cathodic generation of hydrogen in contact with the metal being co-deposited. Hydrogen is evolved primarily from the reaction of the mildly acidic medium with the surface of the

metal. This reaction occurs at a much slower rate than during electroplating. The porous coating does not trap hydrogen and allows hydrogen to effuse at room temperature. Voorhis studied the impact of phosphate coating, a chemical conversion process in acidic medium, on the embrittlement of high strength military submunitions under sustained loading at 65% of the fracture strength for 200 hours. He concluded that the process which takes place in a zinc-rich phosphoric acid bath causes hydrogen embrittlement failure. However, baking at 90 °C for three hours, or natural degassing at room temperature for 30 days, eliminated the problem. These findings can be attributed to the porosity of the zinc phosphate coating. He also observed that better control of the zinc phosphate bath chemistry can reduce the degree of embrittlement.[27] One area of weakness in this study is that the sustained loading method does not provide any reliable quantitative data on the degree of embrittlement because it does not measure threshold stress. Phosphate coating standards for fasteners are specified in ASTM F1137.[28]

Mechanical zinc

Mechanical plating and mechanical galvanising apply a zinc coating by impaction of particulate zinc in a liquid medium filled with glass beads. Surface preparation typically consists of degreasing and caustic descaling, followed by pickling in a dilute acid. After surface preparation, varying sizes of glass beads are added to a rubber lined tumbler, along with water and a "chemical starter" which ensures an optimal chemical balance for the coating process. Next, a small quantity of copper sulphate is added to the now rotating tumbler barrel, producing a copper flashover which will act as active substrate for the zinc coating. Very fine zinc powder is then added to the process. The forces exerted by the tumbling action cause the impact media (glass beads ~1-10mm) to

cold weld the much smaller and softer zinc particles (~3-5 microns) onto the surface of the parts.[29]

The desired coating thickness is achieved by controlling the quantity of zinc powder and tumbling time. Typical coating thickness can range from 5 to 12 microns, for mechanical plating, and 25 to 110 microns for mechanical galvanising. The coating coverage by this process is smooth and uniform, albeit porous.

The principal driving force behind the development of mechanical galvanising was the ability to coat parts with minimal risk of internal hydrogen embrittlement. From the perspective of IHE avoidance, this process offers a number of advantages to zinc plating and hot dip galvanising. First, the process is at room temperature, thus avoiding the thermal impact of hot dip galvanising on hydrogen mobility. Second, because the process does not involve electroplating, there is no cathodic generation of hydrogen in contact with the metal being co-deposited. Hydrogen is evolved primarily from the reaction of the mildly acidic medium with the surface of the metal. This reaction occurs at a slower rate than during electroplating. The cold welding of the relatively large zinc particles does not tend to trap hydrogen gas during impaction. Third the coating itself is less dense and more porous than zinc plating or galvanising. Fourth, the abrasive nature of mechanical galvanising precludes the need for aggressive acid pickling. The metal surface is cleaned by the glass beads as the coating is being deposited.[29] On the other hand, it should be noted that the variability in compaction rate and the porosity of the mechanically galvanised coating results in poorer corrosion protection than with the hot dip process. Mechanical galvanising coating standards are specified in ASTM B695.[30]

DACROMET®

DACROMET® is a proprietary coating system licensed by Metal Coatings International (MCII) in Chardon, OH. It is a water-based inorganic zinc-aluminium dispersion coating comprised of overlapping zinc and aluminium flake in a chromium-oxide binder system. Typically a sodium silicate based sealer is applied over the basecoat for additional corrosion protection and also to control the lubricity of parts, which can be a very important application design feature. Surface preparation consists of alkaline degreasing followed by mechanical descaling. Acid pickling is not permitted in the DACROMET® process, thus effectively eliminating the risk of internal hydrogen embrittlement.[31]

DACROMET® is usually applied to small and medium sized metal components such as fasteners and stampings that can be coated in bulk by the dip-spin process. "Dip-spin" refers to an application process whereby product is placed in a mesh basket, submerged in coating solution, and then spun centrifugally to remove excess coating material. Larger parts such as tubes, large bolts and rods are racked, then either sprayed or immersed. If immersion is used, excess coating material is removed by draining and/or centrifuging. Each application step in the DACROMET® emulsion is followed by a 15 minute curing cycle of the basecoat at roughly 320°C part metal temperature. Once the sealer is applied, also by spray or immersion, the parts undergo a 15 minute curing cycle at roughly 175 °C part metal temperature.[31]

Typical coating thickness can range from 6 to 12 microns. Coating thickness may be varied by applying successive layers of the basecoat and by controlling the viscosity of the DACROMET® emulsion. The coating coverage by this process is very smooth and

uniform. Non proprietary requirements for DACROMET® are specified in ASTM F1136 and F1136M.[32]

Magni 555®

Magni 555® is a proprietary coating system licensed by The Magni Group based in Birmingham, MI. This coating system, which originally targeted the automotive market, applies an aluminium/zinc organic topcoat (epoxy) over a zinc rich primer base coat. The basecoat is designed to provide sacrificial protection of the steel substrate. The topcoat is designed to provide a well adhered, durable barrier that also has the effect of passivating the zinc basecoat.[33]

Surface preparation consists of alkaline degreasing followed by acid pickling in sulphuric acid at 42 °C for 10-15 minutes. This step is followed by the application of a medium weight zinc phosphate (Z24) to promote adhesion of the basecoat.

Similar to DACROMET®, this coating is typically applied to small parts by the dip-spin process and to large parts by the rack-spray process.

The application of basecoat is followed by an 18 minute curing cycle at roughly 220 °C part metal temperature. Once the topcoat is applied, the parts undergo an 18 minute curing cycle at roughly 225 °C metal part temperature.[33]

Typical coating thickness can range from 12 to 20 microns. The coating coverage by this process is very consistent and uniform. Non proprietary requirements for Magni 555® are specified in ASTM F1136 and F1136M.[32]

2.5.3.3 Thermal diffusion processes – hot dip zinc (galvanising)

Hot-dip galvanising is the process of applying a zinc coating to fabricated iron or steel material by immersing the material in a molten zinc bath. The galvanising process consists of surface preparation followed by zinc immersion.[34]

Surface preparation typically consists of three steps: (i) degreasing and caustic descaling, (ii) acid pickling or abrasive cleaning, and (iii) fluxing which removes oxides and prevents further oxides from forming on the surface of the metal prior to galvanising. It also promotes bonding of the zinc to the steel.[34]

Following surface preparation, the parts are completely immersed in a bath consisting of molten zinc (~ 98% Zn, 1% Pb, 0.01% Al). The bath temperature is maintained at about 450°C. Parts are immersed in the bath long enough (~ 3-5 minutes) until they reach bath temperature. This process is also referred to as "cooking". The articles are withdrawn slowly and the excess zinc is removed by draining, vibrating and/or centrifuging. Small parts such as fasteners are transported into the zinc bath by means of a perforated metal basket, and are typically cooled in water immediately after withdrawal from the bath. Large articles are typically cooled in ambient air.[34]

During galvanising molten zinc reacts with the surface of the steel part to form a series of successive layers composed of zinc/iron alloy phases. These layers provide excellent bond strength. The adherence of a galvanised coating to the underlying steel is in the order of 0.2 MPa. By contrast, the adherence of other coatings is one order of magnitude lower.[34] Figure 2.3 illustrates the cross section of a hot dip galvanised coating.

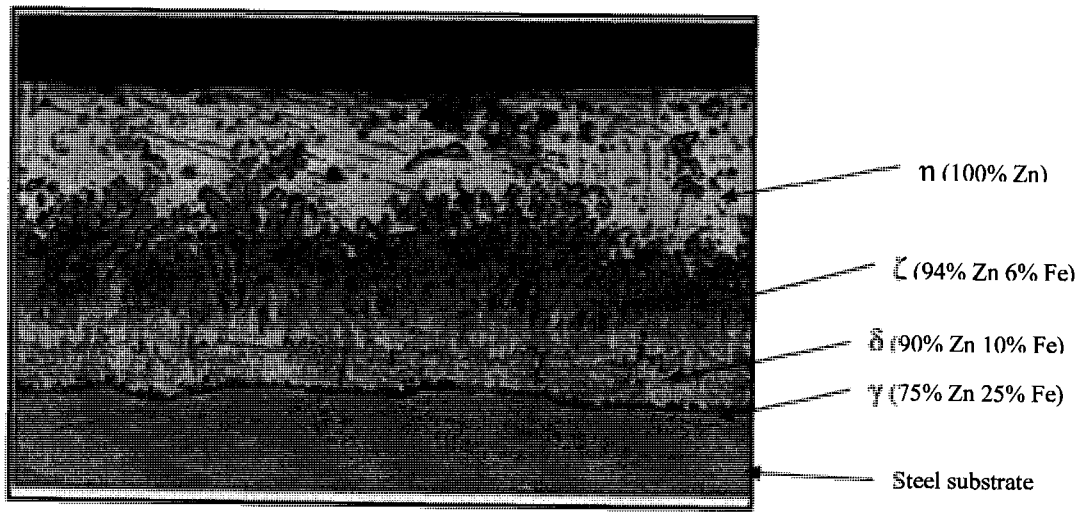

Figure 2.3. Microstructure of hot-dip zinc coating illustrating successive Zn/Fe phases.[34]

Factors influencing the thickness and appearance of the galvanised coating are: (i) chemical composition of the steel, (ii) steel surface condition, (iii) bath temperature, (iv) bath immersion time, (v) bath withdrawal rate, and (vi) steel cooling rate. As the galvanising reaction is a diffusion process, higher zinc bath temperatures and longer immersion times will produce heavier alloy layers. Like all diffusion processes, the reaction proceeds rapidly at first and then slows as layers grow and become thicker.[34]

Galvanised coatings are impermeable, and if damaged will continue to provide cathodic protection to the exposed steel. In his study on the effects of zinc coatings on stress corrosion cracking and hydrogen embrittlement, Townsend[17] confirmed that the galvanic nature of zinc coatings can be an additional source of cathodic hydrogen, as was discussed earlier. However, he also made an interesting observation about hot dip galvanised (zinc) coatings. Despite the fact that *hot dipping* in molten zinc does not introduce any hydrogen, hot dip galvanised test specimens with a fatigue pre-crack exhibited a substantial drop in threshold stress, even in the absence of acid pickling. He

postulated that internal hydrogen bound in trap sites was being released by the thermal energy of hot dipping, but was prevented from escaping by the intermetallic coating layer. Brahimi[35] made the same observation in a similar study on hot dip galvanising using the incremental step load method.

Galvanised coatings are typically rough and dull. Coating in recesses such as internal socket drives and internal threads, where zinc has a tendency to accumulate, can be problematic. Hot dip galvanising coating standards for fasteners are specified in ASTM F2329.[36]

2.5.4 Baking

The potentially deleterious effects of hydrogen absorbed during plating or surface cleaning can usually be eliminated by a baking heat treatment after processing. The severity of hydrogen damage is normally determined by the strength level or the amount of cold work within a fastener. Troiano demonstrated that time to failure can be varied as a function of hydrogen content, or bake time.[9] Baking reduces interstitial (free) hydrogen, thus increasing the threshold stress and the time to failure. Baking is thought to either expel hydrogen or cause it to migrate to stable trap sites, making it immobile.[17]

The key factors that influence baking effectiveness are: (i) time, (ii) temperature, (iii) the permeability of the surface (coating, case, oxides, etc.), and (iv) material hardness. These factors lead to a high variability of effective baking response. Current industry practice calls for baking plated parts above 35 HRC for 4 hours at 190°C, within a few hours of plating. However, it has been shown in many studies that this is inadequate for truly susceptible parts.[37] Robinson and Sharp,[38] and others observed that insufficient bake times can sometimes result in a lowering of threshold stress by releasing hydrogen

from irreversible (i.e., innocuous) traps, to the metal lattice, or to lower energy reversible traps.

2.6 INCREMENTAL STEP LOADING TEST METHOD

Most studies in the literature have used some form of mechanical testing to measure fracture stress as the parameter for assessing the degree of embrittlement after plating and plating/baking combinations. Prior to the 1980's, 200 hour sustained loading was the method of choice. The shortcomings of this approach have been demonstrated on many occasions. For example, in the mid 1980's Levy and Bruggeman[39] used sustained load testing to determine if suspect high strength cadmium plated aircraft fasteners were embrittled. Although they did not find any parts that failed the test, their findings did not provide any assurance that the parts were not embrittled. The uncertainty compelled them to apply a costly baking process at 190 °C for 48 hours to a very large volume of parts. In a 1988 study, Dreher[40] highlighted not only the technical shortcomings of sustained load testing but also the practical difficulties in applying this approach for production quality assurance purposes.

Beginning in the late 1980's, mechanical test methodology that utilised slowly increasing loading patterns, namely slow strain rate testing (SSRT) and incremental step load testing (ISL), gained wider acceptance. These tests allow for the time-delay mechanisms of HE to evolve, while applying stress at a slowly increasing rate. The result is an accurate measure of the threshold stress. Recently, the ISL test method has demonstrated very promising capabilities as an accelerated test metric to measure the hydrogen susceptibility of materials.[18,41] ISL is unique in that it measures the threshold

stress intensity for hydrogen stress cracking in an accelerated manner (i.e., less than 24 h). It measures the onset of sub-critical crack growth in a notched specimen subjected to a modified, incrementally increasing, slow strain rate load.[42] The test method is well suited for fasteners, as these are naturally notched specimens.

The ISL test method can measure the threshold stress of materials that have had prior exposure to hydrogen (i.e., internal hydrogen). It can also measure the threshold stress of materials that have not had prior exposure to hydrogen by simulating hydrogen charging conditions during the test (i.e., environmental hydrogen). In this case, the test is performed in an environmental chamber containing 3.5% NaCl solution under cathodic potential ranging from -1.2V versus SCE to testing in air. The hydrogen susceptibility ratio H_{sr}, as defined by Raymond,[42] is a parameter that can be used as a measure of the susceptibility of a material to hydrogen assisted cracking, given its threshold stress. H_{sr} is calculated as the ratio of the $K_{I(HE)}$ threshold stress of a material under specific environmental conditions over its fracture stress K_{IC} tested under benign conditions.

In 1999 the incremental step load test method in ASTM F1624[43] was modified and adapted in ASTM F1940[44] to provide a methodology for quantifying the risk of internal hydrogen embrittlement (IHE) posed by coating processes. The test consists of using a test specimen as a *witness* by processing it with other production parts. By doing so, it is exposed to the same hydrogen charging conditions as the production parts. The test specimen is a standardised notched square bar (SQB) made of highly susceptible AISI E4340 steel heat treated to 50-52 HRC. In terms of HE susceptibility, this specimen represents a worst case scenario. In other words production fasteners will never be more susceptible than the SQB specimens. Fastener product specifications for class 12.9

fasteners, which is the highest *standard* strength grade, set a maximum allowable hardness limit of 44 HRC.

ASTM F1940 specifies a test protocol with pre-defined load/strain increments and hold times. The SQB specimen is subjected to a sustained four-point bending load and slow strain rate under displacement control. The test indirectly quantifies the amount of residual hydrogen by measuring the threshold stress, represented by the fracture load, called Notch Fracture Strength (NFS).

Pristine (unexposed) SQB specimens are tested in the same manner to establish a *baseline* notch fracture strength. The ratio of the fracture strength for each *witness* over the baseline represents the percent Notch Fracture Strength (%NFS), which is another expression for the hydrogen susceptibility ratio H_{sr}.

$$NFS_{\%} = \frac{NFS_{(W)F1940}}{NFS_{(B)}} \times 100 \qquad \textbf{(21)}$$

where:

$NFS_{\%}$ = Percent notch fracture strength
$NFS_{(B)}$ = Notch fracture strength of "pristine" SQB specimen
$NFS_{(W)F1940}$ = Notch fracture strength of coated SQB "witness" specimen

The $NFS_{\%}$ ratio, when statistically validated, represents a measure of the embrittling potential of a coating process. ASTM F1940 establishes an acceptability limit of 75% notch fracture strength[a]. In other words a coating process that obtains a $NFS_{\%}$

[a] ASTM F1940 proposes an acceptability limit of 75% when $NFS_{\%}$ is calculated using the ***fast fracture*** strength of pristine specimens as the denominator. This corresponds to roughly 85% when $NFS_{\%}$ is calculated using the ***same incremental step loading pattern*** used for the coated specimens.

above 75% is not at risk of causing IHE, whatever the susceptibility of the parts being coated. Such a process is considered to be "safe".[42,45]

CHAPTER 3: EXPERIMENTAL PROCEDURE

3.1 EXPERIMENTAL PROCEDURES

As was stated earlier, the primary objective of this research was to quantify the risk of embrittlement from residual hydrogen (i.e., IHE) from coating processes commonly utilised to coat high strength mechanical fasteners. More specifically, the effects of coating process variables and certain coating characteristics, such as thickness and permeability were investigated. The overall methodology consisted of sampling a number of industrial electroplating and coating processes in accordance with the ISL test method described in ASTM F1940. This is the first time that ASTM F1940 has been used to test a broad cross section of fastener coating processes to assess the relative impact of key processing variables for the risk of causing IHE. The sampling procedure consisted of coating "witness" test specimens by each process along with actual production parts. One important reason for utilising a standardised test method was to make it possible for the results to be used as a benchmark for future academic studies, and also for industry based process evaluation and process control.

The ISL fracture loads obtained with coated specimens were compared to the baseline ISL fracture load, obtained with pristine specimens. This relationship was expressed as the "percent notch fracture strength" ($NFS_{\%}$), which is the ratio of the threshold over the baseline fracture strength shown in equation 21, section 2.6.

Each process was sampled within a "window" defined as the process being under reproducible conditions within the *normal range of processing parameters*. Apart from obtaining the processed specimens, standard sampling procedures included measuring the resulting *coating thicknesses*, recording all of the *process parameters* at the time of sampling, and wherever possible obtaining *technical data sheets* pertaining to each process. Each condition was sampled using specimen subgroups comprising five test specimens processed simultaneously.

While waiting to be tested, processed specimens were stored in a desiccator at room temperature. In most cases the specimens were tested within one week of having been coated to minimise any influence of time delay on the test results.

3.2 ISL TEST METHOD

The test equipment used for this investigation consisted of two RSL® loading frames, manufactured by Fracture Diagnostics Inc. An RSL® loading frame, shown in Figures 3.1 and 3.2, is a computer-controlled *four-point bend* displacement control frame that is capable of holding a displacement within ± 0.13 μm and reaching target loads within ± 1.78 N (0.4 lb). The load readings were generated by a calibrated load cell in each unit having a maximum capacity of 2.224 kN (500 lb). All of the tests were conducted in air, meaning that no hydrogen was being electrolytically charged during the test. The tests were automatically halted at a 5% drop in load, which was taken to indicate the onset of cracking.

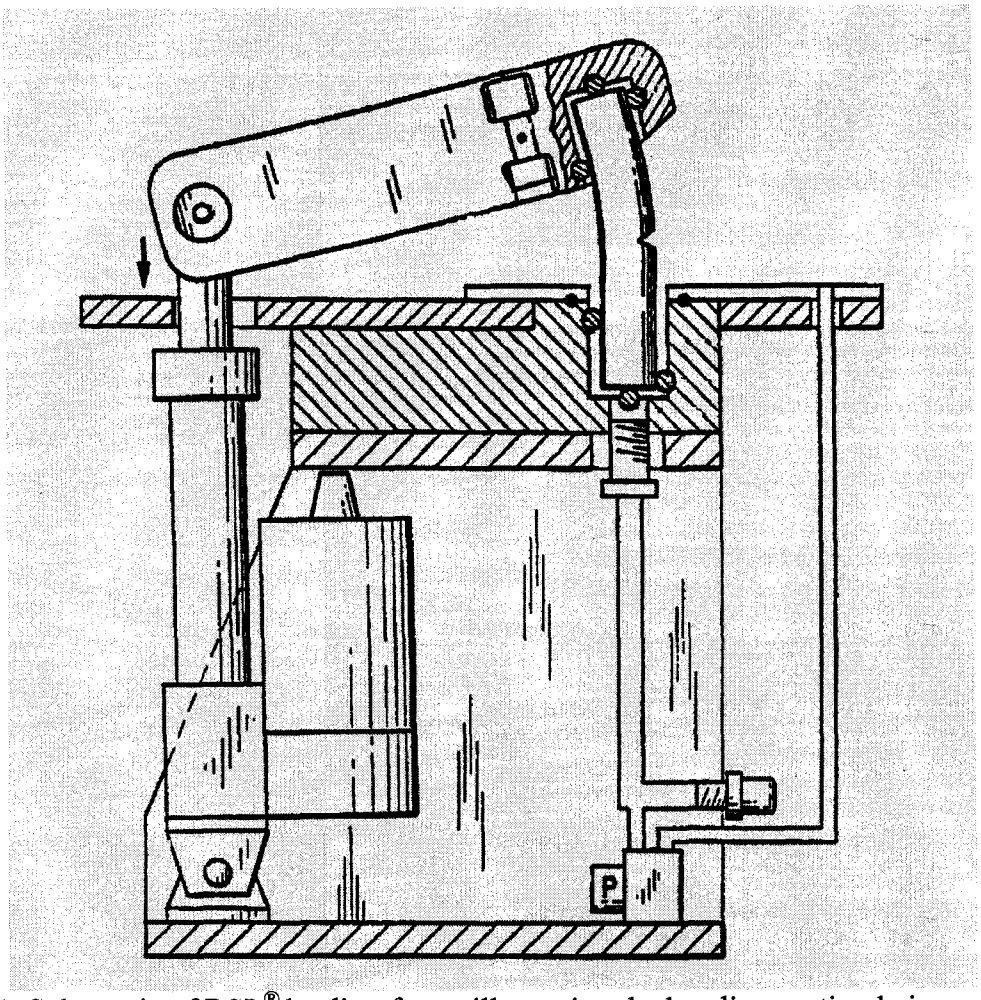

Figure 3.1. Schematic of RSL® loading frame illustrating the bending motion being applied to a test specimen.[46]

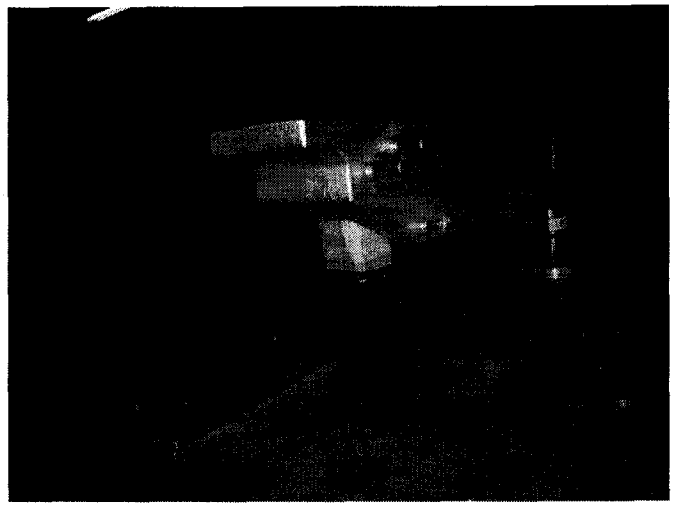

Figure 3.2. RSL® loading frame.

The duration of each test cycle ranged from 5 to 20 hours and was dependent upon the degree of embrittlement of the specimen. The ASTM F1940 loading protocol shown in Table 3.1 was applied. This loading protocol was designed to achieve sufficient sensitivity within a reasonable testing time. It initially increases load rapidly by five one-hour steps at 10% notch fracture strength increments. In order to maximise sensitivity in the middle portion of the test range, the step size is reduced to four one-hour steps at 5% increments, followed by five one-hour steps at 2% increments. Step size is again increased in the last stage to six one-hour steps at 5% increments. Figure 3.3 illustrates a typical loading pattern obtained during a single test where fracture occurred after 12 hours.

Table 3.1. ISL loading protocol per ASTM F1940[44]
(5 x 10%) + (4 x 5%) + (5 x 2%) + (6 x 5%) at one hour intervals

Percent notch fracture strength ($NFS_{\%}$)	Step duration (h)	Total duration (Σh)
10	1	1
20	1	2
30	1	3
40	1	4
50	1	5
55	1	6
60	1	7
65	1	8
70	1	9
72	1	10
74	1	11
76	1	12
78	1	13
80	1	14
85	1	15
90	1	16
95	1	17
100	1	18
105	1	19
110	1	20

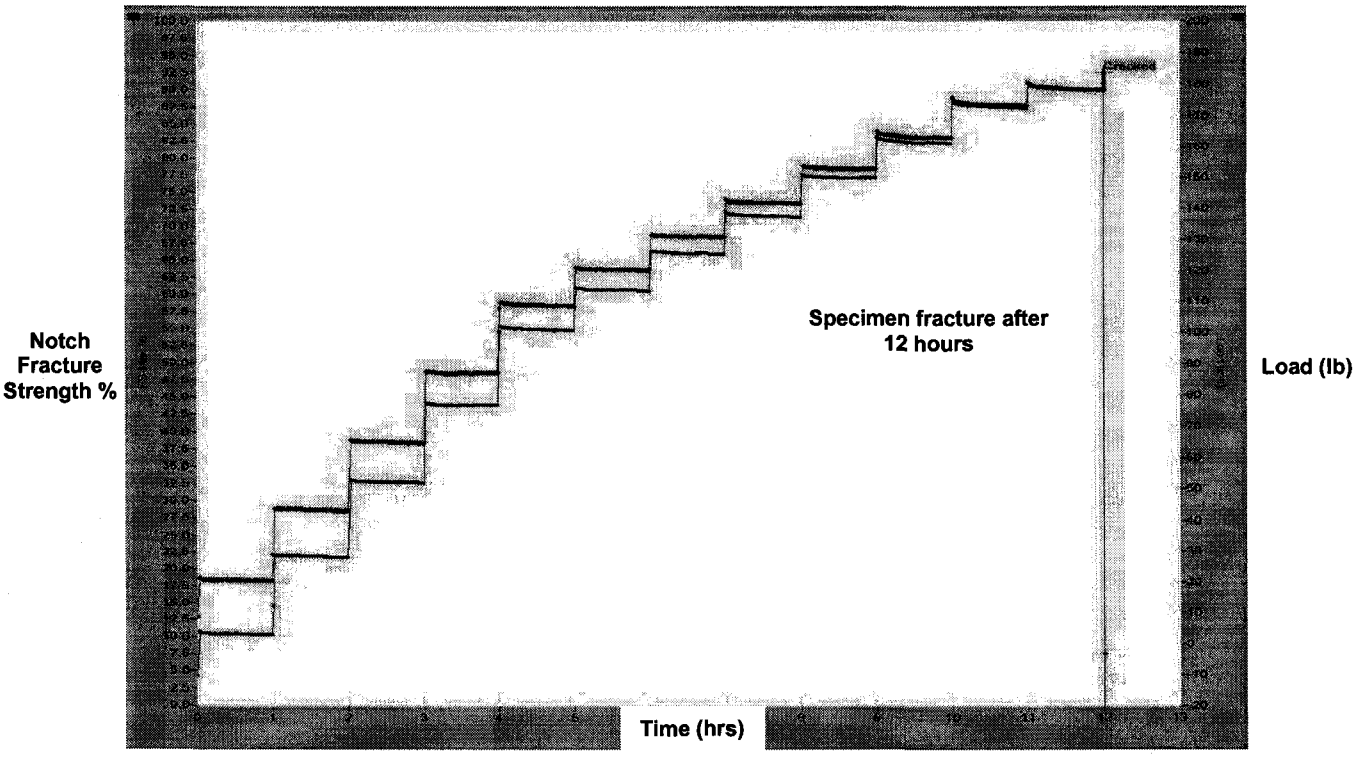

Figure 3.3. Example of typical ISL loading profile.

3.3 TEST SPECIMENS

3.3.1 Dimensional, physical and metallurgical specifications

The coating processes were sampled using test specimens manufactured to ASTM F519 (type 1e) requirements.[47] The F519-1e test specimen is almost identical to the one specified in ASTM F1940, with two notable exceptions: (i) F519-1e requires a hardness range of 51-53[b] Rockwell C instead of 50-52 Rockwell C for F1940, and (ii) the root radius at the base of the notch for the F519-1e specimen is 0.25 mm instead of 0.50 mm. The higher hardness makes the F519-1e specimens slightly more susceptible to hydrogen embrittlement. The smaller root radius increases the predicted stress intensity factor K_t in

[b] At the time this study was initiated, ASTM F519 hardness requirement for test specimens was 51 to 53 HRC. The latest revision of the standard (F519-06) has a hardness requirement of 52 to 54 HRC.

the notch from 3.10 ± 0.20 to 4.27 ± 0.32, which has the effect of increasing the notch sensitivity of the specimen. In other words, this configuration was selected to increase the sensitivity of the test.

The test specimen, shown in Figures 3.4 and 3.5, is a single notched bend square bar made from AISI 4340 steel per SAE-AMS-S-5000[48] (alloy composition is given in Table 3.2). The manufacturing process begins by cutting the raw material, typically in bar form, into blanks. The blanks are quenched and tempered per SAE AMS 2759/2D[49] to a hardness of 51 to 53 Rockwell C. Heat treatment as a first step (prior to machining) eliminates any distortion effect on the specimen, and straightening after final heat treatment is prohibited. The notch is rough machined in the LS-orientation by wire electrical discharge machining (EDM) within 0.5 mm of the final notch depth. Final notch depth and specimen dimensions, with the exception of length, are produced by low stress grinding. The surface finish of the notch is 0.4 μm (16 micro-inch) root square mean (RMS) or better, with the other surfaces at 0.8 μm (32 micro-inch) RMS or better. No chemical or mechanical cleaning is allowed after final machining. The last manufacturing step consists of a stress relief at 190°C for no less than 4 hours. The specimens are typically coated with light oil to prevent corrosion during storage. The appearance of any amount of corrosion may compromise the integrity the test specimen and validity of the test.

The uniformity, mechanical properties and sensitivity to IHE, must be demonstrated for each lot of test specimens as per the requirements in ASTM F1940 or F519. A *lot* consists of only those specimens cut from the same heat of steel in the same orientation, heat treated together in the same furnace, quenched and tempered together,

and subjected to the same manufacturing processes. Sensitivity testing must be performed on every lot prior to its sale by the manufacturer.

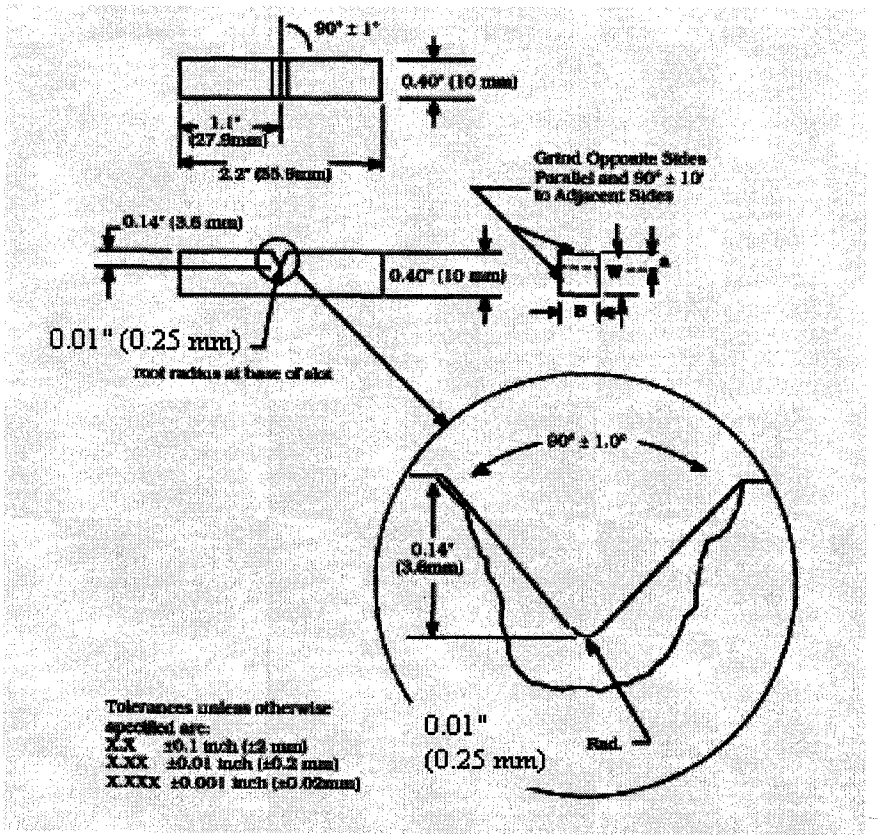

Figure 3.4. Dimensional specifications of ASTM F519 (type 1e) single notch bend square bar.[47]

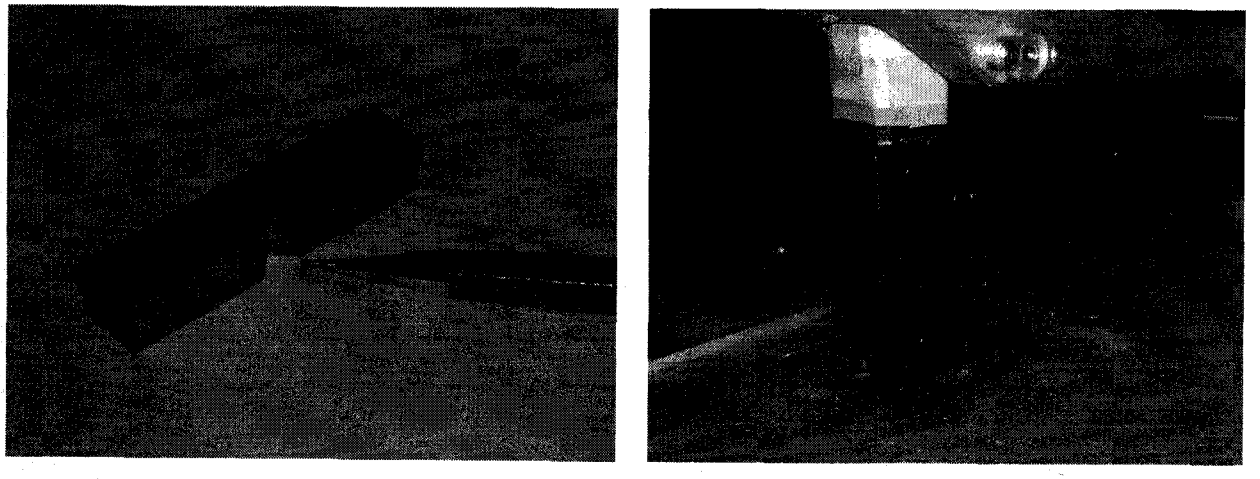

Figure 3.5. ASTM F519 (type 1e) single notch bend square bar. Right hand image shows the specimen mounted in the test fixtures.

3.3.2 Supplier certification and properties

For this study 285 specimens of a single lot (identified as S2) were purchased from Green Specialty Services in Fort Worth, Texas, in April, 2006. Certification was supplied by the vendor indicating compliance with all specified requirements. The chemical composition, heat treatment and final mechanical properties for the S2 lot of test specimens are as follows:

Table 3.2. Chemical composition of lot S2 test specimens.

	Weight %	
	Actual	**AISI 4340 requirements**
Carbon	0.40	0.38-0.43
Manganese	0.78	0.65-0.85
Phosphorus	0.007	0.025 max.
Sulfur	0.030	0.025 max.
Silicon	0.22	0.15-0.30
Copper	0.18	-
Nickel	1.72	1.65-2.00
Chromium	0.82	0.70-0.90
Molybdenum	0.28	0.20-0.30
Aluminium	0.016	-
Vanadium	0.001	-

Heat treatment:

- Preheated at 538 °C for 2 hours
- Austenitised at 816 °C for 45 minutes at temperature
- Quenched in oil at 70 °C
- Air tempered at 246 °C for 2 hours at temperature followed by air cooling
- Second air tempered at 266 °C for 2 hours at temperature followed by air cooling

Manufacturer certified average surface hardness: 51.4 HRC

Baseline load measurements:

Baseline loads were established by two methods: (i) fast fracture (FF) mode and, (ii) incremental step load mode. Fast fracture testing was performed at a continuous loading rate of 445 N/min (100 lb/min). Incremental step load testing was performed in accordance with the loading protocol in Table 3.1. All percent notch fracture strength ($NFS_{\%}$) results presented in this work were calculated using the ISL baseline instead of the FF baseline in the denominator of equation 21 (sect. 2.6). The former is generally considered a more valid baseline because it is derived using the same loading method as that of the actual test. For high hardness materials, such as the test specimens used in this work, the ISL baseline is typically 10% lower than the FF baseline. This difference is thought to be a manifestation of embrittlement caused by residual hydrogen already present in the pristine test specimens.

Baselines were established independently for each of the two RSL test frames. All the results were calculated using the baseline ISL fracture strength corresponding to the test frame in which the test was conducted.

Table 3.3. ***Fast fracture*** baseline – specimen lot S2.

	Fast fracture **load of pristine specimens** $NFS_{(B)FF}$		
	Avg.*	**Std. dev.**	**Percent std. dev.**
Unit 1	949 N (213.24 lb)	12.9 N (2.91 lb)	1.36
Unit 2	962 N (216.34 lb)	14.9 N (3.34 lb)	1.54

Note: five specimens were tested per condition.

Table 3.4. ***ISL*** baseline – specimen lot S2.

	ISL **fracture load of pristine specimens** $FS_{(B)F1940}$		
	Avg.*	**Std. dev.**	**Percent std. dev.**
Unit 1	838 N (188.46 lb)	19.6 N (4.2 lb)	2.23
Unit 2	881 N (198.08 lb)	13.4 N (3.02 lb)	1.52

Note: five specimens were tested per condition.

3.4 COATING PROCESS SAMPLING

The coating processes sampled in this study were classified under three categories: (i) electroplated coatings, (ii) non electrolytic coatings, and (iii) thermal diffusion coatings, specifically hot dip zinc (galvanising).

3.4.1 Electroplating processes

Electroplating is the most important and largest coating process category in the scope of this work. Electroplated coatings are very common to fasteners, and are routinely specified for high strength fasteners. Electroplating is also the most complex category to evaluate for several reasons. There are many varieties of electroplated coatings ranging from single element coatings such as zinc and cadmium, to alloy coatings such as zinc-nickel, zinc-cobalt, and zinc-iron. The method of coating can vary between *direct current plating* which is most common, and alternating current *pulse plating* which is growing in use. There also exists a panoply of proprietary bath chemistries combined with innumerable electroplating cells varying in configuration and size. The manner in which parts are handled can also vary. Fasteners are most often

coated in bulk "barrel" processes. However, larger bolts in particular are often coated in "rack" processes to minimise thread damage that can otherwise occur during tumbling in a barrel.

The great many permutations of processes and processing methods make an exhaustive sampling impractical. Instead, a number of electroplating processes were selected for evaluation, based either on their prevalence in the fastener industry, or on their relevance to high strength fasteners. The list of selected electroplating processes is given in Table 3.5.

Table 3.5. List of sampled electroplating processes

Zn – acid chloride – barrel
Zn – alkaline (non cyanide) – barrel

Zn/Ni – acid chloride – barrel
Zn/Ni – alkaline (non cyanide) – barrel
Zn/Ni – alkaline (non cyanide) – rack

Zn/Fe – alkaline (non cyanide) – barrel

Cadmium – cyanide – rack

As was described in section 2.3.2, electroplating generates hydrogen that adsorbs onto the cathode (bolt) surface. In theory, the amount of hydrogen generated depends on the cathode efficiency of the plating bath, the plating current density, and the plating time. The amount of hydrogen actually *absorbed* by the bolt also depends upon the permeability of the coating as it begins to build up on the surface of the bolt during plating. The ease with which hydrogen can effuse or escape from a coated bolt, either by baking or at room temperature, is a function of both the permeability and final thickness of the coating.

The method of surface preparation can also have a significant impact on the amount of hydrogen that is absorbed. Acid pickling in particular used for the removal of oxide scale will generate hydrogen on the surface of the bolt by the mechanism described in section 2.3.1. The type of acid, its concentration and temperature, and the residence time in the acid will influence the kinetics of oxidation, and therefore, the quantity of hydrogen generated. For this reason, a growing number of processes utilise mechanical descaling methods such as grit blasting instead of acid pickling for coating high strength fasteners.

In light of the immense number of variables at play, the electroplating process was reduced to its basic components in order to normalise the test data and facilitate the interpretation of results. More precisely, the F1940 sampling conditions were designed to make a first attempt at assessing the relative effect of the following of three factor groups: (i) electrochemical parameters (i.e., cathode efficiency, current density, and plating time), (ii) surface preparation methods (i.e., type, concentration and temperature of pickling acid), and (iii) coating material permeability (ease of hydrogen effusion, either at room temperature or through baking).

In terms of the sampling methodology, this meant separating the plating process from any chemical surface preparation steps that preceded it (i.e., alkaline degreasing and acid pickling). This was done by sampling two primary conditions: (i) the "full process," which included acid pickling when applicable to the process, and (ii) electroplating alone, without any surface preparation. The proper adherence of the coating in the latter case was not a concern because the test specimens were already clear of surface oxides. Consequently, for sampling plating processes alone, the test specimens only required

removal of the protective oil by immersion in acetone, followed by surface activation in *very dilute* hydrochloric acid (~1-3 % v/v) for no more than 10 seconds. If the process normally included a post bake for hydrogen relief, an additional distinction was made by sampling the process *with* and *without* baking.

Additionally, in order to examine the effect of acid pickling in the absence of a subsequent coating, a number of samples were generated in the laboratory by dipping the test specimens in hydrochloric acid at various immersion times and concentrations. The specimens were either tested immediately after exposure, or after fixed waiting periods. This test procedure was designed to validate the theory regarding the barrier effect of metallic coatings.

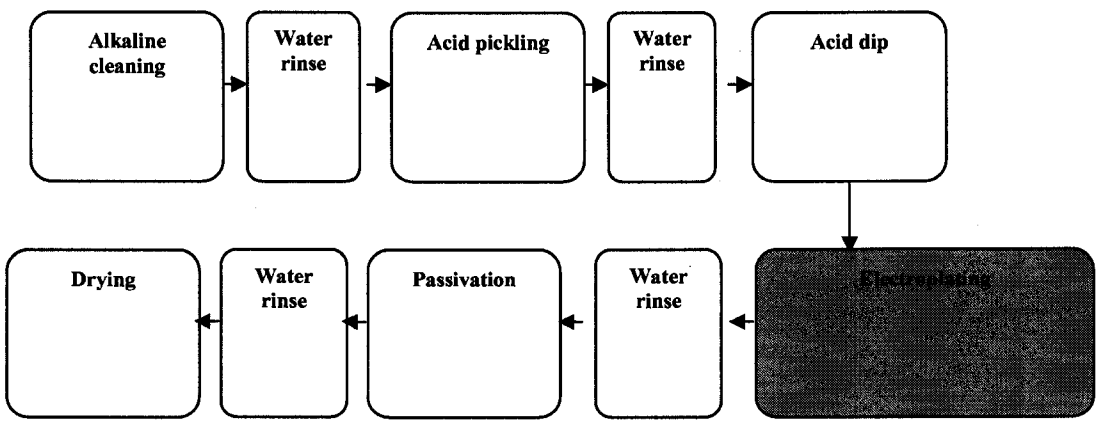

Figure 3.6. Generic electroplating processing steps – barrel.

3.4.2 Non electrolytic processes

Non electrolytic processes have the common benefit of offering coating mechanisms that are recognised as being "hydrogen free." This benefit is particularly

attractive for coating high strength fasteners. The reasons for this common benefit are different for each process. Just as with electroplating, the method of surface preparation is an important consideration for minimising exposure to hydrogen. In some cases such as with DACROMET®, which is a proprietary Zn/Al organic emulsion coating, acid pickling is forbidden by the licensor of the product. In other cases such as with phosphate coatings, acid pickling is often used, yet it is the porosity of the coating that allows hydrogen to naturally effuse at room temperature.

Four types of non electrolytic processes were selected for evaluation, based on their prevalence in the fastener industry. The list of selected processes is given in Table 3.6. The sampling methodologies specific to each process follow.

Table 3.6. List of sampled non electrolytic processes

Mechanical zinc – bulk drum
Zn phosphate – barrel
Dacromet® – bulk dip spin
Magni 555® – bulk dip spin

Mechanical zinc

Sampling methodology consisted of sampling the "full process" condition which included light acid pickling. It was not necessary to separate surface preparation from the coating step. The rationale for this procedure was based on the anticipated effusion of hydrogen at room temperature, because the porous coating should not block hydrogen escaping. Consequently, the source of hydrogen is less relevant. The process did not include a post bake for hydrogen relief.

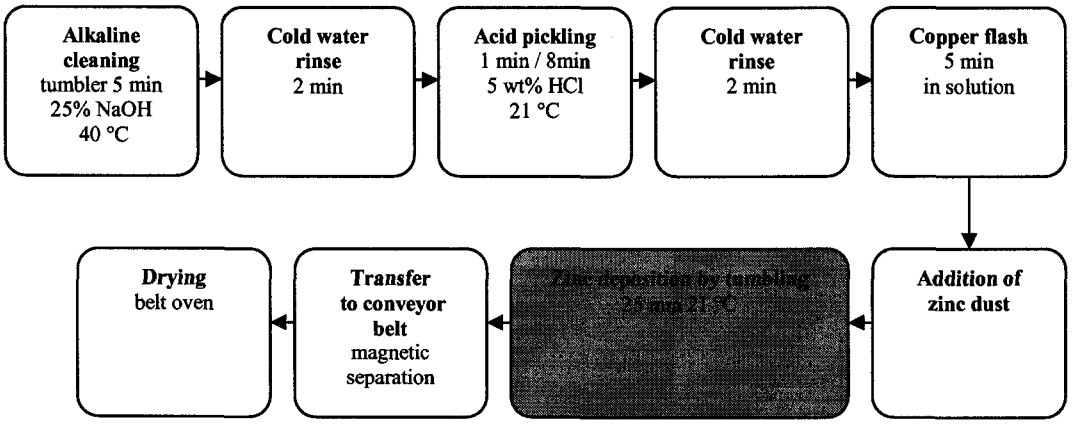

Figure 3.7. Mechanical galvanising processing steps – tumbler system. Target coating thickness of 60 μm.

Zinc phosphate

Sampling methodology consisted of sampling the "full process" condition which included acid pickling. It was not necessary to separate surface preparation from phosphating. Similar to mechanical zinc, the same rationale applied because room temperature effusion of hydrogen through the porous coating was anticipated, making the source of hydrogen less relevant. The process did not include a post bake for hydrogen relief.

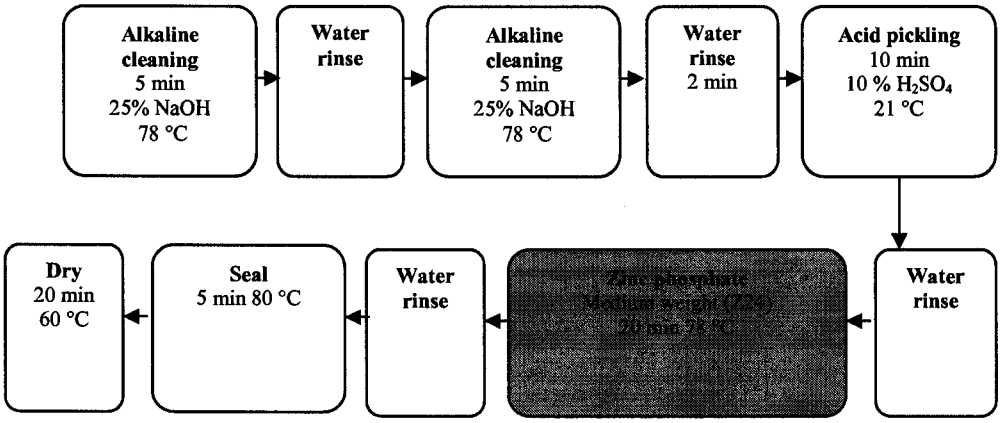

Figure 3.8. Zinc phosphate processing steps – barrel.

DACROMET®

Sampling methodology consisted of introducing the test specimens only after surface preparation for the following two reasons: (i) acid pickling was not allowed in the process, and (ii) grit blasting might have introduced compressive stresses into the test specimens, which would have changed their hydrogen sensitivity. Note that because the curing temperatures exceeded the tempering temperature of the F519-1e specimens, hardness after coating was measured.

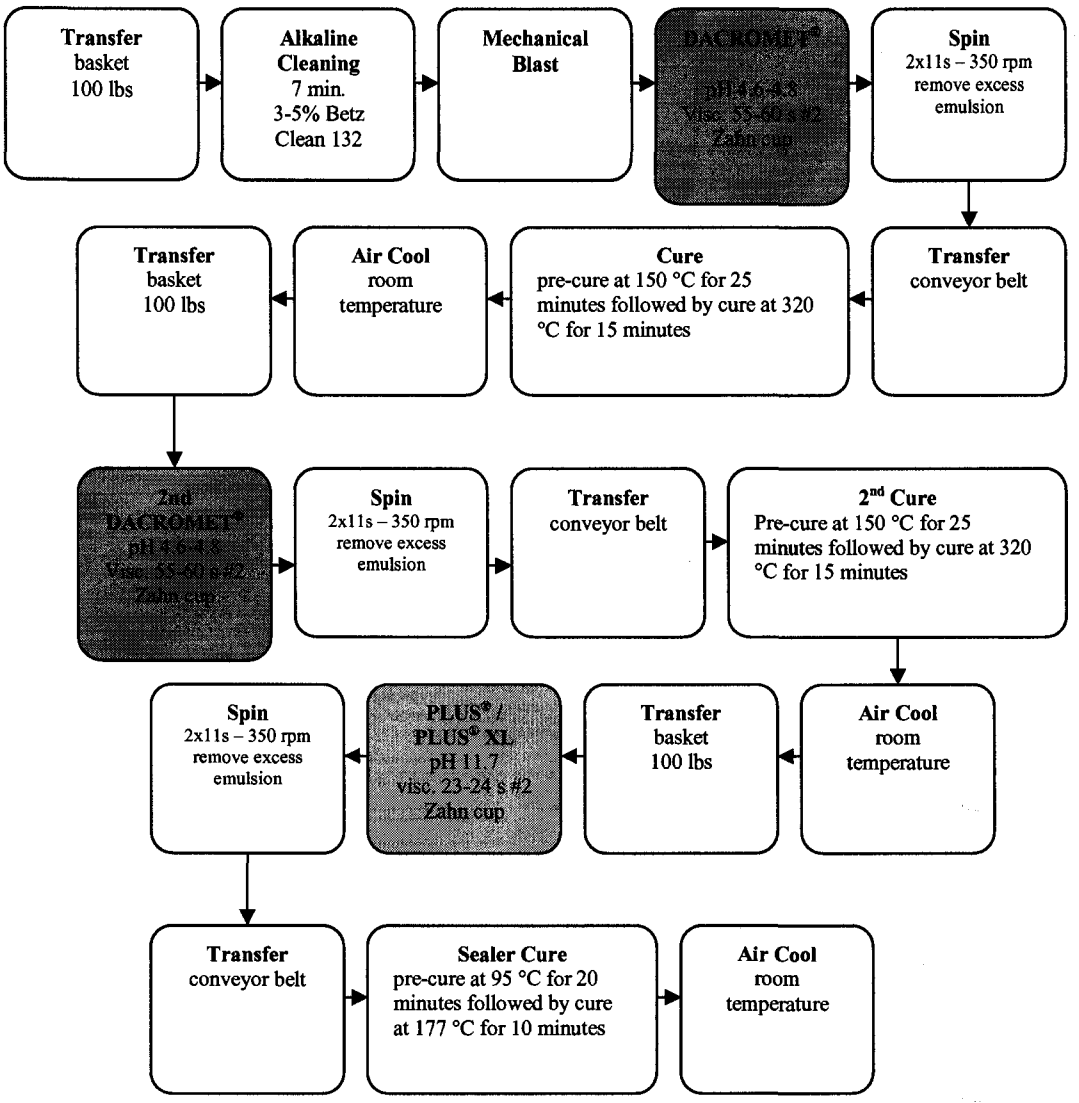

Figure 3.9. DACROMET® processing steps – applied by dip-spin in two basecoats plus one topcoat. Target coating thickness of 8 μm.

Magni 555®

Sampling methodology consisted of sampling the "full process" condition which included surface preparation by alkaline degreasing, acid pickling, and zinc phosphating. Although the curing temperatures were lower than those for DACROMET®, they still exceeded the tempering temperature of the F519-1e specimens. Similarly, hardness after

coating was measured to correlate any drop in hardness with a proportional drop in ISL fracture strength.

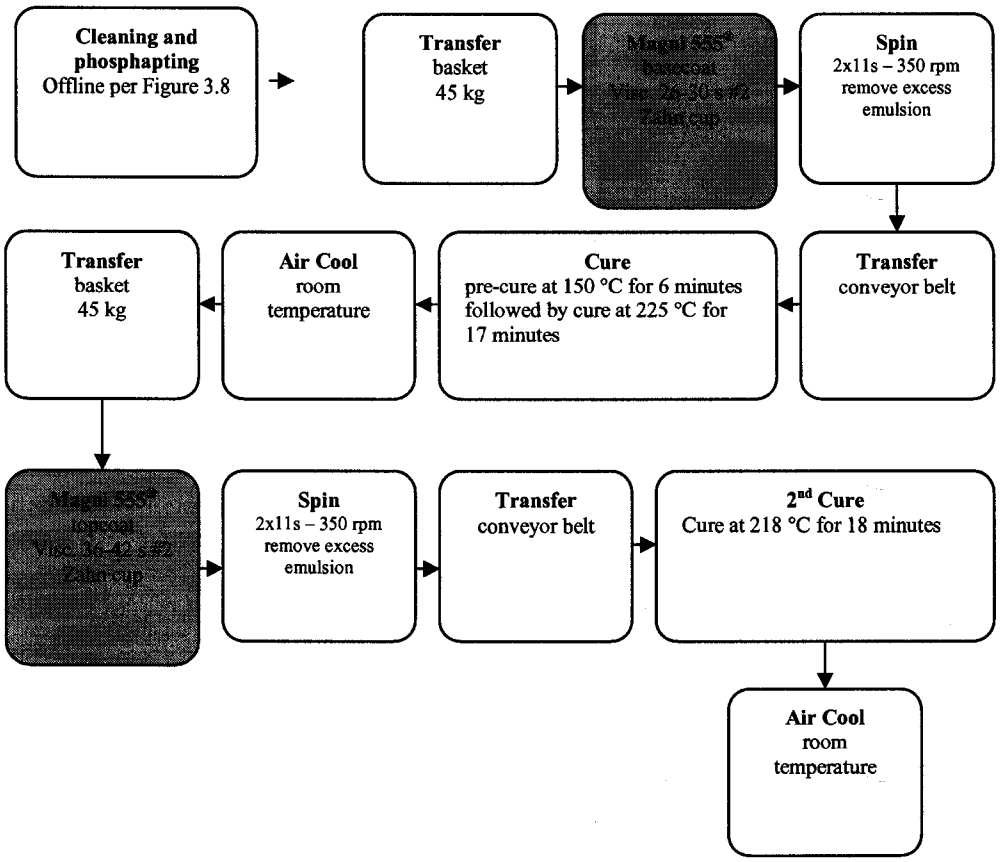

Figure 3.10. Magni 555® processing steps - applied by dip-spin in two coats. Target coating thickness of 8 μm.

3.4.3 Hot dip zinc (galvanising)

As was stated earlier, the incremental step load methodology in ASTM F1940 is designed to correlate the quantity of residual hydrogen retained in a standard test specimen (after coating) to a reduction of its fracture strength. Any alteration of specimen properties by phenomena other than hydrogen absorption would constitute a deviation from the standard conditions prescribed, and would have an unknown effect on test

results. It also follows that results obtained in such a scenario could not be interpreted within the parameters defined in the standard. The initial objective of including the hot dip zinc process in this work was to determine if and how ASTM F1940 could be applied to the process. Hot dip galvanising can modify the specimen properties in two ways. First, by exposure to heat at 450 °C; this far exceeds the temperature at which the specimens are tempered, constituting a de facto change of specimen material. Second, because zinc diffuses into the surface of the steel specimen, a localised impact on the sensitivity of the notch may occur.

In order to determine the applicability of ASTM F1940 to hot dip galvanising, an *initial* sampling event was designed to isolate process components such as acid pickling, fluxing, and hot dipping. Three primary conditions were sampled: (i) the "full process," which included acid pickling and flux solution, (ii) flux solution without prior pickling, followed by galvanising, and (iii) galvanising alone without any surface preparation or flux solution. For conditions (ii) and (iii), the protective oil was removed by prior immersion of the specimens in acetone. Proper coating adherence was not a concern because the test specimens were already clear of surface oxides. A fourth condition was generated by exposing test specimens for 7 minutes at 450 °C in a conventional furnace in air. This is approximately double the time in the molten zinc bath. Subsequent sampling events were performed to test hypotheses proposed to explain the results obtained from the first sampling event. Subsequent sampling conditions will be described in section 4.3, of the Results chapter.

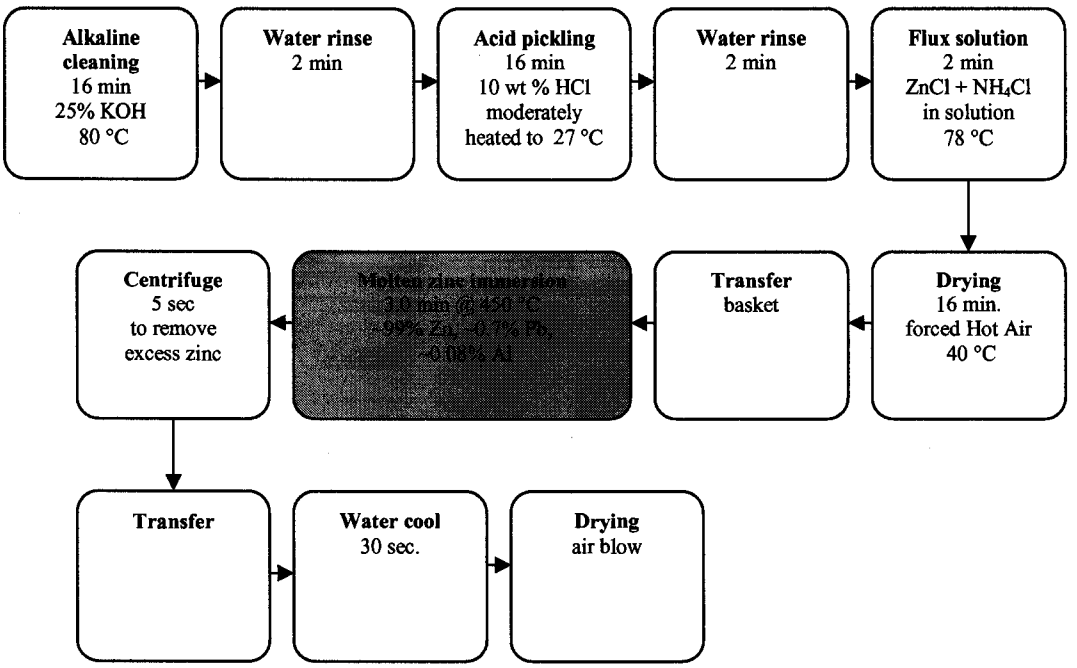

Figure 3.11. Hot-dip zinc processing steps – applied by dip spin. Target coating thickness of 60 μm.

3.5 ANALYTICAL TECHNIQUES

A number of specimens were examined by a series of test methods to supplement and interpret ISL test results. The following is the list of analyses performed, followed by brief descriptions of the methodologies adopted for each test.

3.5.1 Coating thickness measurement

Coating thickness for the electroplated processes was measured using a CMI eddy current thickness tester. Hot dip, mechanical zinc and other coatings that exceed 20 μm in thickness were measured using a Fisherscope MMS magnetic induction tester.

3.5.2 Rockwell hardness testing (C scale)

In preparation for hardness testing, specimens with a zinc coating were immersed in 25% v/v hydrochloric acid to dissolve the zinc. Following the complete dissolution of the coating, the specimens were rinsed, dried and buffed using 600 grit SiC paper. Coatings that did not readily dissolve in hydrochloric acid were mechanically removed using 240 to 600 grit SiC paper. Hardness was measured on the surface of the fractured half specimens using the Rockwell C scale at the specified test force of 150 Kg.

3.5.3 Vickers macro and micro-hardness testing

Core hardness was measured on mounted specimens prior to etching using both macro and micro-Vickers hardness testers. A test force of 5 Kg was used for macro-Vickers testing. A test force of 50 g was used for micro-Vickers testing.

3.5.4 Microstructure

Specimens were sectioned in half using a diamond saw and mounted in Bakelite. An automatic polisher was used to grind the samples respectively with 120, 240, 320, 400 and 600 grit SiC paper. The mounts were then polished respectively with 9μm, 3μm and 1μm diamond suspension. Finally the mounts were etched using 3% Nital solution. The microstructures were examined using a CLEMEX optical metallograph and recorded as digital photo-micrographs.

3.5.5 Fractography

A JEOL JSM-840A scanning electron microscope (SEM) was used to perform the fractographic analysis. Clear topographical images of the specimen fracture surfaces were generated at 2000X and 15KV with secondary electrons (SE) collected by an Everhart-

Thornley (E-T) detector. The working distance (WD) was set to 38 mm and the aperture selector set to 3. The entire fracture surfaces of selected specimens were observed, mapped and digitally recorded.

CHAPTER 4: RESULTS

The results of this investigation are presented by coating category: (i) electroplating processes, (ii) non electrolytic processes, and (iii) hot dip zinc, which falls under the category of thermal diffusion processes. The results of each category will be presented and discussed separately.

For each coating category, the ISL results are organised in the first order by process codes that are unique to each sampling event (e.g., P1). The process code identifies the coating process, the sampling conditions and the process parameters at the time of sampling. The process code is unique, meaning that the *same process* sampled twice under the *same conditions*, but at *different times* is attributed a different (*unique*) process code. This approach is adopted because it cannot be assumed that process parameters and processing conditions were exactly duplicated from one sampling event to the next. In the second order, the results are organised in *groups* based on defined variable(s) that correspond to a specific theme of interest.

The test results are presented as bar charts summarising the data by process code (e.g., P1). As a rule, each coded condition comprised five test specimens. The individual bars show the *average* percent notch fracture strength ($NFS_{\%}$), the *standard deviation*, and *minimum/maximum* values. The numerical data are presented below each bar. When appropriate, additional results obtained from analytical tests are also presented to supplement the ISL results (e.g., hardness, metallography, fractography). Process

descriptions and conditions for each sampling event are given in detail by order of process code in Appendix A.

As a final note, hydrochloric acid concentrations are given in weight percent to avoid confusion regarding dilution ratios. The highest concentration at which hydrochloric acid can be commercially obtained is 38 wt%. Therefore, for example, an acid concentration of 19 wt% corresponds to 50% v/v dilution of concentrated acid.

4.1 ELECTROPLATING PROCESSES

4.1.1 Zinc – acid chloride

Zinc acid chloride processes were sampled at three different suppliers having *barrel* processes. The data are divided into five groups: Groups 1 and 2 were sampled at Supplier A, Groups 3 and 4 at Supplier B, and Group 5 at Supplier C. Results are shown in Figure 4.1.

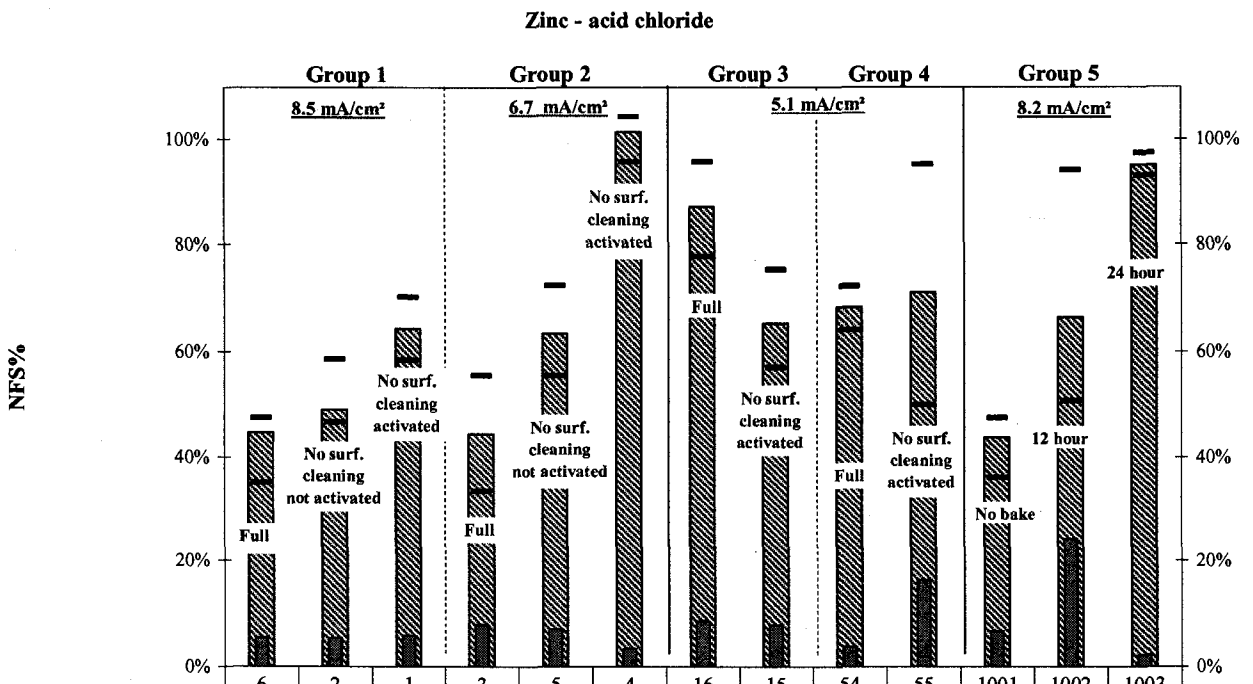

	6	2	1	3	5	4	16	15	54	55	1001	1002	1003
Average	44.7%	49.1%	64.2%	44.5%	63.3%	101.3%	87.0%	65.2%	68.1%	70.9%	43.8%	66.2%	95.0%
Standard deviation	5.42%	5.26%	5.81%	7.85%	6.97%	3.33%	8.54%	7.75%	3.69%	16.22%	6.69%	24.07%	2.17%
Minimum	35.0%	46.7%	58.4%	33.3%	55.5%	95.6%	77.7%	57.1%	64.0%	50.1%	36.0%	50.8%	92.9%
Maximum	47.6%	58.5%	70.0%	55.5%	72.2%	104.3%	95.6%	75.2%	72.1%	95.1%	47.6%	93.9%	97.2%

Figure 4.1. Zinc – acid chloride, percent fracture strength ($NFS_{\%}$) by process condition.

In Group 1, three conditions were sampled: (i) "full process" (P6) which included alkaline degreasing and pickling in hydrochloric acid at 13 wt% for 14 minutes, (ii) "no surface cleaning – not activated" (P2) which consisted of exposing the specimens only to the electroplating step, and (iii) "no surface cleaning – activated" (P1) which was the same as the previous condition, except that the specimen surfaces were activated manually in dilute hydrochloric acid for 30 seconds prior to electroplating. As expected, the "full process" resulted in the lowest $NFS_{\%}$ average at 44.7%. This is explained by the fact that the specimens were exposed to hydrogen both from pickling and electroplating. The elimination of pickling in conditions P2 and P1 resulted in notable improvements, up to 49.1% and 64.2% respectively. It is interesting to note that surface activation resulted

in the least amount of embrittlement. It is conceivable that surface activation leads to a more permeable coating morphology that offers hydrogen an easier escape path.

Group 2 consists of a repetition of the same conditions on the same plating line as Group 1, but several weeks later. These were the only sampling events where the effect of surface activation was tested. The average current density was 6.7 mA/cm^2 as compared to 8.5 mA/cm^2 for Group 1. This difference was due to the smaller size of production parts being plated. The trends in Group 1 are also observed in Group 2, where in addition, the lower current density seemed to result in decreased embrittlement of the specimens that were not pickled. In fact for the condition "no surface cleaning – activated" (P4), no loss in fracture strength was detected. This observation might be explained by the fact that electrolytic hydrogen generation decreases with current density. For both groups, the same $NFS_{\%}$ values were obtained for the "full process" conditions P6 and P3. Evidently, the hydrogen contribution from acid pickling negated the improvement from the lower current density in Group 2.

Group 3 consists of two conditions: (i) "full process" (P16) which included alkaline degreasing and pickling in hydrochloric acid at 7.6 wt% for 8 minutes and (ii) "no surface cleaning – activated" (P15). Both conditions were plated at a current density of 5.1 mA/cm^2. In this group, the full process P16 resulted in a $NFS_{\%}$ average of 87.0%, which was unexpectedly higher than the 65.2% obtained for P15.

Because this result is contrary to the expected trend, the same plating line was sampled again under the same conditions, identified as P54 and P55. The results are presented as Group 4, where "full process" (P54) included alkaline degreasing and pickling in hydrochloric acid at 8.0 wt% for 7 minutes. Both conditions were plated at a

current density of 5.1 mA/cm^2, the same as for Group 3. This time, the "full process" (P54) resulted in a $NFS_{\%}$ average of 68.1%. This result was slightly lower than for P55 at 70.9%. However, the difference of 2.8% between the two conditions is statistically insignificant. Evidently, for the process sampled in Groups 3 and 4 the effect of acid pickling was negligible in comparison to the hydrogen contribution from electroplating.

Group 5 consists of an attempt to assess the impact of baking time on embrittlement. Three conditions were sampled: (i) "full process without baking" (P1001) which included alkaline degreasing and pickling in hydrochloric acid at 13 wt% for 10 minutes, (ii) "full process followed by a 12 hour bake at 204 °C" (P1002), and (iii) "full process followed by a 24 hour bake at 204 °C" (P1003). The current density for Group 5 was 8.2 mA/cm^2. The first observation is that "full process without baking" (P1001 resulted in the similar $NFS_{\%}$ values (~44%) as in the previous groups. This seems to indicate that the zinc acid chloride process is generally a high risk process. The second observation is that the average $NFS_{\%}$ value after 12 hours of baking had increased to 66.2%. The large data scatter for this condition (43 percentage points) can be explained by the fact that in this region, small changes in hydrogen concentration can result in large changes of $NFS_{\%}$. This concept will be developed later in the discussion section. Finally, the average $NFS_{\%}$ value after 24 hours of baking had increased to 95%, meaning that ductility had been fully restored. This finding is encouraging as it validates the theory regarding the *reversibility* of IHE. On the other hand, full recovery required 24 hours of baking time, which is six times greater than the 4 hour baking time specified in most industry standards. It must be emphasised that these observations are limited to the acid chloride zinc plating process.

4.1.2 Zinc – alkaline non cyanide

One alkaline non cyanide zinc *barrel* process was sampled under two conditions: (i) "full process" (P10) which included alkaline degreasing and pickling in hydrochloric acid at 13 wt% for 7 minutes, and (ii) "no surface cleaning – activated" (P9) which is the same as the previous condition, except that the specimen surfaces were activated manually in dilute hydrochloric acid for 30 seconds prior to electroplating. In both cases the plating time was 120 minutes. Current densities were 7.5 mA/cm^2 for P10 and 8.1 mA/cm^2 for P9. Results are shown in Figure 4.2.

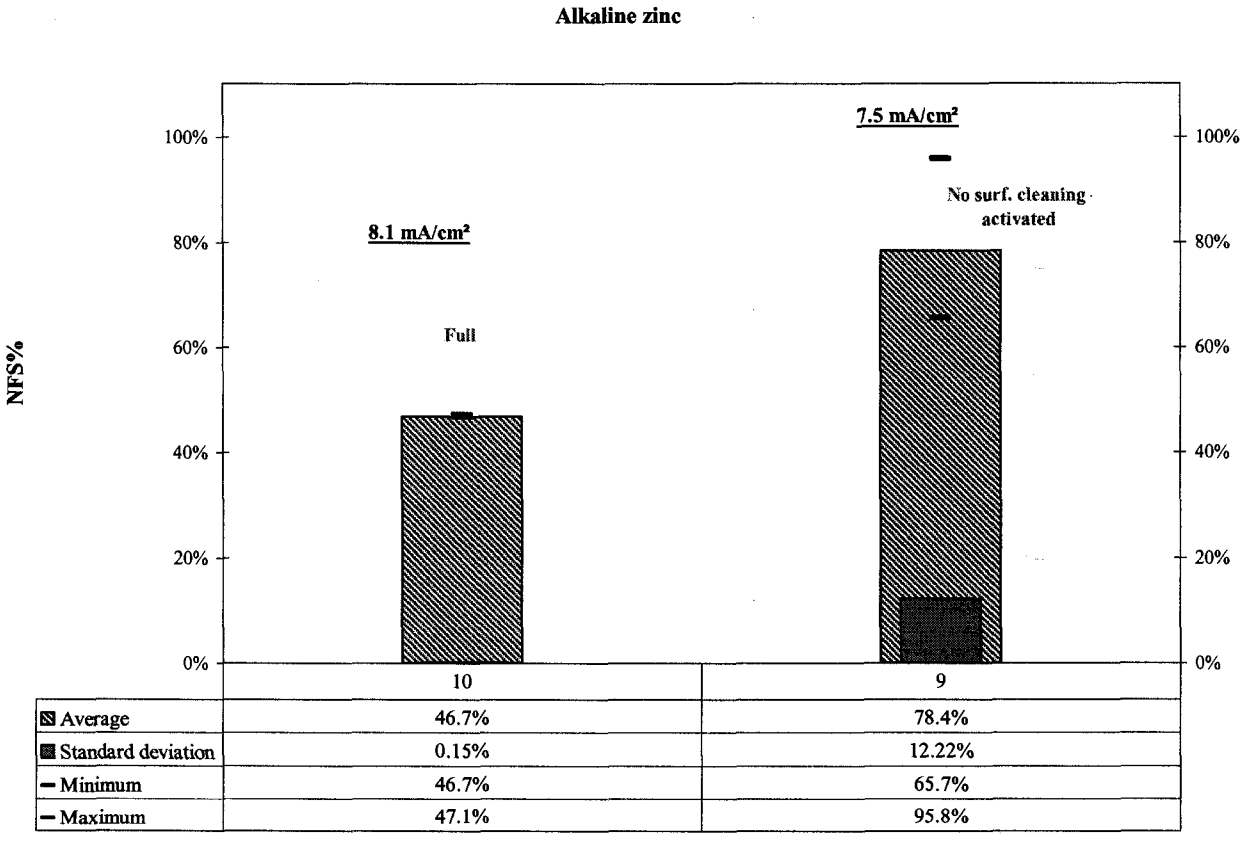

Figure 4.2. Zinc – alkaline non cyanide, percent fracture strength ($NFS_{\%}$) by process condition.

As was anticipated, the "full process" (P10) resulted in lower $NFS_{\%}$ values, with an average of 47.7% as compared to 78.4% for P9. Again, this can be attributed to the hydrogen contribution of acid pickling. When comparing P9 to the acid chloride process in P1, both of which do not include pickling, it is interesting to note at roughly the same current density but twice the plating time, the alkaline zinc process still yielded higher $NFS_{\%}$ values, with an average of 78.4% as compared to 64.2% for P1. This seems to indicate that alkaline non cyanide zinc is less embrittling than acid chloride zinc.

4.1.3 Zinc nickel – acid chloride

One acid chloride zinc nickel *barrel* process was sampled under two conditions: (i) "full process" (P12) which included alkaline degreasing and pickling in hydrochloric acid at 17 wt% for 5 minutes, and (ii) "no surface cleaning – activated" (P11) which is the same as the previous condition, except that the specimen surfaces were activated manually in dilute hydrochloric acid for 30 seconds prior to electroplating. Both conditions were plated at 5.2 mA/cm^2 for 60 minutes. Results are shown in Figure 4.3.

Both conditions were found to be non-embrittling with average $NFS_{\%}$ values of 92.1% for P12 and 99.8% for P11. The lower result in the case of P12 can once again be attributed to the hydrogen contribution of acid pickling.

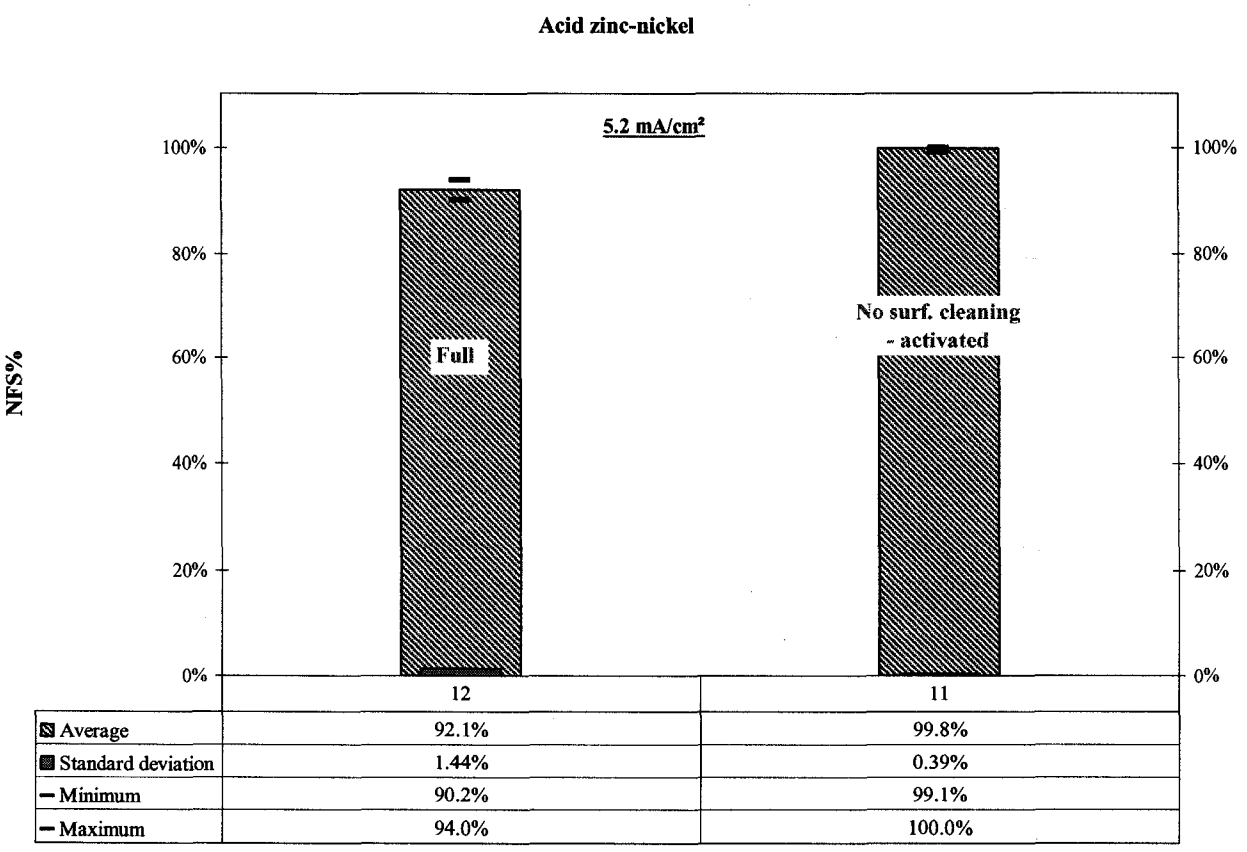

Figure 4.3. Zinc nickel – acid chloride, percent fracture strength ($NFS_{\%}$) by process condition.

4.1.4 Zinc nickel – alkaline non cyanide

Three alkaline zinc nickel processes were sampled as is shown in Figure 4.4. Group 1 was a *barrel* process sampled under two conditions: (i) "full process" (P8) which included alkaline degreasing and pickling in hydrochloric acid at 12 wt% for 10 minutes, and (ii) "no surface cleaning – activated" (P7) which is the same as the previous condition, except that the specimen surfaces were activated manually in dilute hydrochloric acid for 30 seconds prior to electroplating. Both conditions were plated at 5.4 mA/cm^2 for 90 minutes. Both conditions were non-embrittling with average $NFS_{\%}$ values around 100%.

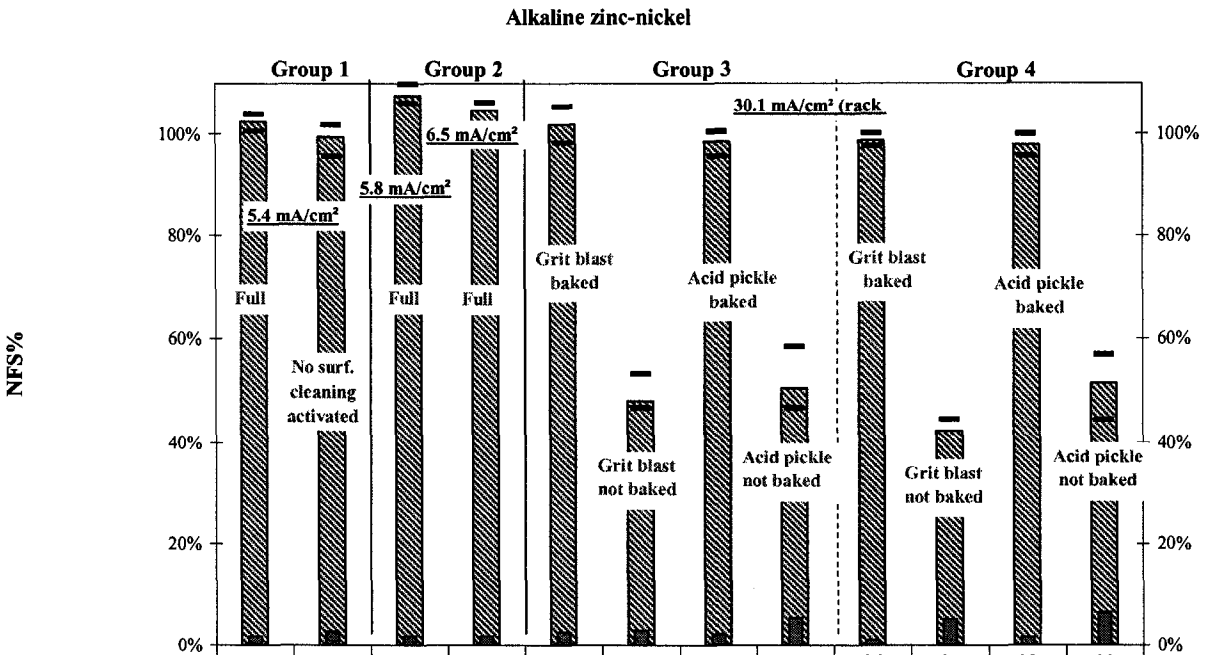

	8	7	52	53	32	33	34	35	36	37	38	39
Average	102.4%	99.3%	107.4%	104.6%	101.7%	48.0%	98.4%	50.4%	98.7%	42.2%	97.7%	51.4%
Standard deviation	1.73%	2.61%	1.69%	1.69%	2.54%	2.87%	2.19%	5.36%	1.04%	4.98%	1.53%	6.35%
Minimum	100.5%	95.6%	106.0%	101.8%	98.2%	46.7%	95.6%	46.7%	97.6%	33.3%	95.6%	44.4%
Maximum	103.9%	101.7%	109.8%	106.1%	105.3%	53.2%	100.4%	58.4%	100.1%	44.5%	99.9%	56.8%

Figure 4.4. Zinc nickel – alkaline non cyanide, percent fracture strength ($NFS_{\%}$) by process condition.

Group 2 was another *barrel* process sampled under two conditions, both classified as "full process" with the following distinction: (i) P52 included pickling in hydrochloric acid at 18.2 wt% for *4 minutes*, and plating current density of 5.8 mA/cm^2, while (ii) P53 comprised pickling in hydrochloric acid at 18.2 wt% for *10 minutes*, and plating current density of 6.5 mA/cm^2. P53 was to be the high risk condition with maximum exposure to acid for this particular process. P53 was also plated at a slighly higher current density than P52. Both conditions were found to be non-embrittling with average $NFS_{\%}$ values in excess of 100%.

Groups 3 and 4 were identical sampling events of a *rack* process under four separate conditions. The conditions were selected to separately test the effects of baking, and mechanical surface preparation (versus acid pickling). The four conditions are as follows: (i) "grit blast – baked" (P32 & P36), (ii) "grit blast – not baked" (P33 & P37), (iii) "acid pickle – baked" (P34 & P38) and, (iv) "acid pickle – not baked" (P35 & P39). Acid pickling was performed in hydrochloric acid at 25 wt% for 3 minutes. Baking was performed at 191 °C for 24 hours. In all cases, the oil on the specimens was removed using a commercial solvent. Also, all the specimens were rack plated at 30.1 mA/cm^2, which is five to six times greater than the plating current density in a typical barrel process.

From the results it can be seen that in the absence of baking this process resulted in significant embrittlement of the specimens with average $NFS_{\%}$ values between 40 and 50%. This is most likely due to the high current density in comparison to Groups 1 and 2. When considering the effect of mechanical surface preparation versus acid pickling, no significant difference was observed in Group 3, with average $NFS_{\%}$ values of 48.0% for P33 and 50.4% for P35. In Group 4, the acid pickled condition P39 had a higher average $NFS_{\%}$ value (51.4%) than the grit blasted condition P37 (42.2%). Due to the relatively high standard deviations, 4.98% and 6.35%, this difference may not be significant. When considering the effect of baking, the results clearly point to full recovery following the *lengthy* baking time of 24 hours with average $NFS_{\%}$ values nearing 100%. Once again, this observation is consistent with the theory of reversibility of IHE.

4.1.5 Zinc iron – alkaline non cyanide – rack

One alkaline non cyanide zinc iron *barrel* process was sampled under two conditions: (i) "full process" (P14) which included alkaline degreasing and pickling in hydrochloric acid at 17 wt% for 5 minutes, and (ii) "no surface cleaning – activated" (P13) which is the same as the previous condition, except that the specimen surfaces were activated manually in dilute hydrochloric acid for 30 seconds prior to electroplating. Results are shown in Figure 4.5.

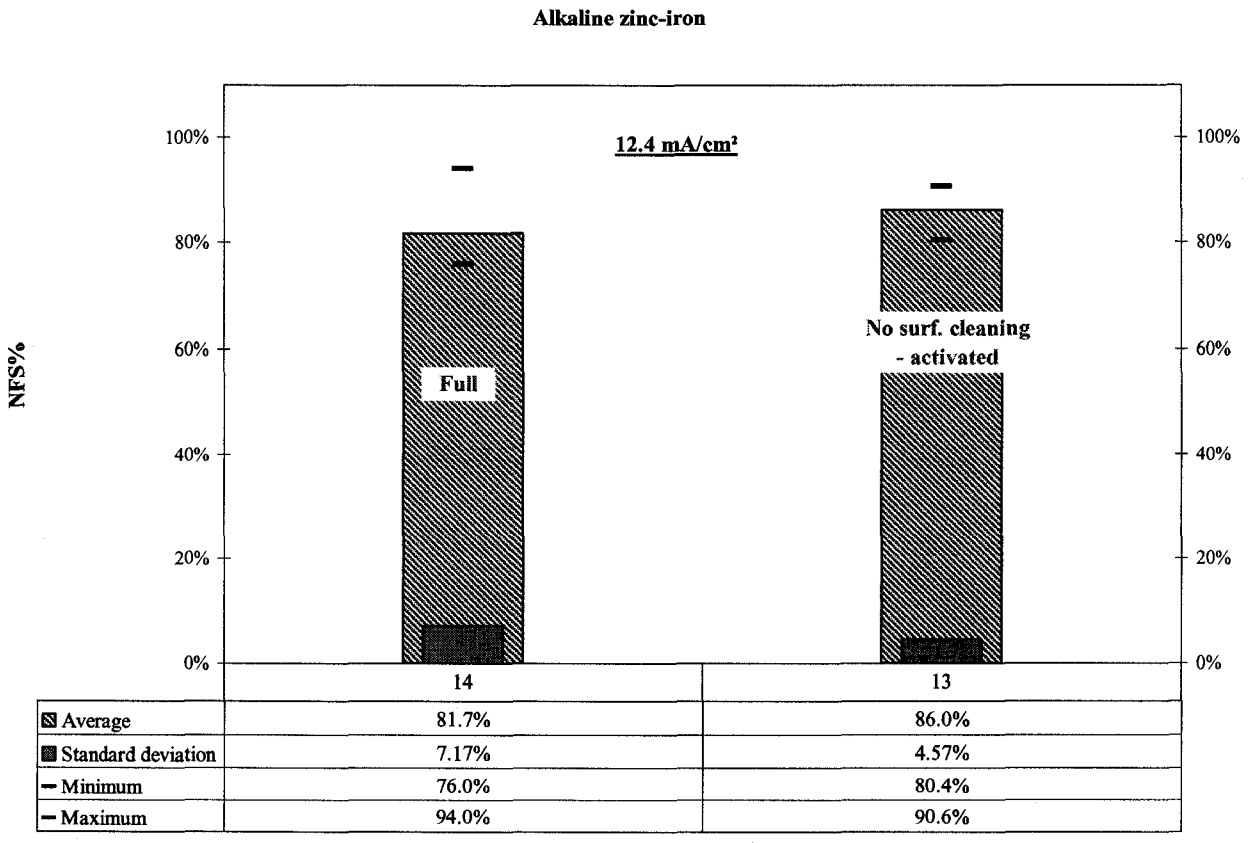

Figure 4.5. Zinc iron – alkaline non cyanide, percent fracture strength ($NFS_{\%}$) by process condition.

Both conditions were plated at a current density of 12.4 mA/cm^2 for 50 to 55 minutes. Both conditions were found to be moderately embrittling with average $NFS_{\%}$ values of 81.7% for P14 and 86.0% for P13. The slightly lower result in the case of P14 may be attributed to the hydrogen contribution of acid pickling. However, considering the standard deviations in the order of 5 to 7%, this difference may not be statistically significant.

4.1.6 Cadmium – cyanide

One bright cyanide cadmium *rack* process was sampled under two conditions: (i) "not baked" (P41) which comprised alkaline degreasing, no pickling, and manual activation in dilute hydrochloric acid for 30 seconds prior to electroplating, and (ii) "baked" (P41) which is the same as the previous condition, except that the specimen was baked at 204 °C for 4 hours. Both conditions were plated in two phases, first a *strike* at 86.1 mA/cm^2 current density for 45 seconds, followed by *plating* at 21.5 mA/cm^2 current density for 20 minutes, both in the same bath. The initial high current density strike prior to plating is an industrial practice designed to minimise hydrogen penetration by rapidly creating a barrier on the surface of the workpiece before starting the actual plating process. Results are shown in Figure 4.6.

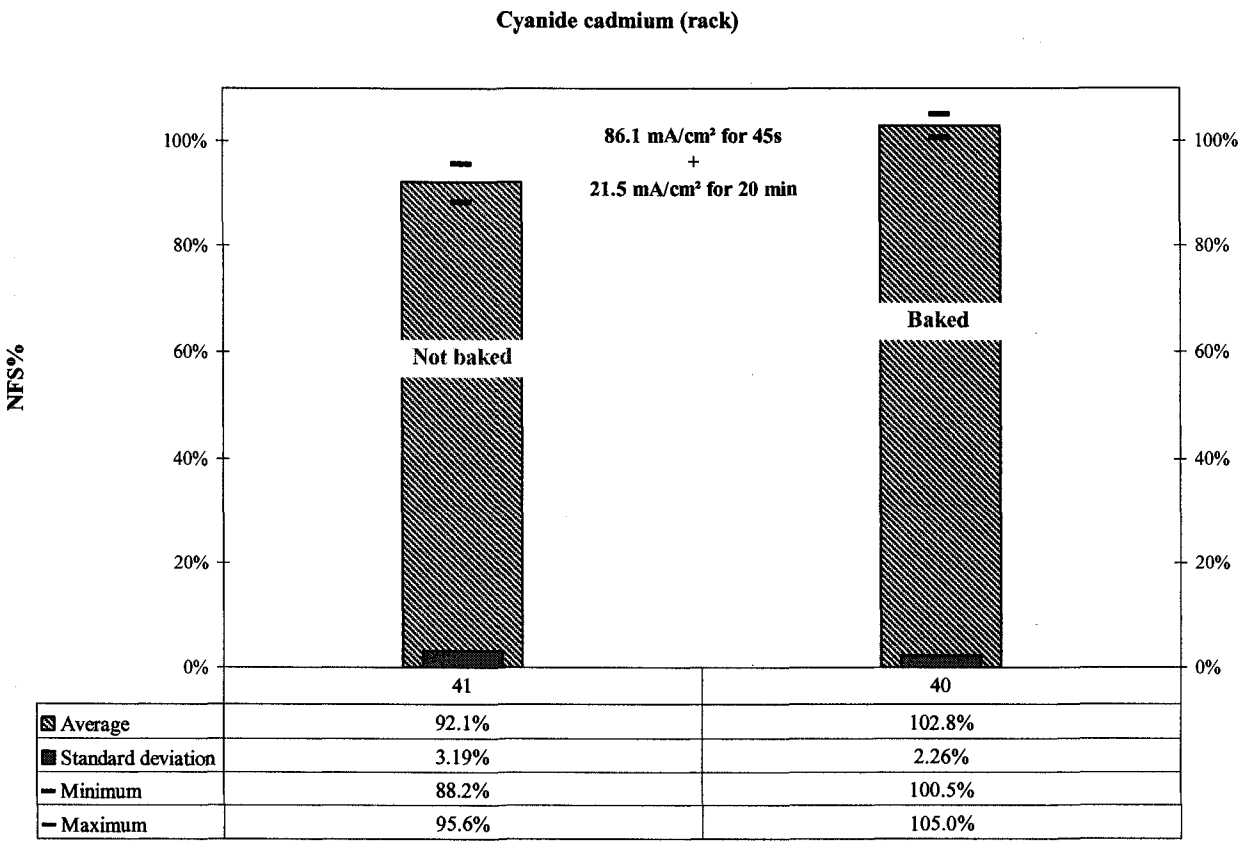

Figure 4.6. Cadmium – bright cyanide, percent fracture strength ($NFS_{\%}$) by process condition.

The un-baked condition P41 resulted in an average $NFS_{\%}$ value of 92.1%, which is considered non-embrittled by the ASTM F1940 standard. This result may have been achieved thanks to the initial high current density strike, although this hypothesis must be validated by testing the same condition with and without the strike. The addition of baking in P40 increased the average $NFS_{\%}$ value to 102.8%, signifying full recovery after only four hours baking time.

4.1.7 Acid dip – laboratory

The data generated by the acid dip process are shown in Figure 4.7.

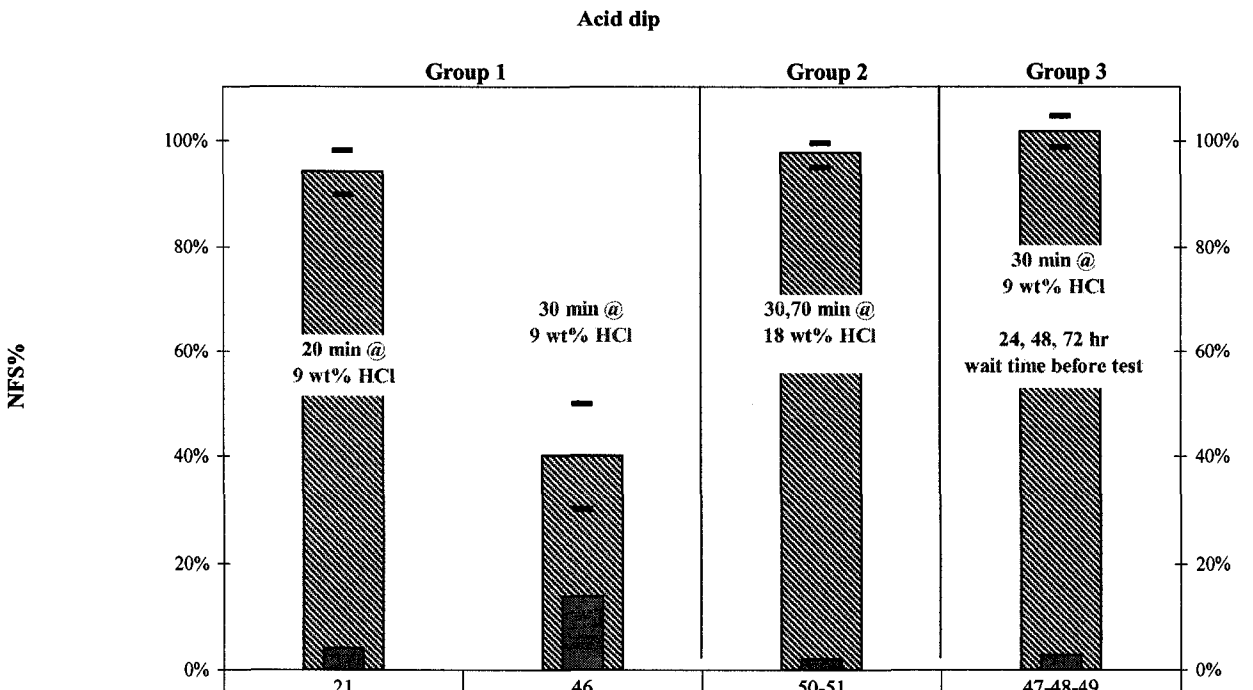

	21	46	50-51	47-48-49
Average	94.2%	40.1%	97.7%	101.7%
Standard deviation	4.22%	14.10%	2.06%	2.88%
Minimum	89.8%	30.1%	95.0%	98.8%
Maximum	98.2%	50.0%	99.6%	104.5%

Figure 4.7. Acip dip, percent fracture strength ($NFS_{\%}$) by process condition.

The conditions for acid dipping are divided into three groups designed to illustrate the effect of *immersion time*, *concentration* and *time before testing*. Group 1 comprised two conditions: immersion in 9 wt% HCl for (i) 20 minutes (P21), and (ii) 30 minutes (P46). P21 was found not to be non-embrittling, yet P46 yielded an average $NFS_{\%}$ value of 40.1%. It seemed improbable that the additional 10 minutes of immersion for P46 could have caused such a sharp drop in fracture strength, so additional conditions were generated to verify this result. Conditions for Group 2 consisted of: immersion in 18 wt%

HCl for (i) 30 minutes, and (ii) 70 minutes. Both conditions are represented in the same bar. The doubling of both immersion time and acid concentration from Group 1 was designed to generate an extreme case of acid exposure, yet the average $NFS_{\%}$ value obtained was 97.7%. In Group 3, wait times ranging from 24 to 72 hours were imposed before ISL testing. Once again the results showed no sign of specimen embrittlement, with $NFS_{\%}$ values around 100%.

Except for the anomalous result obtained for P46, all of these data seem to indicate that even the most severe acid pickling conditions will not cause embrittlement in the absence of a barrier to prevent hydrogen escaping.

4.1.8 Fractography

A thorough examination and mapping of a sampling of fracture surfaces of electroplated test specimens was performed by scanning electron microscopy (SEM). The specimens that ruptured at high fracture strength exhibited a mix of ductile dimples and some brittle transgranular (cleavage) fracture morphology. In comparison, specimens with low fracture strengths, such as an acid-chloride zinc plated specimen from P1001, exhibited intergranular fracture morphology, but *only in the area below the notch* where stress, and therefore hydrogen concentration were highest. Interestingly, a specimen from P1003 (zinc plated, 24 hr bake) exhibited almost entirely ductile and transgranular morphology. A sample from P1002 (zinc plated, 12 hour bake) had evidence of intergranular morphology below the notch area, and a predominance of ductile and transgranular morphology elsewhere.

4.2 NON ELECTROLYTIC PROCESSES

Fracture strength results for all of the non-electrolytic processes are shown in Figure 4.8.

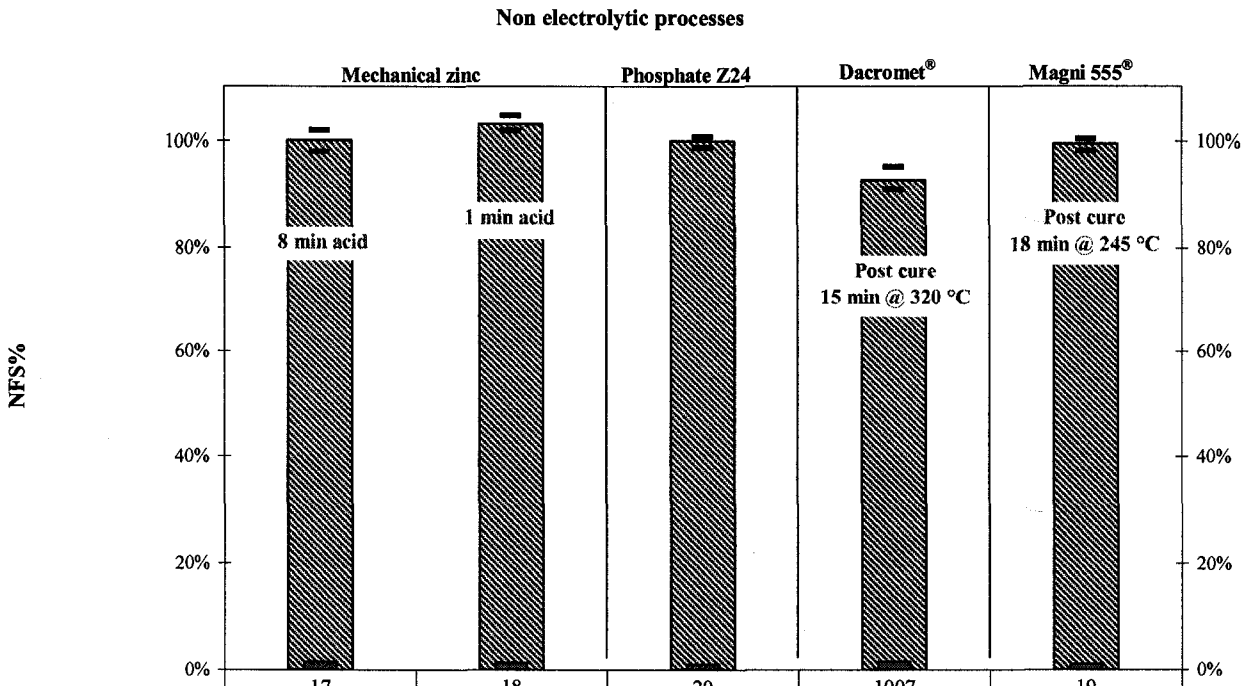

	17	18	20	1007	19
Average	100.1%	103.0%	100.0%	92.7%	99.5%
Standard deviation	1.54%	1.40%	1.00%	1.54%	1.12%
Minimum	98.0%	101.8%	98.8%	91.0%	98.2%
Maximum	101.9%	104.6%	100.7%	95.2%	100.3%

Figure 4.8. Non electrolytic processes, percent fracture strength ($NFS_{\%}$) by process.

4.2.1 Mechanical zinc – bulk drum

The mechanical zinc process was sampled under two conditions: (i) P17 at eight minutes of pickling time, which was the maximum pickling time for this process, and (ii) P18 at one minute of pickling time. Hydrochloric acid at 5 wt% was used for both conditions. The resulting $NFS_{\%}$ values in both cases exceeded 100%. These results are

consistent with the literature which holds that mechanical zinc is a non-embrittling process.

4.2.2 Zinc phosphate – barrel

The zinc phosphate process sampled (P20) included 10 minutes of pickling time in 10% v/v sulphuric acid. As expected, the average $NFS_{\%}$ value was 100%. This result is consistent with the literature which holds that phosphating is a non-embrittling process.

4.2.3 Dacromet® – bulk dip spin

The Dacromet® process (P1007) resulted in an average $NFS_{\%}$ value of 92.7%. This marginal reduction in fracture load is not thought to be related to hydrogen embrittlement phenomena. Rather, it is explained by a parallel reduction of specimen hardness resulting from the 15 minute curing cycle at 320 °C, which significantly exceeds the specimen tempering temperature of 220 °C. The specimen hardness measured after processing was 48.1 HRC, instead of 51 HRC originally.

In order to test the validity of the hypothesis that the drop in fracture strength is solely related to a lowering of specimen hardness rather than hydrogen embrittlement phenomena, an additional sampling was conducted to verify if the deterioration in fracture strength is time dependent. A single Dacromet® coated condition (P56) was tested by two methods: (i) fast fracture (FF), and (ii) incremental step loading (ISL). The loading rate for FF testing was 445 N/min, and each test took less than two minutes to complete. The ASTM F1940 loading protocol resulted in test durations of roughly 16 hours for the Dacromet® coated specimens, the same as for the pristine specimens. The results in figure 4.9 are given in the form of absolute fracture loads.

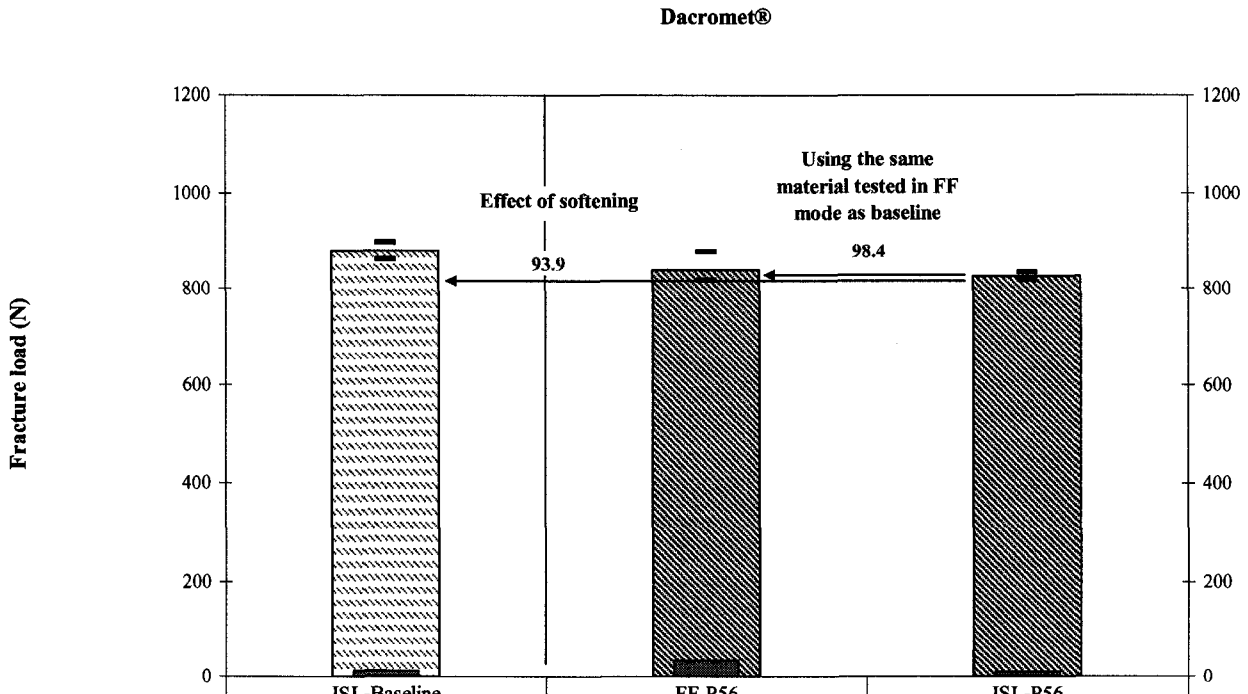

	ISL-Baseline	FF-P56	ISL-P56
Average	880	839	826
Standard deviation	12.2	34.4	10.3
Minimum	863	818	819
Maximum	898	879	834

Figure 4.9. Dacromet ®, considering material modification by using the fast fracture strength of a Dacromet ® coated specimen as the baseline.

The average *ISL* fracture strength of Dacromet® coated specimens was 826 N, which represents 93.9% the ISL fracture strength of uncoated pristine specimens, the standard baseline used for calculating $NFS_{\%}$ values. This result is consistent with the results obtained in the previous sampling. Because the curing of the specimens effectively modifies the standard specimen material to a lower hardness, *non-standard* material, a Dacromet® coated specimen would more accurately reflect the material condition being tested. Therefore, the FF strength of Dacromet® coated specimens (i.e. 839 N) would be a

more appropriate baseline for comparison with ISL results. The alternate baseline eliminates hardness as a variable. With this approach, the average Dacromet® coated ISL fracture strength was 98.4% of the baseline strength, which is essentially unchanged. This result confirms that the Dacromet® process is non-embrittling. This finding is also consistent with the fact that pickling or other contact with acidic media is prohibited in the Dacromet® process.

4.2.4 Magni 555® – bulk dip spin

The Magni 555® process (P19) resulted in an average $NFS_{\%}$ value of 99.5%, indicating no embrittlement, despite some exposure to acid during phosphating. Similar to Dacromet® the process includes a curing cycle, but at a significantly lower temperature of at 225 °C for 18 minutes. Although this is slightly higher than the 220 °C at which the specimens were tempered, it did not have a significant effect on fracture strength. The specimen hardness measured after processing was 50.4 HRC, instead of 51 HRC originally. This result confirms that the Magni 555® process is non-embrittling.

4.2.5 Fractography

A thorough examination and mapping of a sampling of fracture surfaces of non-electrolytically coated test specimens consistently found a mix of ductile dimples and some brittle transgranular (cleavage) fracture morphology. This observation was consistent with the fact that all the specimens had ruptured at high fracture strengths, indicating no embrittlement.

4.3 THERMAL DIFFUSION PROCESS – HOT DIP GALVANIZING

The ISL results obtained from the hot dip zinc process are divided into five separate groups that follow the chronological progression of sampling and testing. Also presented are results of mechanical, microstructural and fractographical analyses performed on broken test specimens.

4.3.1 Group 1

Group 1 comprised the first sampling event as was described in section 3.4.3 of the experimental procedure. Three primary conditions were sampled: (i) the "full process," which included acid pickling and flux solution, (ii) flux solution without prior pickling, followed by galvanising, and (iii) galvanising alone without any surface preparation or flux solution. A fourth condition was generated by exposing test specimens for 7 minutes at 450 °C in a conventional furnace in air.

The ISL results clearly show a significant loss of fracture strength for all specimens that were hot dip galvanised (P1008, P1009, P1010), regardless of whether they were exposed to acidic media prior to galvanising. The average $NFS_{\%}$ values ranged from 41.0 to 44.9%. The drop in fracture strength was also accompanied by a drop in specimen hardness to roughly 45 HRC from the initial 51 HRC, resulting from heat exposure in the galvanising kettle. The elimination of acid pickling in P1009 and P1010 did not increase fracture strength. Therefore, hydrogen absorbed during acid pickling was not a factor, despite the relatively aggressive pickling conditions (16 min, 10 wt% HCl, heated to 27 °C). Group 1 results are shown in Figure 4.10.

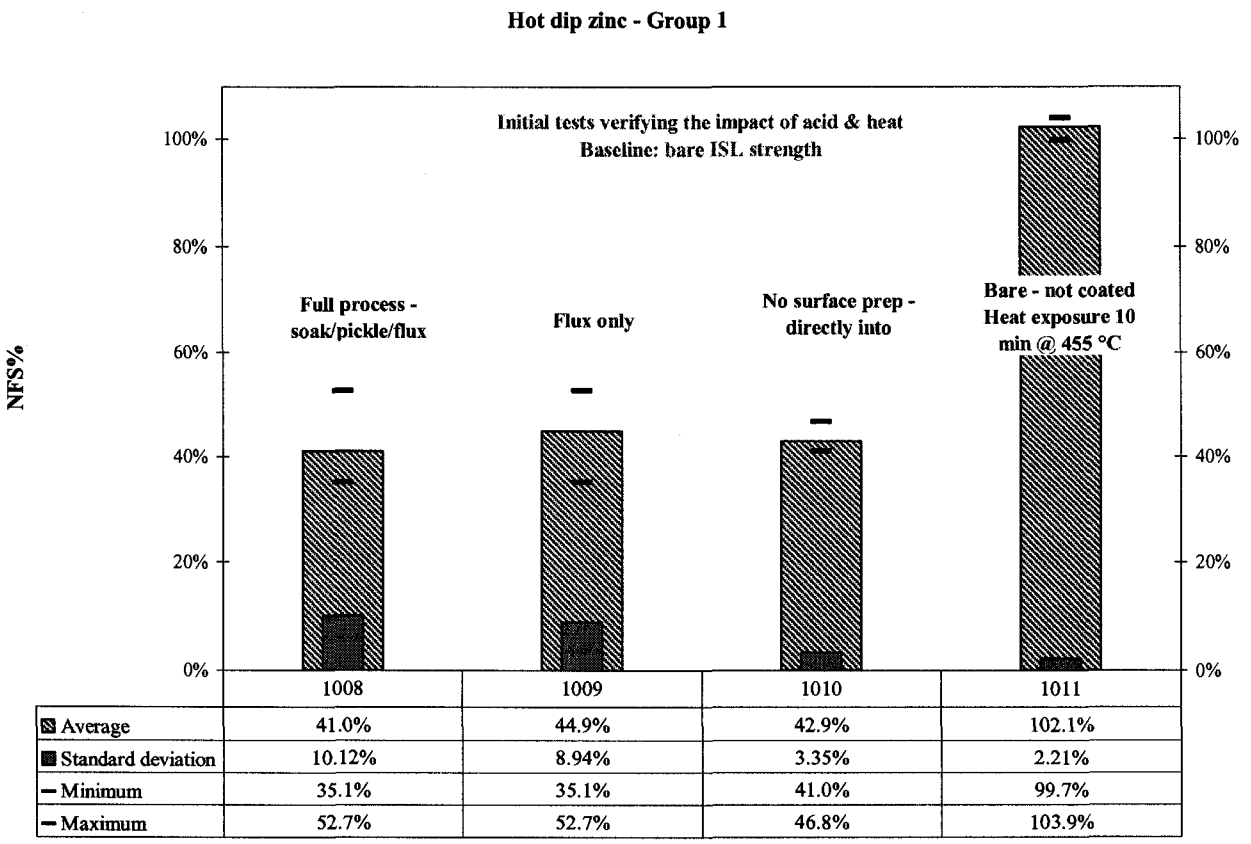

	1008	1009	1010	1011
Average	41.0%	44.9%	42.9%	102.1%
Standard deviation	10.12%	8.94%	3.35%	2.21%
Minimum	35.1%	35.1%	41.0%	99.7%
Maximum	52.7%	52.7%	46.8%	103.9%

Figure 4.10. Hot dip zinc Group 1, $NFS_{\%}$ values obtained from initial tests verifying the effects of acid and heat.

In an attempt to recreate conditions of heat exposure, P1011 specimens in were placed in a standard furnace in air for 7 minutes at 450 °C, and then quenched in water. This is approximately double the immersion time in the zinc bath. The resulting fracture strength values exceeded 100%, and specimen hardness remained unaffected. This is consistent with published empirical data for 4340 steel which states that the specimen would have had to be tempered for two hours in order to reach a hardness of 44 HRC from the as quenched hardness of 60 HRC.[50] It is clear that the conditions in the furnace could not possibly have duplicated the extreme heat transfer rate in molten zinc, which in effect induced thermal shock by up-quenching. The hardness data are summarised in Figures 4.11 and 4.12.

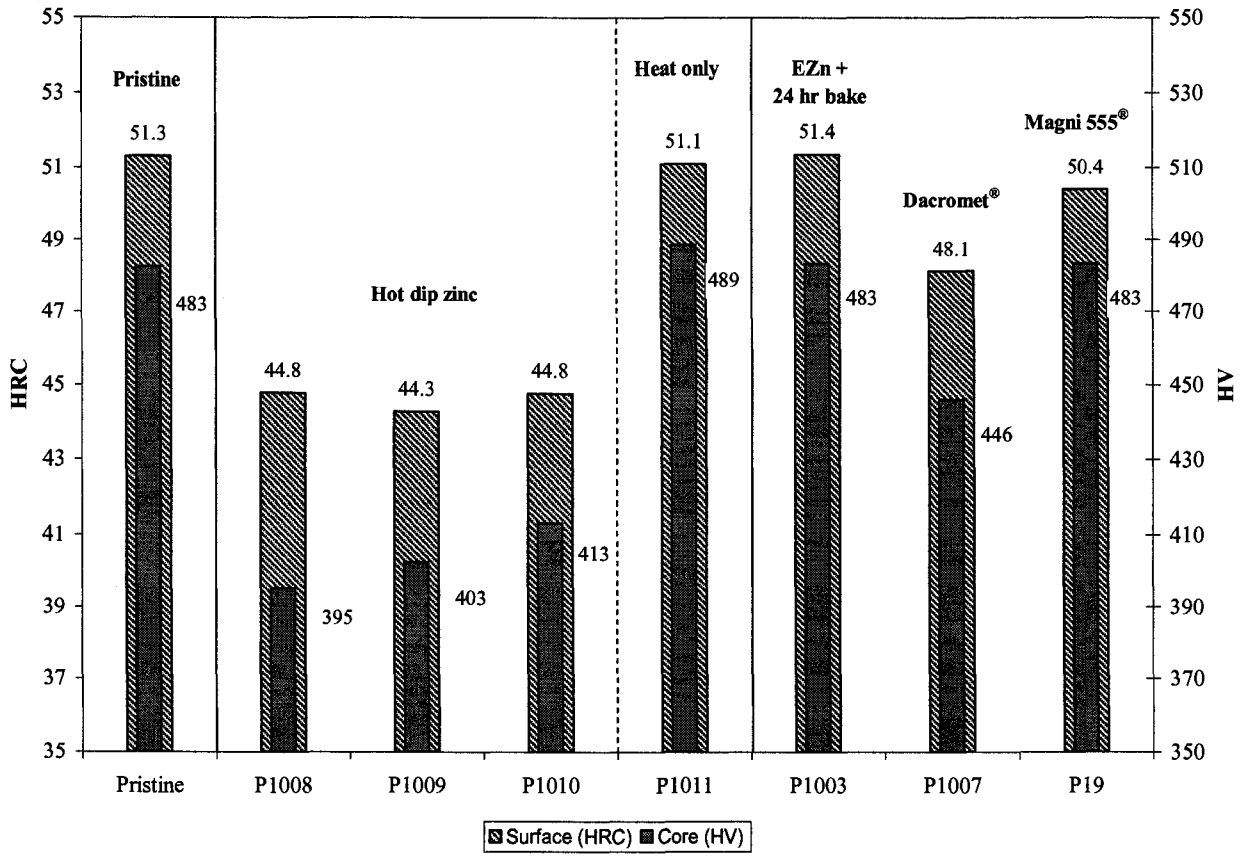

	Surface (HRC)		Core (HV)	
	Average	Std dev.	Average	Std dev.
Pristine	51.3	1.6	482.6	11.3
P1008	44.8	0.4	395.2	9.3
P1009	44.3	0.6	402.5	5.4
P1010	44.8	0.4	413.2	4.7
P1011	51.1	0.7	488.6	8.4
P1003	51.4	0.4	483.4	3.7
P1007	48.1	0.5	445.9	4.9
P19	50.4	0.3	483.5	7.8

Figure 4.11. Hardness of hot dip galvanised specimens compared to the pristine condition and to other coating processes. The same trends were observed for both core and surface hardness values.[c, d]

[c] Surface hardness was measured using a Rockwell tester in the C scale. Surface hardness measurements were supplemented by core hardness measurements on sectioned and mounted specimens using a macro-Vickers tester to avoid any possible effect of the coating or its removal on surface hardness.

[d] Any conversion of values between HRC and HV scales are approximate and should not be used as a measure of specimen through-hardness. See Figure 4.12 for hardness profiles.

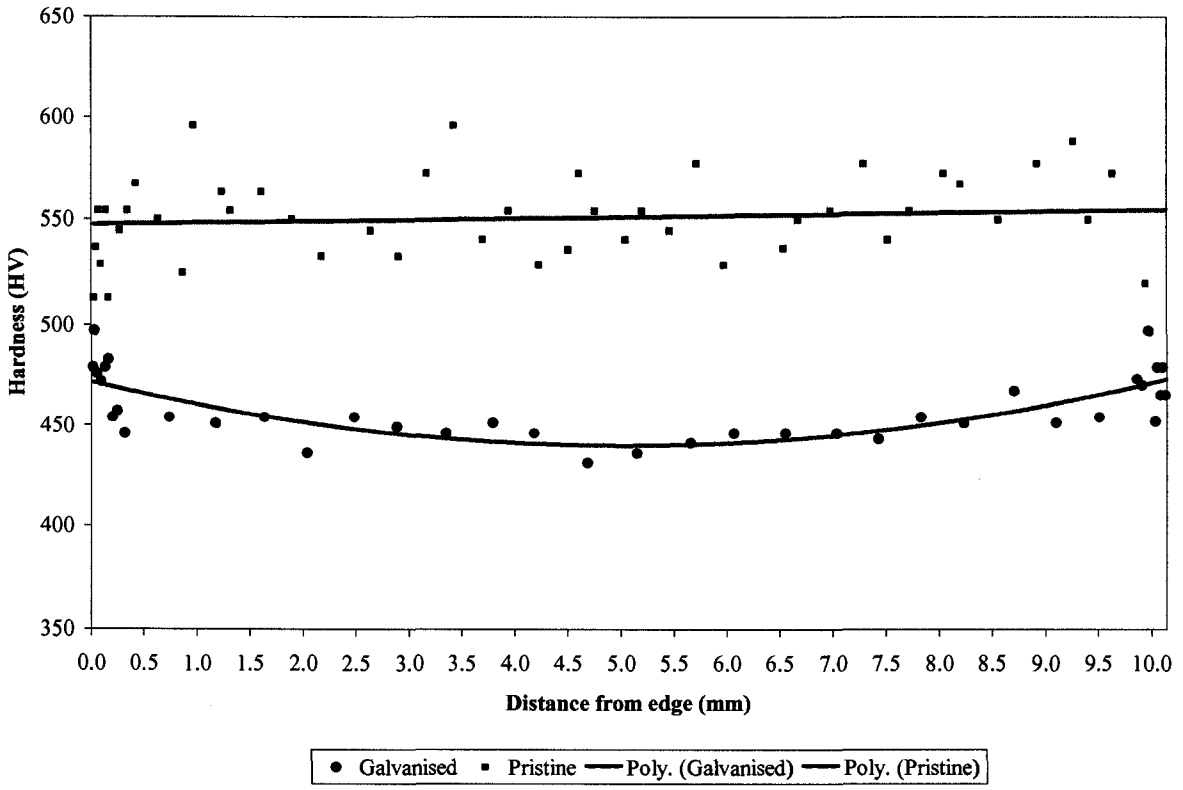

Figure 4.12. Hardness profile of pristine specimens as compared to hot dip galvanised specimens. Pristine specimens were uniformly through-hardened with very little difference between core and surface hardness. Galvanised specimens were slightly softer in the centre due to the slower cooling of the core after hot dipping.

The microstructures observed at a magnification of 1000X consisted of tempered martensite for pristine specimens (Fig. 4.13). The galvanised specimens were also tempered martensite, which was to be expected because the galvanising temperature of 450 °C is far below the transformation temperature. Nevertheless, the microstructures appeared different, with more clearly delineated martensite lathes (Fig. 4.14). This finding seems to indicate that galvanising caused a second order alteration in the microstructure. The structure of a heat exposed specimen from P1011 was similar to the pristine specimens, which is consistent with the fact that hardness was unchanged (Fig.

4.15). The reason why the zinc bath treatment changed the microstructure, whereas the furnace heat treatment did not, is difficult to explain. However, it may be a manifestation of the thermal shock/up-quenching during immersion in molten zinc.

The constancy of results for the galvanised conditions, regardless of acid exposure, was unexpected. The lowered hardness would certainly account for a loss of fracture strength, but it is not yet clear if it accounted for all of the loss. If on the other hand hydrogen embrittlement has occurred, the source of hydrogen is not obvious. Another possibility is that the rapid heating and cooling to and from 450 °C is causing a form of temper embrittlement, which is an altogether different failure mechanism.

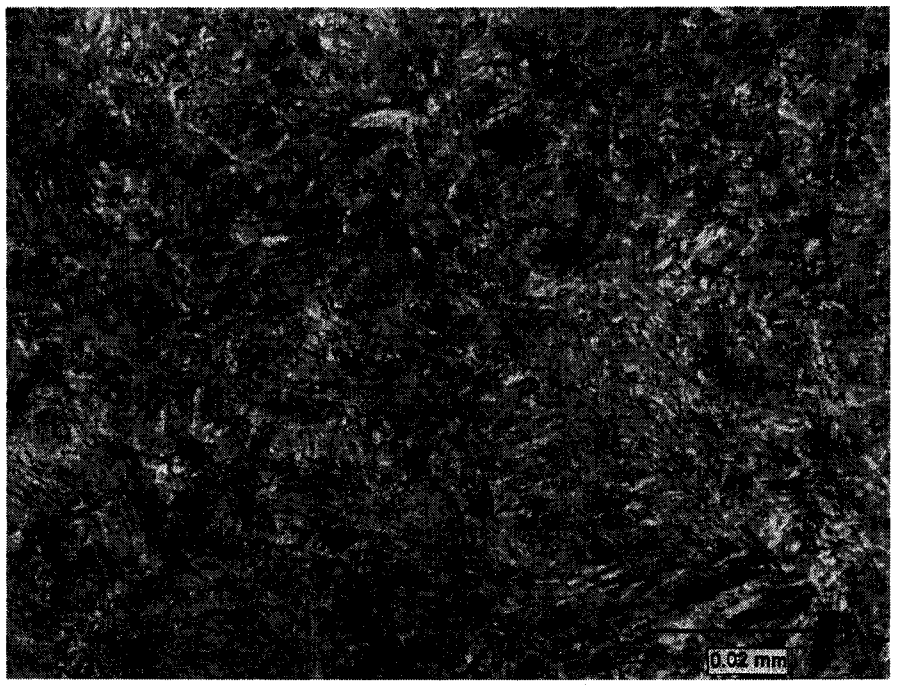

Figure 4.13. Metallurgical structure of pristine specimen consisting of tempered martensite. (1000X)

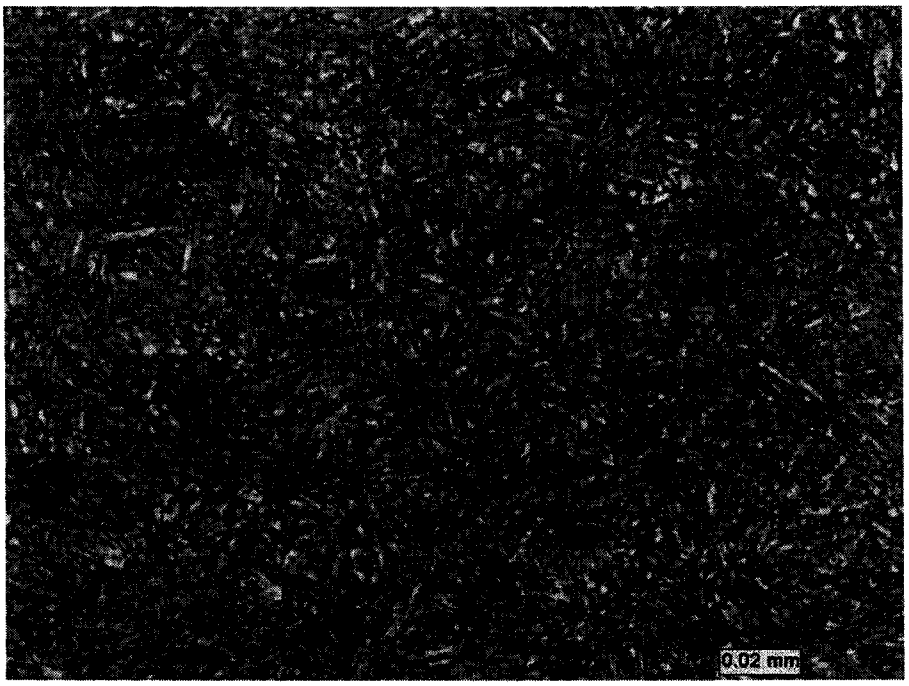

Figure 4.14. Metallurgical structure of galvanised specimen from P1009 composed of martensite with modified appearance. (1000X)

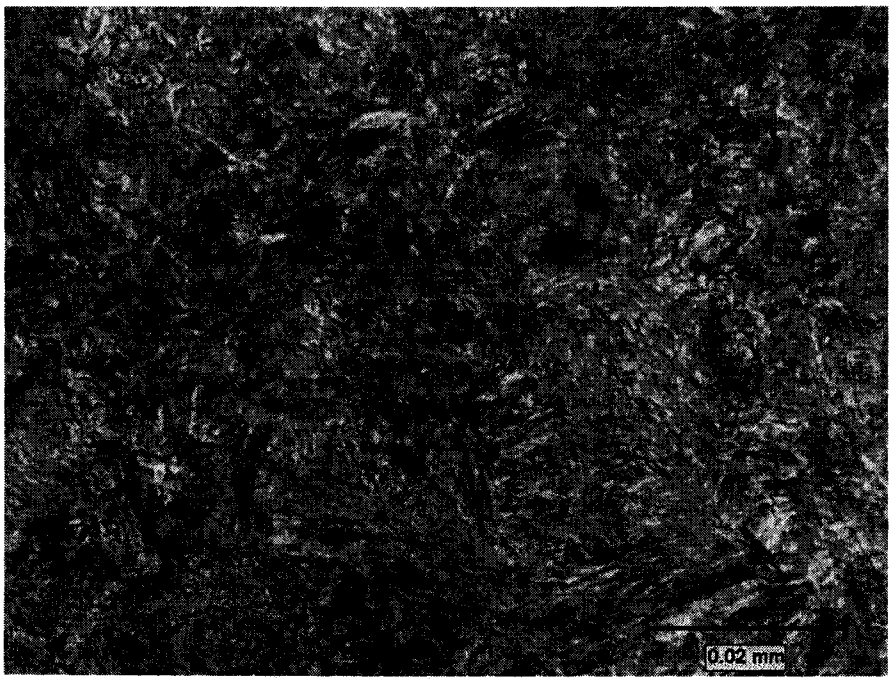

Figure 4.15. Metallurgical structure of heat exposed specimen from P1011 which was very similar to the pristine specimen. (1000X)

A thorough examination and mapping of fracture surfaces was performed by scanning electron microscopy (SEM). Figure 4.16 is an annotated overview of a fracture surface, indicating locations and observed morphologies. Examples of morphologies observed are shown in Figures 4.17 and 4.18. Fracture surfaces of a heat exposed specimen from P1011 and that of a broken baseline (pristine) specimen were found to be predominantly ductile with some brittle transgranular (cleavage) morphology. All of the galvanised specimens showed a predominance of brittle intergranular fracture morphology, with some ductile morphology at ridges on the periphery. For all three galvanised conditions the intergranular morphology extended throughout the *entire fracture surface.* In comparison, the acid-chloride zinc plated specimens (P1001) referenced earlier exhibited intergranular fracture morphology only in the area below the notch. For the electroplated specimens, hydrogen was absorbed as a result of the plating process. Therefore, hydrogen entered the specimen from the surface, penetrated inward, and concentrated at the root of the notch. In the case of the galvanised specimens, if hydrogen was at play, it must already have been present in the matrix, perhaps in trap sites, to have resulted in such predominantly intergranular morphology.

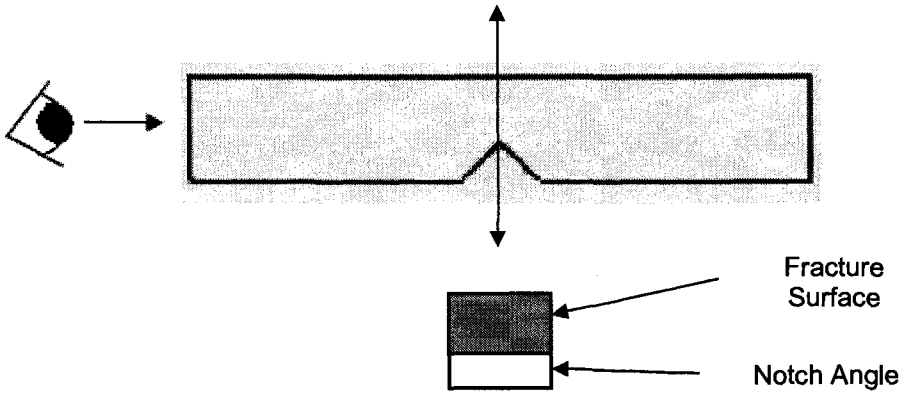

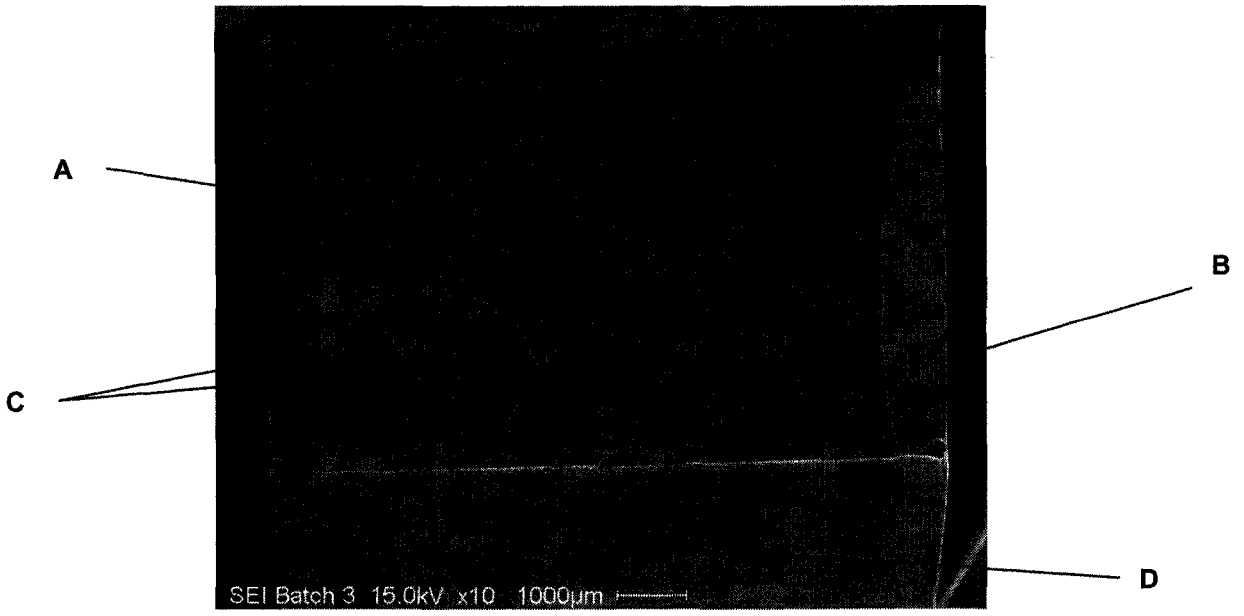

A: Center of fracture surface, characterised by predominantly brittle intergranular morphology in the hot-dip galvanised specimens, and predominantly ductile dimple morphology in the zinc electroplated specimens.

B: Edge of fracture below the notch radius, typically the only brittle intergranular region in the zinc electroplated specimens. The hot-dip galvanised samples also exhibited intergranular morphology in this region.

C: Ductile ridges

D: Notch Angle

Figure 4.16. Fracture surface overview with schematic of specimen orientation. (10X)

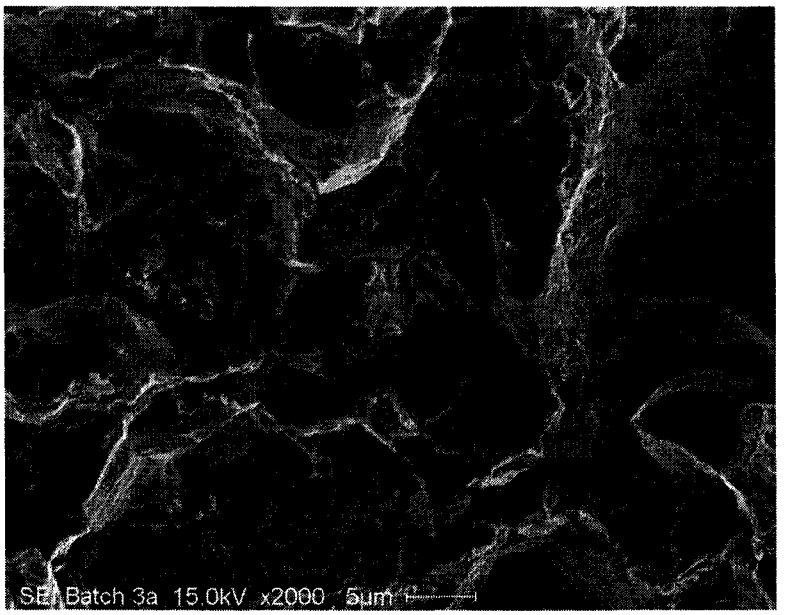

Figure 4.17. Fracture surface of hot dip galvanised sample from P1008 – brittle intergranular morphology.

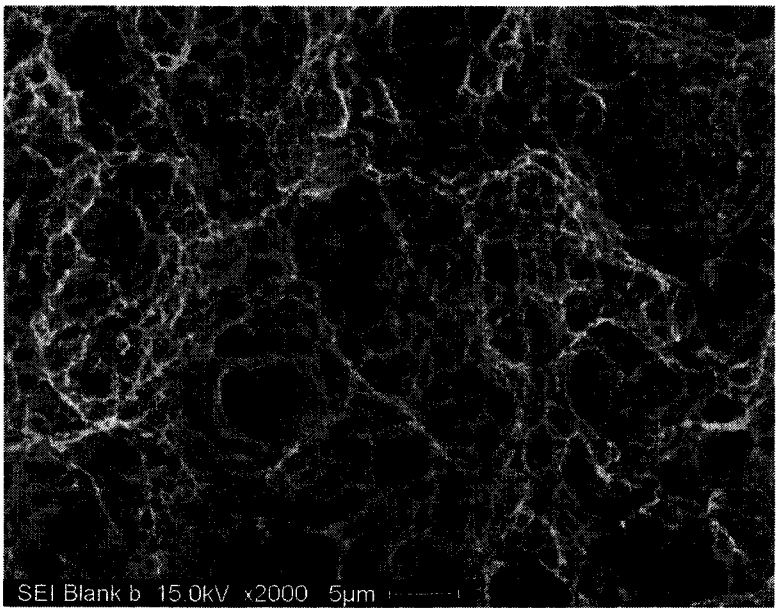

Figure 4.18. Fracture surface of pristine sample – ductile "dimple" morphology.

4.3.2 Group 2

Group 2 was designed to test the validity of the trapped hydrogen hypothesis by applying "pre-bake" cycle at 205 °C prior to galvanising. The baking temperature was

carefully selected so as not to exceed the specimen tempering temperature of 220 °C, thus avoiding any change in mechanical properties. The follwing three pre-bake times were selected: (i) 24 hours (P23), (ii) 48 hours (P25), and (iii) 72 hours (P26). An additional condition consisting of a "post-bake" for 4 hours at 190 °C was also generated. Group 2 results are shown in Figure 4.19.

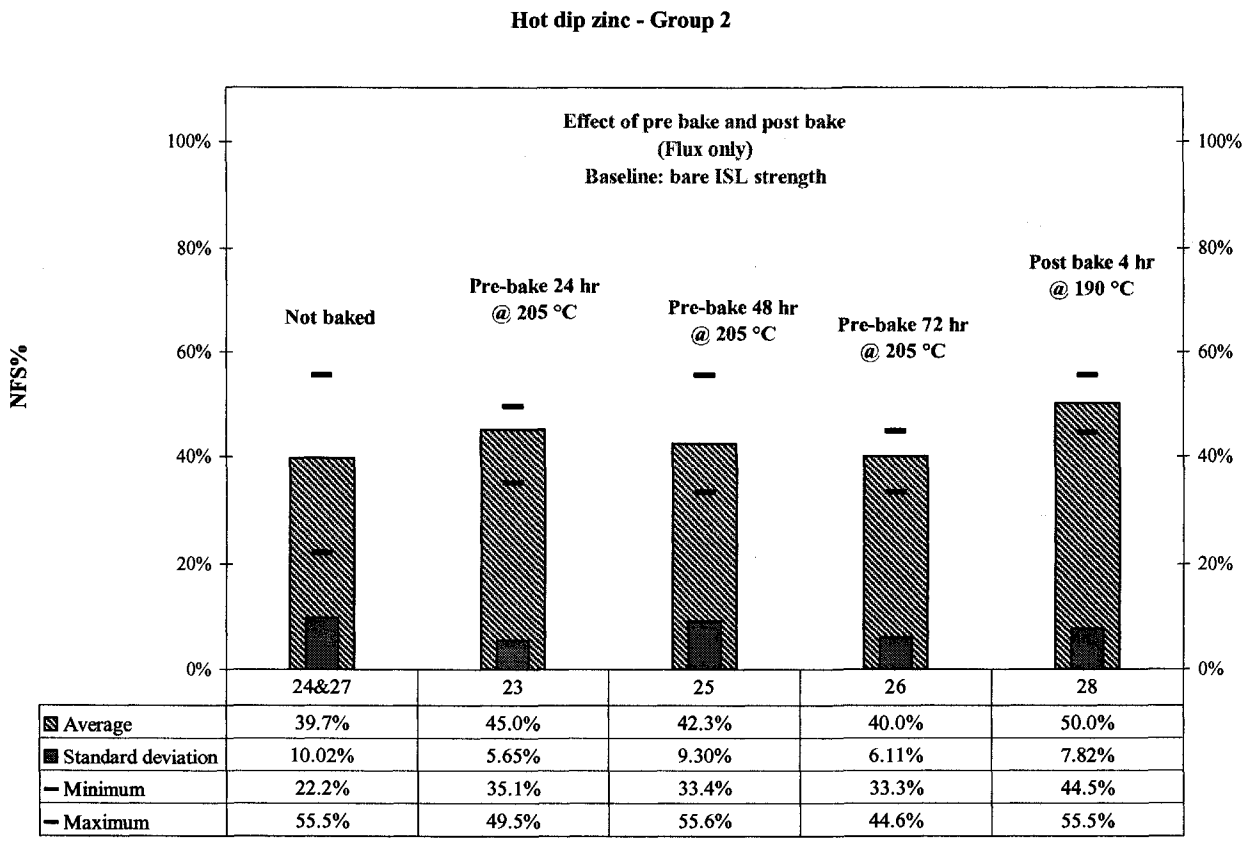

	24&27	23	25	26	28
Average	39.7%	45.0%	42.3%	40.0%	50.0%
Standard deviation	10.02%	5.65%	9.30%	6.11%	7.82%
Minimum	22.2%	35.1%	33.4%	33.3%	44.5%
Maximum	55.5%	49.5%	55.6%	44.6%	55.5%

Figure 4.19. Hot dip zinc Group 2, comparing the effects of pre-baking and post baking.

The results showed average $NFS_{\%}$ values in the range of 40 to 45%, i.e., no significant improvement in any of the conditions. Group 2 comprised a concerted, attempt to dislodge or effuse hydrogen from the test specimen by applying heat, before and after galvanising. The lack of success in obtaining different results from Group 1 does not rule

out the presence of trapped hydrogen. The principal limitation of this effort was that the pre-baked heating conditions did not duplicate the conditions in the zinc kettle. Not only was the baking temperature less than half that of molten zinc in the kettle, but also the heat transfer rate was also exponentially slower.

4.3.3 Group 3

Group 4 was designed to test the validity of the trapped hydrogen hypothesis by verifying if the deterioration in fracture strength was time dependent. A single galvanised condition (P27) was tested by two methods: (i) fast fracture (FF), and (ii) incremental step loading (ISL). The loading rate for FF testing was 445 N/min, and each test took less than two minutes to complete. The ASTM F1940 loading protocol resulted in test durations ranging from 1.5 to 4.3 hours for the galvanised specimens, and up to 16 hours for the pristine specimens. The results in figure 4.20 are given in the form of absolute fracture loads.

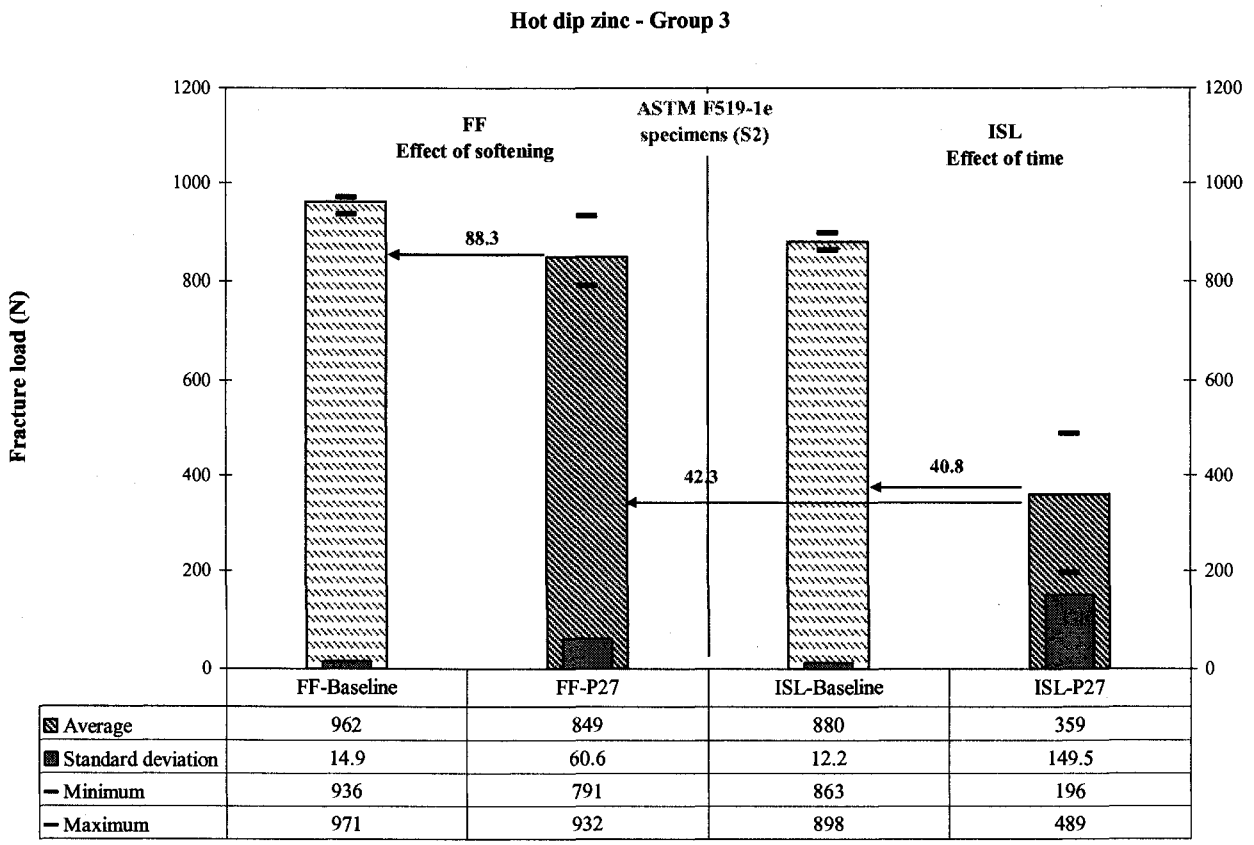

Figure 4.20. Hot dip zinc Group 3, considering material modification by using the bare fast fracture strength as the baseline.

The average *FF* strength of galvanised specimens was 849 N, which is equal to 88.3% of the FF strength of uncoated pristine specimens. The drop of roughly 12% is primarily attributed to the lowering of specimen hardness to 45 HRC from the initial 51 HRC.

The average *ISL* fracture strength of galvanised specimens fell to 359 N, which represents 40.8% the ISL fracture strength of uncoated pristine specimens, the standard baseline used for calculating $NFS_{\%}$ values. The lower fracture strength is apparently related to the longer testing times, which is a characteristic of hydrogen embrittlement phenomena. However, similar to the Dacromet® process, it can be argued that the

galvanising process effectively modifies the standard specimen material to a *non-standard* material, and that the standard material cannot be used as a valid baseline. A specimen that has been galvanised would more accurately reflect the material condition being tested. Therefore, the FF strength of galvanised specimens should be used as an alternate baseline for comparison with ISL results. In this scenario, the average galvanised FF strength of 849 N would serve as baseline. Even with this approach, at 359 N, the average galvanised ISL fracture strength represents only 42.3% of the baseline strength. Either way, the results show a significant deterioration of fracture strength as testing time is prolonged. *This result is the most solid evidence in support of the trapped hydrogen hypothesis*, because the time dependence of hydrogen embrittlement is well established. Other embrittlement mechanisms such as temper embrittlement are not time dependant. Had temper embrittlement occurred, galvanised specimens would have exhibited lower fracture strengths, in the range of 359 N, when tested in FF mode.

4.3.4 Group 4

Group 4 was designed to test the effect of hardness on susceptibility to brittle failure. The intention was to reduce the *starting specimen hardness* to within the hardness range of high strength structural fasteners (i.e., ASTM A490[51] bolts). Standard F519-1e test specimens were tempered for one hour at 560 °C. The resulting surface hardness was reduced to an average of 36.5 HRC from the initial 51 HRC. A single galvanising process condition (P45) was tested using the modified specimens. Hardness of the modified specimens after galvanising was measured and found to be unchanged. Group 5 results are shown in Figure 4.21.

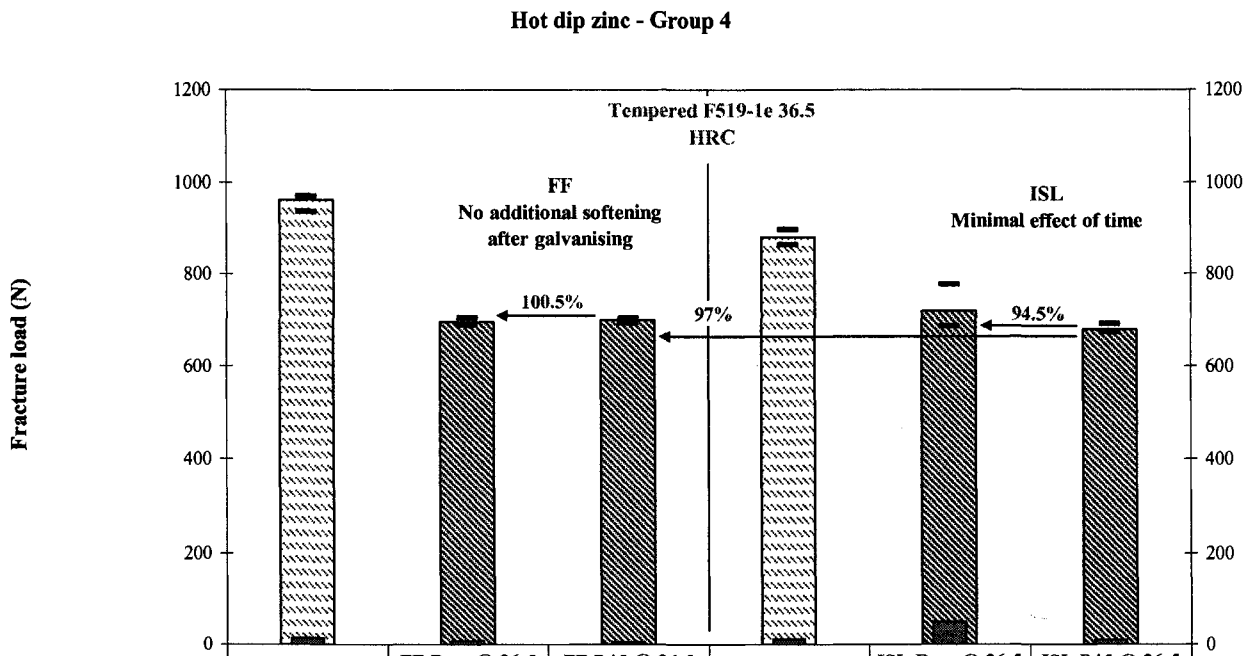

	FF-Baseline	FF-Bare @ 36.5 HRC	FF-P45 @ 36.5 HRC	ISL Baseline	ISL-Bare @ 36.5 HRC	ISL-P45 @ 36.5 HRC
Average	962	696	700	880	718	679
Standard deviation	14.9	8.0	5.8	12.2	50.3	10.0
Minimum	936	688	693	863	686	673
Maximum	971	704	703	898	776	690

Figure 4.21. Hot dip zinc Group 4, galvanising of specimens re-tempered to 36.5 HRC.

The average FF and ISL fracture strengths of bare (uncoated) *modified* specimens were roughly the same at 696 and 718 N respectively. This reflected the lower hardness of the *modified* specimens in comparison to *standard* specimens. The average FF strength of galvanised *modified* specimens was 700 N which was unchanged from the bare condition tested in FF mode. The average ISL fracture strength of galvanised *modified* specimens was 679 N, which equals 94.5% of the bare condition tested in ISL mode. Using the same alternate baseline as in the previous group, 679 N equals 97% of the FF strength of galvanised modified specimens.

These results can be restated as follows. First, unlike with the high hardness standard specimens, there was no difference between FF strength and ISL fracture

strengths of bare specimens. Second, the galvanising process did not alter the specimen FF strength, which is consistent with the fact that hardness was also unchanged. Third, increasing testing time per the ASTM F1940 loading protocol had a minimal effect. These results all point to decreased hydrogen susceptibility at the lower starting hardness of the specimens, which is also consistent with HE theory.

CHAPTER 5: DISCUSSION

The intention of the sampling methodology adopted for this study was to obtain a cross section of coating processes used in the fastener industry. Consequently, the processes were sampled "as-is," without modifying any parameters or processing conditions. The information will serve as a baseline for further investigations into improving process performance. Naturally the results have raised many questions that will need to be answered in future work.

5.1 GENERAL OBSERVATIONS

The results of the hot dip zinc process in particular and also of the Dacromet® process highlight the relationship between hardness and baseline *fast fracture* strength, notably that a lowering of specimen hardness is accompanied by a similar lowering of FF strength. Figure 5.1 illustrates this relationship by plotting six distinct specimen hardness conditions, each with the corresponding FF strength. This empirical observation is important because it demonstrates that there is no overriding notch effect which could have reversed the described relationship. A sharp notch might have caused fracture strength to fall with increasing hardness due to higher notch sensitivity. The absence of a notch effect is likely the result of having a relatively large radius of 0.25 mm at the root of the specimen notch (i.e., dull notch). As a final note, FF strength is used as the reference here because it represents a conventional measure of strength, without the influence of testing time such as with ISL testing.

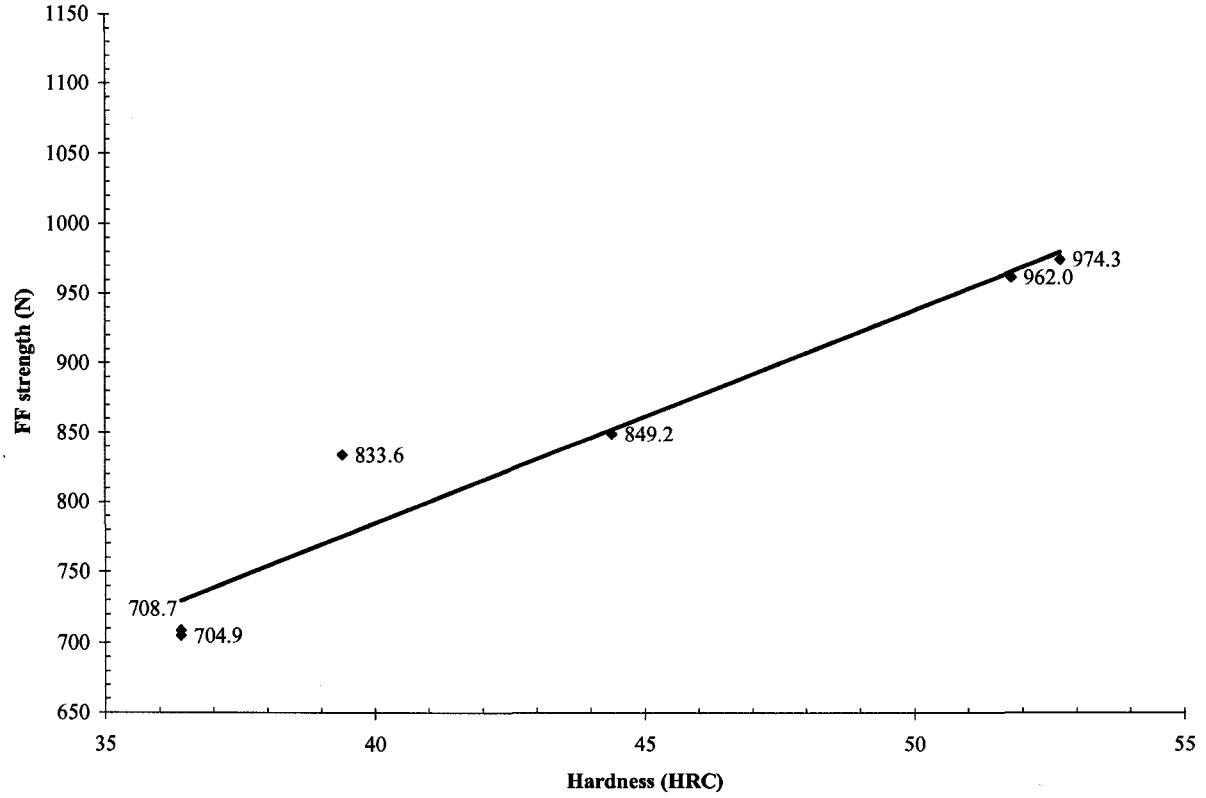

Figure 5.1. Relationship between specimen hardness and fast fracture strength.

In section 4.1.1, a statement was made to the effect that small changes in hydrogen concentration can, under certain conditions, lead to large changes in $NFS_{\%}$ value. This statement was in reference to the large scatter of fracture strength results with zinc electroplated specimens baked for 12 hours. Indeed, the relationship between hydrogen concentration and ISL fracture strength shows a "ductile to brittle" transition. This point is illustrated in Figure 5.2 showing the threshold curve for F1940 notched square bar specimens. The curve was empirically generated by plotting $NFS_{\%}$ as a function of cathodic charging potential (i.e., hydrogen concentration). Hydrogen charging is greatest at -1.2V (i.e. origin of the x axis), and is nil in air (i.e. far right of the x axis). The slope of the curve is steepest between the two inflection points (i.e. -0.8 to -0.9V). In

this region, *relatively* small changes in hydrogen concentration can lead to fracture strengths ranging from 45 to 80%. Therefore, $NFS_{\%}$ data will typically exhibit greater variability within this middle range.

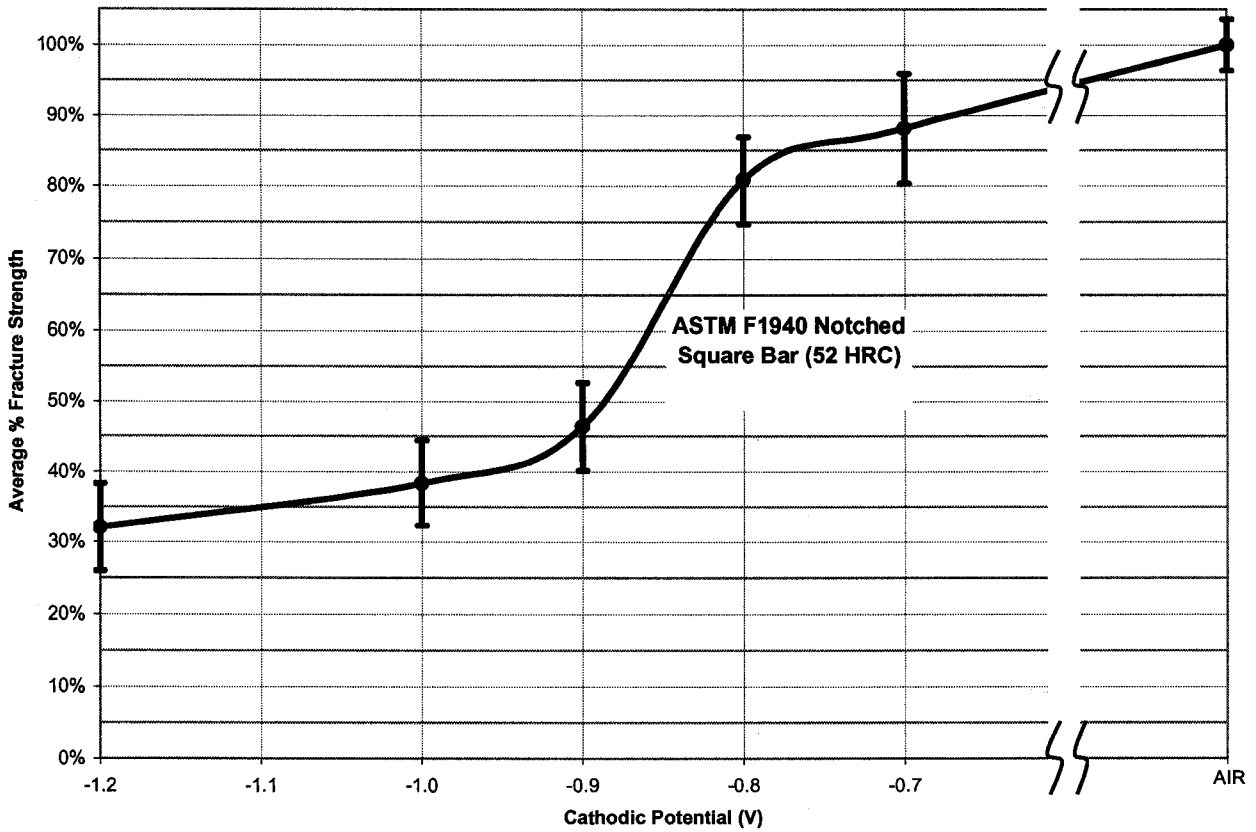

Figure 5.2. ASTM F1940 threshold chart.[44]

SEM analysis of the fracture surfaces revealed a close correlation between the lowering of fracture strength, and the presence of intergranular morphology, which is the footprint of hydrogen embrittlement. The fractographic evidence confirmed the causal relationship between the presence of residual hydrogen from processing and the reduction of fracture strength, which is the premise upon which the ASTM F1940 test method is based. This finding supports the use of the ISL test method as a predictor of hydrogen assisted brittle failure, both IHE and EHE.

Finally, it is important to point out that the findings presented in this research constitute a new paradigm through which coating processes will be evaluated. Currently, coatings are evaluated based on their corrosion protection, electrochemical, and mechanical characteristics. The availability of an additional metric to quantify the embrittling nature of the coating process and the resulting coating will have a significant impact on the selection of coatings.

5.2 ELECTROPLATING PROCESSES

Viewed from a mechanistic perspective, the results obtained with electrolytic processes support the assertion that the multitude of complex processing variables and coating characteristics can be grouped into two basic parameters affecting IHE: (i) the amount of hydrogen introduced by the process, and (ii) the permeability of the coating. It will be shown that *coating permeability* has a first order effect, while the *quantity of hydrogen* introduced by the process has a second order effect.

The results of the acid dip tests and the phosphating process showed that in the absence of a coating barrier, hydrogen had a tendency to freely "out-gas" or escape, rather than be attracted to areas of stress concentration. The data seem to indicate that this statement can hold true even with the most severe acid pickling. This finding is consistent with the literature and industry standards that do not require phosphated parts to be baked, owing to the highly porous nature of phosphate coatings.

When a coating barrier is present, the effect of permeability is evident when comparing Zn-Ni coatings to other coatings. The Zn-Ni coated specimens plated at the

same current density as Zn coated specimens were not embrittled. This result is thought to be related to the porosity of the Zn-Ni coating.[52] Although this point will be thoroughly investigated in future work, preliminary characterisation by electron microscopy showed the Zn-Ni coatings to be considerably more fractured than pure zinc coatings, thus allowing hydrogen easier escape paths.[53] These results highlight the relationship between the coating metal and permeability. In the case of alloy coatings such as Zn-Ni, Zn-Fe or Zn-Co, the alloy ratio may also have an effect on coating permeability. The degree of influence of nickel ratio in Zn-Ni can be tested in future work.

The results of the cadmium process showed the reverse effect of coating permeability. In this process, the application of an impermeable layer at the start of plating was used to prevent additional hydrogen being absorbed during plating build-up. The very high current density apparently resulted in an impermeable structure. This result can be easily validated in future work by sampling the same cadmium process *with* and *without* the initial strike. Additionally, a thorough characterisation of the two coating structures might reveal the effect of coating morphology (e.g., columnar or platelet) on permeability.

Other variables, such as bath chemistry, and in particular the type of brighteners used may affect morphology and, therefore, the permeability of a coating. It is also conceivable that surface activation leads to a more permeable coating morphology. The degree of influence of these variables can be tested in future work. An additional topic to investigate in relation to coating permeability is the effect, if any, that hydrogen has when it is trapped in the coating or at the coating/substrate interface.

Quantity of hydrogen is a function of electrolytic parameters (i.e., current density and plating time), and acid exposure conditions (i.e., acid type, concentration, and pickling time). The effect of current density was most evident when comparing Zn-Ni rack plating to barrel plating. The current densities were as much as six times greater and fracture strengths as low as 45% for the rack process as compared to 100% for barrel processes. To a lesser extent the effect of current density was also observed in comparing Groups 1 and 2 of the acid chloride zinc process, where lower current density seemed to result in decreased embrittlement for Group 2.

The hydrogen contribution of acid pickling was evident when comparing the results of the "full process" conditions to the "no surface cleaning" conditions. The latter consistently produced higher fracture strength results than the former. The effect of acid pickling was most evident in the acid-chloride zinc process, which is thought to produce the least permeable coating. Conversely, the effect of acid pickling was least evident for the Zn-Ni processes which are thought to produce the most permeable coatings.

Although conventional wisdom supported by theory has always held that high efficiency baths are less embrittling because they generate less hydrogen, there was no apparent effect of bath efficiency on ISL results. It may be that the effect of bath efficiency is minor in relation to current density/time and pickling concentration/time. It is also possible that the limiting current density i_L, defined in equation 14 (sect. 2.4 of the literature review) is not readily achieved in the course of an industrial plating process.

In summary, the results of ASTM F1940 testing showed that the zinc acid chloride process was the most embrittling process (i.e., highest risk) because it consistently produced the lowest $NFS_{\%}$ results. Next in the order of risk, the alkaline zinc

process was found to be slightly less embrittling with higher $NFS_{\%}$ values, even at twice the plating time. These results are attributed to low permeability of pure zinc coatings. The fact that the acid zinc chloride bath is an acidic medium might explain its slightly more embrittling nature versus the alkaline zinc bath. Pure zinc processes were followed by the alkaline zinc-iron process, which at 86% fracture strength was classified as moderately embrittling. This result reflects the mixed effects of coating permeability and hydrogen contribution. The least embrittling processes were zinc-nickel, both alkaline and acid. In barrel processes, where plating current densities were around 6 mA/cm^2, the zinc-nickel processes produced no measurable embrittlement. In a rack process where plating current density was five times greater, embrittlement had occurred, but ductility was fully restored after 24 hours of baking at 191 °C. These results are attributed to the permeability of Zn-Ni coatings.

The cyanide cadmium plating process cannot be ranked against the others because the coating was applied in two steps: (i) a quick high current density "strike" followed by, (ii) lower current density plating. Despite being applied at a relatively high current density (~ 22 mA/cm^2), the initial strike evidently succeeded in preventing subsequent hydrogen absorption. This assertion is supported by the fracture strength result of roughly 92%, obtained without the benefit of baking. The technique of creating an impermeable absorption barrier prior to plating is not widespread in the general plating industry. However, it is used by some electroplaters specialising in the coating of high strength and ultrahigh strength components for the aerospace industry. Incidentally, a process similar in principal was described in the 1970 Canadian Patent by Bednar et al.,[23] noted in the literature review (Sect. 2.5.2).

It must be emphasised that results obtained for electroplating processes are only a measure of the ***potential*** for internal hydrogen embrittlement. Ultimately, whether or not hydrogen embrittlement will occur depends upon the degree of susceptibility of parts being plated. If a process is deemed "high-risk" by this method, it may still be suitable for plating parts that have low susceptibility. On the other hand, if a process is deemed non-embrittling or "safe" by this method, then there is no risk of embrittlement, regardless of the susceptibility of parts being plated. The only exception to this rule is if the hardness of the production parts exceeds that of the test specimens. In very rare cases, *non-standard ultrahigh strength* parts, or in some cases *surface hardened* parts may exceed a hardness of 52 HRC. In these cases, non-embrittling coating processes should be used.

5.3 BAKING

When considering the effect of baking, fracture strength results supported by fractographic analysis showed that ductility can be fully restored by baking at temperatures ranging from 190 to 204 °C. This finding is significant because it not only validates the theory regarding the *reversibility* of IHE, but it also signifies that baking can be used as an effective countermeasure for preventing IHE related failures. It should be noted that baking is limited to this temperature range, as higher temperatures may increase the risk of liquid metal embrittlement with metallic coatings such as zinc and cadmium.

Current industrial standards overwhelmingly, although not exclusively, specify a "one size fits all" approach for baking electroplated high strength fasteners. The typical approach comprises four hours of baking at 204 °C. However, this study demonstrated

that baking response depends upon the permeability of the coating and, therefore, varies with coating type. Zinc plating, which is the most widespread electroplated coating applied to fasteners, achieved full recovery only after 24 hours of baking at 204 °C.

Clearly, the fact that IHE related failures are relatively rare with zinc plated fasteners has little to do with the effectiveness of baking practice. Instead, the absence of failures is a consequence of the *low hydrogen embrittlement susceptibility* of most fastener materials. This point is illustrated in the following example. Class 10.9 (metric) and Grade 8 (inch) screws are the most common "high strength" fasteners in use, and are often zinc plated with the provision of a baking cycle of 4 hours at 204 °C. These grades and have a hardness of 33 to 39 HRC, and manufacturers typically target the middle of the specified hardness range (i.e., 35 to 37 HRC). At this hardness, steel typically has very low HE susceptibility and baking is often not even necessary. On the other hand, four hours of baking at 204 °C will likely be insufficient for zinc plated Class 12.9 fasteners (39-44 HRC). Class 12.9 fasteners may be safely electroplated provided an *effective* baking cycle is applied. The term *effective* implies that ASTM F1940 methodology was used to validate the effectiveness of the baking cycle. In the case of zinc electroplating an effective baking cycle would be 24 hours at 204 °C.

The findings of this research warrant a comprehensive revision of industrial baking standards and practices. The economic and infrastructural impact on industry of increasing baking times to 24 hours (for zinc plated parts) may appear at first to be insurmountable. However, a revision of baking practice should also seek to eliminate baking where it is not needed. The resulting scenario would be one where a considerably smaller quantity of parts would be baked for longer periods.

5.4 NON ELECTROLYTIC PROCESSES

All four of the non-electrolytic processes tested, mechanical zinc, zinc phosphate, Dacromet®, and Magni 555® were found to be non-embrittling. In the cases of phosphate and mechanical zinc, the results were attributed to the permeability of the coating. A drop in fracture strength for Dacromet® by roughly 7% was attributed to a lowering of specimen hardness caused by curing at 320 °C. The relationship between hardness and fracture strength was elaborated in the general observations (sect. 5.1 and Fig. 5.1).

5.5 THERMAL DIFFUSION PROCESS – HOT DIP GALVANIZING

With hot dip galvanising, the evidence heavily points to hydrogen embrittlement as the mechanism causing brittle failures in test specimens, with fracture strengths as low as 40%. The most compelling evidence supporting this finding is that the embrittlement phenomenon was found to be time dependant. Other embrittlement mechanisms such as temper embrittlement are not time dependant, and would have resulted in similarly low *fast fracture* strengths. But this was not the case.

In this scenario, hydrogen is present in reversible traps and is then released by the thermal shock of up-quenching that occurs upon immersion in molten zinc. The presence of a thick zinc coating prevents hydrogen escaping, instead causing it to accumulate at grain boundaries. It is important to emphasise the concept of *reversible trap*. If hydrogen is not trapped, it will have a tendency to effuse, even at room temperature. If hydrogen is trapped, the traps must be "reversible" for hydrogen to be released.

The most plausible source of hydrogen is residual hydrogen trapped in the matrix of the steel specimens. Hydrogen is a known and inevitable impurity that is present in steel made by conventional steelmaking practice. Depending on the effectiveness of the vacuum degassing method used, concentrations in the final product can vary between 0.5 to 7 ppm.[54] Samples of the test specimens used in this work (lot S2) were submitted to a certified laboratory for analysis. The reported hydrogen concentration was 0.7 ppm.[55] Despite being at the very low end of the impurity spectrum, the presence of this residual hydrogen can also explain the drop in fracture strength, by roughly 10%, when pristine specimens are tested in ISL mode versus FF mode.

It can be argued that prior heat exposure undergone by the test specimens would have provided similar opportunities for releasing trapped hydrogen, and would have done so in the absence of a coating barrier to block effusion from the matrix. To address this point, a closer look at the manufacturing history of the specimens is required (sect. 3.3). The heat exposure history can be summarised as follows: (i) austenitise at 816 °C for 45 minutes, (ii) temper at 220 °C for two hours, (iii) second temper at 220 °C for two hours, and (iv) stress relief at 190 °C for four hours. Although the initial heating to the austenitic range provides a great deal of energy, the solubility of hydrogen in steel increases with temperature, from less than 1 ppm at room temperature to about 12 ppm at 815 °C.[54] Therefore there is no opportunity for the elimination hydrogen at this stage. The tempering and stress relief temperatures are ideal for baking out residual interstitial hydrogen. However, if hydrogen is trapped in the lattice or at grain boundaries, these moderate to low heating temperatures may not succeed in dislodging it.

A very important result highlighted in Group 4 is that lower hardness specimens (i.e., 36-37 HRC) were not embrittled by the hot dip zinc process. The primary scientific significance of this finding is that it further strengthens the hydrogen embrittlement hypothesis by agreeing with the theory which states that HE susceptibility decreases with hardness. An important practical significance of this finding is the confirmation that lower hardness materials can be galvanised without the risk of hydrogen embrittlement, and without affecting hardness, strength or metallurgical properties.

A better understanding of the relationship between hardness and embrittlement by the hot dip zinc process will have far reaching implications for the structural fastener industry. ASTM A490[51] is the pre-eminent product standard for high strength structural bolts. These products are characterised by a tensile strengths ranging from 1034 to 1193 MPa (150,000 to 173,000 psi), and hardness ranging from 33 to 39 HRC. Reports of field failures in the 1970's, although poorly documented, prompted the ASTM committee F16 on fasteners to explicitly prohibit the application of metallic coatings on A490 structural bolts. The prohibition specifically spells out hot-dip zinc, mechanical zinc, and electroplated zinc. Townsend's[17] 1975 paper on the effects of zinc coatings on stress corrosion cracking and hydrogen embrittlement of low alloy steel is cited as the basis for the prohibition (also see sect. 2.4.1 of the literature review). In his study, Townsend found that stress corrosion crack growth rates were increased in hot dip zinc coated bolts made of 4140 steel, which he also attributes to residual trapped hydrogen.[16] However, he does not address the relationship between hardness and susceptibility to IHE by hot dipping. Although the intent of the prohibition in ASTM A490 was to institute a blanket

measure that eliminated the risk of hydrogen embrittlement, in hindsight, it may have been *too* extensive.

With the advent of new coating processes and processing technologies, the broadness of the prohibition is now being challenged. The most common argument against the prohibition is that Class 10.9 structural bolts, which are equivalent in strength and hardness to ASTM A490 bolts, are routinely hot dip galvanised in Europe without any reports of fastener failures. The absence of failures is commonly attributed to the fact that European practice allows hot dip galvanising on Class 10.9 bolts, with the provision that surface preparation be conducted only by mechanical descaling (i.e., no acid pickling). Based on the correlation established in this work between hardness and embrittlement, it is more likely that the absence of failures is related to the low HE susceptibility of materials being galvanised.

This investigation has shown that non-electrolytic coatings such as mechanical galvanising, Dacromet® and Magni 555® can be safely applied without the risk of internal hydrogen embrittlement. These results should be the basis for allowing these coatings on ASTM A490 high strength structural bolts in the future. In fact, the findings of this research have already prompted ASTM Committee F16 on fasteners to consider approval of Dacromet® for A490 bolts. Continuing research will hopefully lead to a better understanding of the material and process conditions that cause IHE with the hot dip zinc process. Such work may someday lead to A490 bolts being safely hot dip zinc coated.

The most intriguing phenomenon observed in this work was the effect of up-quenching on test specimens. Although the temperature of the galvanising bath is well below the transformation temperatures for steel, the sheer rate of heat transfer evidently

affects both metallurgical and mechanical properties in a manner that is not fully understood. Not only does up-quenching seem to trigger the release of trapped hydrogen with embrittling consequence, but it also significantly lowers hardness. Conventional tempering in air would have required between one and two hours at 450 °C to lower hardness to 45 HRC.[50] Immersion in molten zinc required only 3 to 4 minutes for the same effect. Furthermore, the microstructure of the steel specimen after galvanising, although fundamentally un-changed from the initial martensitic morphology, presented a different appearance. It would be premature to dismiss this difference as an etching artefact without the benefit of high resolution electron microscopy and x-ray analysis, particularly in the area of the grain boundaries.

Another important variable to investigate is the effect of bath temperature. The process sampled in this research was "normal hot dip galvanising," where the bath temperature is 450 °C. There is also a process dubbed "high-temperature galvanising," which is performed at bath temperatures above 530 °C. *High-temperature* galvanising is not as widespread as the *normal* process. However, it offers a number of benefits when used appropriately, such as an exceptionally smooth coating.[34] High-temperature galvanising might affect the mobility hydrogen differently if it promoted hydrogen dissolution instead of causing it to be released.

The engineering benefits of understanding the effects up-quenching are potentially far reaching, not only in hot dip galvanising, but also in the heat treatment of metals. One example is if hours of tempering could, under certain conditions, be substituted by minutes of up-quenching. It is clear that up-quenching warrants further investigation as an independent research topic.

CHAPTER 6: CONCLUSION

The primary objective of this research was to quantify the risk of embrittlement from residual hydrogen (i.e., IHE) from coating processes commonly utilised to coat high strength mechanical fasteners. The effects of coating process variables and certain coating characteristics were investigated, principally by the incremental step loading (ISL) technique, in accordance with test method ASTM F1940. This methodology was used to rank a number of industrial coating processes for their propensity to cause internal hydrogen embrittlement. One topic of particular interest was the use of this test method for evaluating hot-dip zinc (galvanising) which is the preferred coating in the structural fastener industry, but which is also prohibited on high strength fasteners structural fasteners. The following conclusions were derived from this study.

1. Lowering of specimen hardness was accompanied by a similar lowering of FF strength. This finding was attributed to the lack of an *overriding* notch effect, due to a relatively large radius of 0.25 mm at the root of the specimen notch (i.e., dull notch).

2. Fractographic evidence supported the causal relationship between the presence of residual hydrogen from processing and the reduction of fracture strength, which is the premise upon which the ASTM F1940 test method is based.

3. The results supported the assertion that the multitude of complex processing variables and coating characteristics can be grouped into two basic parameters affecting IHE: (i) the amount of hydrogen introduced by the process, and (ii) the

permeability of the coating. *Coating permeability* had a first order effect, while the *quantity of hydrogen* introduced by the process had a second order effect.

4. In the absence of a coating barrier, hydrogen had a tendency to freely "out-gas" or escape, rather than be attracted to areas of stress concentration, even with the most severe acid pickling. In the presence of a coating, the first order effect of permeability was evident with phosphate and Zn-Ni coatings, both of which are porous.

5. The results of the cadmium process showed the reverse effect of coating permeability, where the application of an impermeable layer by high current density strike at the start of plating was used to prevent additional hydrogen being absorbed during plating build-up.

6. Quantity of hydrogen introduced was affected by: (i) electrolytic parameters (i.e., current density and plating time), and (ii) acid exposure conditions (i.e., acid type, concentration, and pickling time). There was no apparent effect of bath efficiency on hydrogen contribution.

7. The process qualification results can be summarised as follows. The zinc acid chloride process was the most embrittling, and therefore the highest risk process. Next in the order of risk, the alkaline zinc process was found to be slightly less embrittling as it produced higher $NFS_{\%}$ values, even at twice the plating time. This was followed by the alkaline zinc-iron process, which at 86% fracture strength was classified as moderately embrittling. The least embrittling processes were zinc-nickel, both alkaline and acid.

8. Baking can fully restore ductility at temperatures ranging from 190 to 204 °C, at times between 4 and 24 hours depending on the coating. This finding validating the theory of *reversibility* of IHE. Baking response depends upon the permeability of the coating. Therefore, baking time must be adapted to the coating type. Zinc plating, which is the most widespread electroplated coating applied to fasteners, achieved full recovery only after 24 hours of baking. The "standard" four hour bake time had no beneficial effect.

9. All four of the non-electrolytic processes tested, mechanical zinc, zinc phosphate, Dacromet®, and Magni 555® were found to be non-embrittling. In the cases of phosphate and mechanical zinc, the results were attributed to the permeability of the coating. A drop in fracture strength for Dacromet® by roughly 7% was attributed to a lowering of specimen hardness caused by curing at 320 °C.

10. Non-electrolytic coatings such as mechanical galvanising, Dacromet® and Magni 555® can be safely applied on ASTM A490 high strength structural bolts.

11. With hot dip galvanising, the evidence heavily points to hydrogen embrittlement as the primary mechanism causing brittle failures in test specimens, with fracture strengths as low as 40%. The most compelling evidence supporting this finding the time dependence of the embrittlement phenomenon.

12. The most plausible source of hydrogen is residual hydrogen trapped in the matrix of the steel specimens. In this scenario, hydrogen is present in reversible traps and then released by the up-quench/thermal shock upon immersion in the molten zinc bath. The presence of a thick zinc coating prevents hydrogen escaping, instead causing it to accumulate at grain boundaries.

13. Lower hardness specimens, in the range of 36-37 HRC were not embrittled by the hot dip galvanising process.

14. Thermal up-quenching that occurs during immersion in molten zinc affects both the metallurgical and mechanical properties of the steel specimens in ways that are not fully understood. Aside from releasing hydrogen from traps, up-queching lowers the hardness in minutes, instead of hours as with conventional air tempering. The effect on the microstructure is more subtle as the martensitic morphology is maintained, albeit with a notably different appearance.

This work should serve the basis for using ASTM F1940, both as a research tool and as a process control tool available to industry, for developing guidelines to optimise coating processes and practices. One example of an important economic benefit would be the elimination of baking requirements for parts that do not need to be baked, while improving baking effectiveness for parts that are truly at risk. The engineering benefit would be the assurance that "at-risk" parts are being effectively safeguarded from internal hydrogen embrittlement.

Continued close collaboration with industry through standards developing bodies such as ASTM and ISO will ensure that these guidelines are incorporated into fastener industry standards, and that the economic, engineering and scientific benefits are realised.

CHAPTER 7: FUTURE WORK

7.1 PHASE TWO INVESTIGATION

The next phase of this research is being undertaken by Sriraman Rajagopalan, a doctoral student at the Department of Mining, Metals and Materials at McGill University. The objective of Phase 2 is to use analytical techniques designed to fundamentally explain the results in terms of physical characteristics of the coatings and permeability of hydrogen. The coatings that will be investigated first are: (i) electrodeposited zinc, (ii) electrodeposited zinc-nickel, and (iii) hot dip zinc. The following describes the analytical techniques being developed.

7.1.1 Coating material characterisation

- Quantification of defects using electron microscopy and image analysis. This will serve as a metric for hydrogen escape pathways.
- Measurement of coating thickness for determination of effective diffusion coefficients by permeation experiments.
- Examination of microstructural parameters such as structure, phase, composition and texture, which can influence the properties of the coatings.

7.1.2 Electrochemical permeation

This technique will be used to determine the permeability of coatings. It consists of electrolytically imposing a potential on the entrance side of a coated steel disk and measuring the current at the discharge side, which in turn is used to quantify permeated hydrogen. The information obtained will allow for the calculation of an effective diffusion coefficient for each coating.

Due to the experimental difficulties associated with electrochemical permeation, it would be useful to verify if comparable results are obtained by an alternate technique using ISL methodology. One alternate technique consists of performing ISL testing on coated notched bar specimens at a cathodic potential of -1.2V, and comparing the results to specimens tested in air.

7.1.3 Thermal desorption spectroscopy (TDS)

This technique will be used to quantify hydrogen in bulk test specimens, both before and after coating. The specimen is placed in a chamber under high vacuum and then heated. The hydrogen discharge is measured downstream by means of a mass spectrometer. The technique will be used primarily to determine the baking response of various coatings. It will also be used to quantify residual hydrogen in bare steel specimens, which will be useful for studying the embrittlement phenomena observed in hot dip galvanising.

7.2 OTHER TOPICS OF INTEREST

The following is a list of topics, specific to each coating type, that warrant further investigation.

7.2.1 Electroplating processes

- Investigate the effect of current density, plating time, and brighteners on coating morphology (i.e., columnar vs. platelet). Explain how coating morphology affects hydrogen permeability.
- Investigate the effect of nickel to zinc ratio in Zn-Ni coating characteristics, with a particular focus on defects and porosity.
- Validate the premise that the high current density cadmium strike creates an impermeable barrier to hydrogen absorption. This can be done by testing the fracture strength of specimens with, and, without the strike.
- Define optimal baking conditions for different selected coatings types by performing baking tests on test specimens using TDS. Results can be validated by ISL testing of the specimens.

7.2.2 Hot dip zinc

- Validate the premise that the zinc coating acts as a barrier preventing hydrogen effusion. This can be done by exposing test specimens to a salt bath up-quench, thus simulating the thermal conditions produced in the galvanising bath, without the actual coating. This experiment may also provide additional insight into the metallurgical effects of the up-quench.
- Measure the effects of pre-baking of pristine specimens and of post-baking galvanised specimens using TDS. The findings would supplement the results obtained by ISL testing.

- Develop the relationship between hardness and embrittlement by the hot dip zinc process. This can be done empirically by varying the hardness of specimens to be galvanised, and using the same investigative methodology adopted in this work. An additional variable could be the effect of steel chemistry. This can be done by manufacturing specimens made of different steel grades commonly used in the fastener industry.

- Investigate the effect of bath temperature by compare "high-temperature" galvanising to "regular" galvanising using the same investigative methodology adopted in this work.

- Up-quenching warrants further investigation as an independent research topic. Such an investigation would include a thorough review of the literature followed by a series of experiments using different media, starting with molten zinc, and moving to non-coating media. Appropriate analytical techniques such as high resolution electron microscopy and x-ray diffraction must to be utilised to study effects on the microstructure, particularly at the grain boundaries.

REFERENCES

1 "ASME B 18.2.1 Square and Hex Bolts and Screws, Inch Series," American Society of Mechanical Engineers.

2 "ASTM F 1789 Standard terminology for F16 mechanical fasteners," in *ASTM Book of Standards*.

3 http://www.avdel.textron.com, "Avdel® Blind Fastening Systems " (Textron Fastening Systems).

4 C. A. Hood, "Fastener materials," in *Handbook of Bolts and Bolted Joints*, edited by John H. Bickford and Sayed Nassar (M. Dekker, New York, 1998), pp. 1-33.

5 "ASTM F 2078 Standard terminology relating to hydrogen embrittlement testing," in *ASTM Book of Standards*.

6 W. H. Johnson, "On some remarkable changes produced in iron and steel by the action of hydrogen and acids," in *Hydrogen Damage*, edited by Cedric D. Beachem (ASM International, Metals Park, OH, 1977), pp. 1-2.

7 L. Raymond, "Evaluation of hydrogen embrittlement," in *ASM Metals Handbook* (ASM International, Metals Park, OH, 1987), Vol. 13 Corrosion, pp. 283-290.

8 B. Craig, "Hydrogen damage," in *ASM Metals Handbook* (ASM International, Metals Park, OH, 1987), Vol. 13 Corrosion, pp. 163-171.

9 Troiano, "The role of hydrogen and other interstitials in the mechanical behavior of metals," in *Hydrogen Damage*, edited by Cedric D. Beachem (ASM International, Metals Park, OH, 1960), pp. 151-177.

10 L. Raymond, "Evaluation of hydrogen embrittlement," in *ASM Metals Handbook* (ASM International, Metals Park, OH, 1987), Vol. 13 Corrosion, pp. 285.

11 M. I. Marek, "Thermodynamics of aqueous corrosion," in *ASM Metals Handbook* (ASM International, Metals Park, OH, 1987), Vol. 13 Corrosion, pp. 283-290.

12 H. Geduld, *Zinc plating*. (ASM International, Metals Park , OH, 1988).

13 J. J. De Luccia, "Electrochemical aspects of hydrogen in metals," in *Hydrogen Embrittlement: Prevention and Control, ASTM STP 962*, edited by L. Raymond (American Society for Testing and Materials, Philadelphia, PA, 1988), pp. 17-34.

14 *Handbook of Chemistry and Physics*. (CRC Press, 1986), 86th ed.

15 Zakroczymski, "Entry of hydrogen into iron alloys from the liquid phase," in *Hydrogen degradation of ferrous alloys*, edited by R.A Oriani, J.P. Hirth, and M Smialowski (Noyes Publications, Park Ridge, NJ, 1985), pp. 215-250.

16 D. C. H. Nevison, "Corrosion of zinc," in *ASM Metals Handbook Corrosion* (ASM International, Metals Park, OH, 1987), Vol. 13 Corrosion, pp. 755-769.

17 H. E. Townsend, Jr., "Effects of zinc coatings on the stress corrosion cracking and hydrogen embrittlement of low-alloy steel," Metall Trans A **6 A** (4), 877-883 (1975).

18 W. J. Pollack and C. Grey, "Assessment of the degree of hydrogen embrittlement produced in plated high-strength 4340 steel by paint strippers using slow strain rate testing," in *Hydrogen Embrittlement: Prevention and Control, ASTM STP 962*, edited by L. Raymond (American Socitey for Testing and Materials, Philadelphia, PA, 1988), pp. 372-386.

19 K. E. Yee, "Corrosion," in *Handbook of Bolts and Bolted Joints*, edited by John H. Bickford and Sayad Nassar (Marcel Dekker, New York, NY, 1998), pp. 709-721.

20 J. A. Smith, M. H. Peterson, and B. F. Brown, "Electrochemical conditions at the tip of an advancing stress corrosion crack in AISI 4340 steel," Corrosion **26** (12), 539-542 (1970).

21 G. T. Murray, "Prevention of hydrogen embrittlement by surface films," in *Hydrogen Embrittlement: Prevention and Control, ASTM STP 962*, edited by L. Raymond (American Society for Testing and Materials, Philadelphia, PA, 1988), pp. 304-317.

22 W. J. Pollack, "Assessment of the degree of hydrogen embrittlement produced in high-strength 4340 steel by plating-and-baking processes using slow strain rate testing," in *Hydrogen Embrittlement: Prevention and Control, ASTM STP 962*, edited by L. Raymond (American Society for Testing and Materials, Philadelphia, PA, 1988), pp. 68-80.

23 J. S. Bednar, W. Dingley, and R. R. Rogers, Canada Patent No. CA 855189 (Nov. 3, 1970).

24 E. D. McCarty, D. Wetzel, and B. S. Kloberdanz, "Hydrogen embrittlement in automotive fastener applications," SAE International Congress #960312, 117-145 (1996).

25 "ASTM F 1941 Standard specification for electrodeposited coatings on threaded fasteners (unified inch screw threads (UN/UNR))," in *ASTM Book of Standards*; "ASTM F 1941M Standard specification for electrodeposited coatings on threaded fasteners [metric]," in *ASTM Book of Standards*.

26 "Practical phosphate coatings," (R.O. Hull & Company, Cleveland, OH, unpublished).

27 G. P. Voorhis, "Hydrogen embrittlement and relief treatment study of zinc phosphate-coated submunitions," in *Hydrogen Embrittlement: Prevention and Control, ASTM STP 962*, edited by L. Raymond (American Society for Testing and Materials, Philadelphia, PA, 1988), pp. 318-334.

28 "ASTM F 1137 Standard specification for phosphate/oil and phosphate/organic corrosion protective coatings for fasteners," in *ASTM Book of Standards*.

29 A. Brooks, "Mechanical plating and hydrogen embrittlement," (Waldes Kohinoor, Inc., Long Island City, NY, 1978 unpublished).

30 "ASTM B 695 Standard specification for coatings of zinc mechanically deposited on iron and steel," in *ASTM Book of Standards*.

31 A. Pfeifer, (2005 personnal communication).

32 "ASTM F 1136M Standard specification for specification for zinc/aluminum corrosion protective coatings for fasteners [metric]," in *ASTM Book of Standards*; "ASTM F 1136 Standard specification for zinc/aluminum corrosion protective coatings for fasteners," in *ASTM Book of Standards*.

33 B. Lowry, (2006 personnal communication).

34 "http://www.galvanizeit.org," (American Galvanizers Association, 2007).

35 Brahimi, "ASTM F1940 testing of hot dip galvanizing processes," (2005 unpublished).

36 "ASTM F 2329 Standard specification for zinc coating, hot-dip, requirements for application to carbon and alloy steel bolts, screws, washers, nuts, and special threaded fasteners," in *ASTM Book of Standards*.

37 K. G. Reddy, S. T. G. Kumar, S. Arumugam, and T. S. Lakshmanan, "Hydrogen embrittlement failure of 30 NCD 16 steel screws," Prakt. Met. **26** (12), 654-659 (1989).

38 M. J. Robinson and R. M. Sharp, "The effect of post-exposure heat treatment on the hydrogen embrittlement of high carbon steel," Corrosion **41** (10), 582-586 (1985).

39 M. Levy and G. A. Bruggeman, "Examination of cadmium-plated aircraft fasteners for hydrogen embrittlement," in *Hydrogen Embrittlement: Prevention and Control, ASTM STP 962*, edited by L. Raymond (American Society for Testing and Materials, Philadelphia, PA, 1988), pp. 335-342.

40 R. V. Dreher, "Accelerated acceptance testing for hydrogen embrittlement control," in *Hydrogen Embrittlement: Prevention and Control, ASTM STP 962*, edited by L. Raymond (American Society for Testing and Materials, Philadelphia, PA, 1988), pp. 60-67.

41 W. R. Crumly, "Screening tests for hydrogen stress cracking susceptibility," in *Hydrogen Embrittlement: Prevention and Control, ASTM STP 962*, edited by L. Raymond (American Socitey for Testing and Materials, Philadelphia, PA, 1988), pp. 173-177; L. Raymond, "Accelerated small specimen test method for measuring the fatigue strength in the failure analysis of fasteners," in *Structural Integrity of Fasteners, ASTM STP 1391*, edited by Pir M. Toor (American Socitey for Testing and Materials, Philadelphia, PA, 2000), Vol. 2, pp. 192-203.

42 L. Raymond, "The susceptibility of fasteners to hydrogen embrittlement and stress corrosion cracking," in *Handbook of Bolts and Bolted Joints*, edited by John H. Bickford and Sayed Nassar (M. Dekker, New York, 1998), pp. 723-756.

43 "ASTM F 1624 Standard Test Method for Measurement of Hydrogen Embrittlement in Steel by the incremental Loading Technique," ASTM Book of Standards.

44 "ASTM F 1940 Standard Test Method for Process Control Verification to Prevent Hydrogen Embrittlement in Plated or Coated Fasteners," in *ASTM Book of Standards*.

45 L. Raymond, "Plating or coating processes for fasteners can be monitored for control of hydrogen embrittlement," American Fastener Journal (Mar/Apr), p26 (1998); Raymond, "Fracture mechanics applied to tensile fasteners, part four in a series...test methods," American Fastener Journal (May/Jun), 48-54 (1990).

46 L. Raymond, US Patent No. 5,549,007 (Aug. 27, 1996).

47 "ASTM F 519 Standard Test Method for mechanical hydrogen embrittlement evaluation of plating/coating processes and service environments," in *ASTM Book of Standards*.

48 "SAE-AMS-S-5000 Steel, chrome-nickel-molybdenum (4340) bars and forging stock," Society of Automotive Engineers.

49 "SAE -AMS-2759/2D Heat treatment of low-alloy steel parts minimum tensile strength 220 ksi (1517 MPa) and higher," Society of Automotive Engineers.

50 H. Chandler, *Heat treater's guide : practices and procedures for irons and steels*. (ASM International, Metals Park, OH :, 1995), 2nd ed.

51 "ASTM A 490 Standard specification for structural bolts, alloy steel, heat treated, 150 ksi minimum tensile strength," in *ASTM Book of Standards*.

52 G. Barcelo, J. Garcia, M. Sarret, C. Muller, and J. Pregonas, "Properties of Zn-Ni alloy deposits from ammonium baths," Journal of Applied Electrochemistry **24** (12), 1249-1255 (1994); G. Barcelo, E. Garcia, M. Sarret, C. Muller, and J. Pregonas, "Characterization of zinc-nickel alloys obtained from an industrial chloride bath," Journal of Applied Electrochemistry **28** (10), 1113-1120 (1998); A. P. Ordine, S. L. Diaz, I. C. P. Margarit, and O. R. Mattos, "Zn-Ni and Zn-Fe alloy deposits modified by P incorporation: anticorrosion properties," Electrochimica Acta **49** (17-18), 2815-2823 (2004).

53 S. Rajagopalan, "Structural aspects of hydrogen embrittlement in zinc coated steel," (2007 unpublished).

54 G. J. W. Kor and P. C. Glaws, "Ladle refining and vacuum degassing," in *The Making, Shaping and Treating of Steel*, edited by R. J Fruehan (AISE Steel Foundation, Pittsburgh, PA, 1998), Vol. Steelmaking and Refining, pp. 661-714.

55 Bodycote Testing Group - Certification of test, 2007.

APPENDIX A

List of processes and conditions

Appendix A: Process descriptions

P1
Electroplating - barrel
Zn clear - acid chloride

No surface cleaning with activation
Not baked

Supplier A

Current density (mA/cm^2):	8.50
Plating time (min):	37
Est. cathode efficiency (%):	Very high: 90-99
Coating thickness (µm):	17.5
Acid type:	Hydrochloric
Acid concentration (wt %):	13
Acid residence time (min):	14

P2
Electroplating - barrel
Zn clear - acid chloride

No surface cleaning no activation
Not baked

Supplier A

Current density (mA/cm^2):	8.50
Plating time (min):	37
Est. cathode efficiency (%):	Very high: 90-99
Coating thickness (µm):	21
Acid type:	Hydrochloric
Acid concentration (wt %):	13
Acid residence time (min):	14

P3
Electroplating - barrel
Zn yellow- acid chloride

Full process soak/pickle
Not baked

Supplier A

Current density (mA/cm^2):	6.67
Plating time (min):	37
Est. cathode efficiency (%):	Very high: 90-99
Coating thickness (µm):	13.8
Acid type:	Hydrochloric
Acid concentration (wt %):	13
Acid residence time (min):	14

P4
Electroplating - barrel
Zn yellow- acid chloride

No surface cleaning with activation
Not baked

Supplier A

Current density (mA/cm^2):	6.67
Plating time (min):	37
Est. cathode efficiency (%):	Very high: 90-99
Coating thickness (µm):	8.7
Acid type:	Hydrochloric
Acid concentration (wt %):	13
Acid residence time (min):	14

P5
Electroplating - barrel
Zn yellow- acid chloride

No surface cleaning no activation
Not baked

Supplier A

Current density (mA/cm^2):	6.67
Plating time (min):	37
Est. cathode efficiency (%):	Very high: 90-99
Coating thickness (µm):	16.8
Acid type:	Hydrochloric
Acid concentration (wt %):	13
Acid residence time (min):	14

P6
Electroplating - barrel
Zn clear - acid chloride

Full process soak/pickle
Not baked

Supplier A

Current density (mA/cm^2):	8.50
Plating time (min):	37
Est. cathode efficiency (%):	Very high: 90-99
Coating thickness (µm):	15.4
Acid type:	Hydrochloric
Acid concentration (wt %):	13
Acid residence time (min):	14

P7
Electroplating - barrel
Zn/Ni - alkaline (non cyanide)

No surface cleaning with activation
Not baked

Supplier B

Current density (mA/cm^2):	5.38
Plating time (min):	90
Est. cathode efficiency (%):	Medium low: 50-60
Coating thickness (µm):	4.7
Acid type:	Hydrochloric
Acid concentration (wt %):	12
Acid residence time (min):	0.5

P8
Electroplating - barrel
Zn/Ni - alkaline (non cyanide)

Full process soak/pickle
Not baked

Supplier B

Current density (mA/cm^2):	5.38
Plating time (min):	90
Est. cathode efficiency (%):	Medium low: 50-60
Coating thickness (µm):	4.3
Acid type:	Hydrochloric
Acid concentration (wt %):	12
Acid residence time (min):	10

P9
Electroplating - barrel
Zn - alkaline (non cyanide)

No surface cleaning with activation
Not baked

Supplier B

Current density (mA/cm^2):	8.07
Plating time (min):	120
Est. cathode efficiency (%):	High: 80-90
Coating thickness (µm):	5.2
Acid type:	Hydrochloric
Acid concentration (wt %):	13
Acid residence time (min):	0.5

P10
Electroplating - barrel
Zn - alkaline (non cyanide)

Full process soak/pickle
Not baked

Supplier B

Current density (mA/cm^2):	7.53
Plating time (min):	120
Est. cathode efficiency (%):	High: 80-90
Coating thickness (µm):	4.5
Acid type:	Hydrochloric
Acid concentration (wt %):	13
Acid residence time (min):	7

P11
Electroplating - barrel
Zn/Ni - acid chloride

No surface cleaning with activation
Not baked

Supplier B

Current density (mA/cm^2):	5.17
Plating time (min):	60
Est. cathode efficiency (%):	Very high: 90-99
Coating thickness (µm):	9.5
Acid type:	Hydrochloric
Acid concentration (wt %):	17
Acid residence time (min):	0.5

P12
Electroplating - barrel
Zn/Ni - acid chloride

Full process soak/pickle
Not baked

Supplier B

Current density (mA/cm^2):	5.17
Plating time (min):	60
Est. cathode efficiency (%):	Very high: 90-99
Coating thickness (µm):	8
Acid type:	Hydrochloric
Acid concentration (wt %):	17
Acid residence time (min):	5

P13
Electroplating - barrel
Zn/Fe - alkaline (non cyanide)

No surface cleaning with activation
Not baked

Supplier B

Current density (mA/cm^2):	12.38
Plating time (min):	55
Est. cathode efficiency (%):	Medium low: 50-60
Coating thickness (µm):	13
Acid type:	Hydrochloric
Acid concentration (wt %):	17
Acid residence time (min):	0.5

P14
Electroplating - barrel
Zn/Fe - alkaline (non cyanide)

Full process soak/pickle
Not baked

Supplier B

Current density (mA/cm^2):	12.38
Plating time (min):	50
Est. cathode efficiency (%):	Medium low: 50-60
Coating thickness (µm):	11.5
Acid type:	Hydrochloric
Acid concentration (wt %):	17
Acid residence time (min):	5

P15
Electroplating - barrel
Zn clear - acid chloride

No surface cleaning with activation
Not baked

Supplier B

Current density (mA/cm^2):	5.06
Plating time (min):	60
Est. cathode efficiency (%):	Very high: 90-99
Coating thickness (µm):	11.5
Acid type:	Hydrochloric
Acid concentration (wt %):	17
Acid residence time (min):	1

P16
Electroplating - barrel
Zn clear - acid chloride

Full process soak/pickle
Not baked

Supplier B

Current density (mA/cm^2):	5.06
Plating time (min):	60
Est. cathode efficiency (%):	Very high: 90-99
Coating thickness (µm):	11.8
Acid type:	Hydrochloric
Acid concentration (wt %):	7.6
Acid residence time (min):	8

P17
Mechanical Zinc

Soak + 8 min pickle
Not baked

Supplier B

Current density (mA/cm^2):	0.00
Plating time (min):	33
Est. cathode efficiency (%):	N/A
Coating thickness (µm):	44
Acid type:	HCl + H2SO4
Acid concentration (wt %):	15
Acid residence time (min):	8

P18
Mechanical Zinc

Soak + 1 min pickle
Not baked

Supplier B

Current density (mA/cm^2):	0.00
Plating time (min):	33
Est. cathode efficiency (%):	N/A
Coating thickness (µm):	6.4
Acid type:	HCl + H2SO4
Acid concentration (wt %):	15
Acid residence time (min):	1

P19
Organic
Magni 555®

Full process - soak/pickle/phos
Post cure

Supplier F

Current density (mA/cm^2):	0.00
Plating time (min):	
Est. cathode efficiency (%):	N/A
Coating thickness (µm):	
Acid type:	Sulphuric at 42 °C
Acid concentration (wt %):	8
Acid residence time (min):	15

P20
Phosphate
Z24 - medium weight

Solvent degrease + acid pickle
Not baked

Supplier F

Current density (mA/cm^2):	0.00
Plating time (min):	15
Est. cathode efficiency (%):	N/A
Coating thickness (µm):	
Acid type:	Sulphuric at 42 °C
Acid concentration (wt %):	7.8
Acid residence time (min):	15

P21
Acid pickle

N/A
Not baked

Supplier M

Current density (mA/cm^2):	0.00
Plating time (min):	
Est. cathode efficiency (%):	N/A
Coating thickness (µm):	
Acid type:	Hydrochloric
Acid concentration (wt %):	9
Acid residence time (min):	20

P22
Hot Dip Zinc

Flux only
Not baked

Supplier A

Current density (mA/cm^2):	0.00
Plating time (min):	
Est. cathode efficiency (%):	N/A
Coating thickness (µm):	
Acid type:	N/A
Acid concentration (wt %):	
Acid residence time (min):	

P23
Hot Dip Zinc

Flux only
Pre-bake 24 h 204 °C (400 °F)

Supplier A

Current density (mA/cm^2):	0.00
Plating time (min):	
Est. cathode efficiency (%):	N/A
Coating thickness (µm):	
Acid type:	N/A
Acid concentration (wt %):	
Acid residence time (min):	

P24
Hot Dip Zinc

Flux only
Not baked

Supplier A

Current density (mA/cm^2):	0.00
Plating time (min):	
Est. cathode efficiency (%):	N/A
Coating thickness (µm):	73.4
Acid type:	N/A
Acid concentration (wt %):	
Acid residence time (min):	

P25
Hot Dip Zinc

Flux only
Pre-bake 48 h 204 °C (400 °F)

Supplier A

Current density (mA/cm^2):	0.00
Plating time (min):	
Est. cathode efficiency (%):	N/A
Coating thickness (µm):	77.0
Acid type:	N/A
Acid concentration (wt %):	
Acid residence time (min):	

P26
Hot Dip Zinc

Flux only
Pre-bake 72 h 204 °C (400 °F)

Supplier A

Current density (mA/cm^2):	0.00
Plating time (min):	
Est. cathode efficiency (%):	N/A
Coating thickness (µm):	77.2
Acid type:	N/A
Acid concentration (wt %):	
Acid residence time (min):	

P27
Hot Dip Zinc

Flux only
Not baked

Supplier A

Current density (mA/cm^2):	0.00
Plating time (min):	
Est. cathode efficiency (%):	N/A
Coating thickness (µm):	
Acid type:	N/A
Acid concentration (wt %):	
Acid residence time (min):	

P28
Hot Dip Zinc

Flux only
Bake 24 h 191 °C (375 °F)

Supplier A

Current density (mA/cm^2):	0.00
Plating time (min):	
Est. cathode efficiency (%):	N/A
Coating thickness (µm):	
Acid type:	N/A
Acid concentration (wt %):	
Acid residence time (min):	

P29
Hot Dip Zinc
Bare - not coated

N/A
Tempered 1h @ 560 °C (1040 °F)

Supplier A

Current density (mA/cm^2):	0.00
Plating time (min):	
Est. cathode efficiency (%):	N/A
Coating thickness (µm):	
Acid type:	N/A
Acid concentration (wt %):	
Acid residence time (min):	

P32
Electroplating - rack
Zn/Ni - alkaline (non cyanide)

Solvent degrease + grit blast
Bake 24 h 191 °C (375 °F)

Supplier C

Current density (mA/cm^2):	30.14
Plating time (min):	35
Est. cathode efficiency (%):	Very low: 30-40
Coating thickness (µm):	11.2
Acid type:	N/A
Acid concentration (wt %):	
Acid residence time (min):	

P33
Electroplating - rack
Zn/Ni - alkaline (non cyanide)

Solvent degrease + grit blast
Not baked

Supplier C

Current density (mA/cm^2):	30.14
Plating time (min):	35
Est. cathode efficiency (%):	Very low: 30-40
Coating thickness (µm):	11.2
Acid type:	N/A
Acid concentration (wt %):	
Acid residence time (min):	

P34
Electroplating - rack
Zn/Ni - alkaline (non cyanide)

Solvent degrease + acid pickle
Bake 24 hr 375F

Supplier C

Current density (mA/cm^2):	30.14
Plating time (min):	35
Est. cathode efficiency (%):	Very low: 30-40
Coating thickness (µm):	11.2
Acid type:	Hydrochloric
Acid concentration (wt %):	25
Acid residence time (min):	3

P35
Electroplating - rack
Zn/Ni - alkaline (non cyanide)

Solvent degrease + acid pickle
Not baked

Supplier C

Current density (mA/cm^2):	30.14
Plating time (min):	35
Est. cathode efficiency (%):	Very low: 30-40
Coating thickness (µm):	11.2
Acid type:	Hydrochloric
Acid concentration (wt %):	25
Acid residence time (min):	3

P36
Electroplating - rack
Zn/Ni - alkaline (non cyanide)

Solvent degrease + grit blast
Bake 24 h 191 °C (375 °F)

Supplier C

Current density (mA/cm^2):	30.14
Plating time (min):	35
Est. cathode efficiency (%):	Very low: 30-40
Coating thickness (µm):	11.2
Acid type:	N/A
Acid concentration (wt %):	
Acid residence time (min):	

P37
Electroplating - rack
Zn/Ni - alkaline (non cyanide)

Solvent degrease + grit blast
Not baked

Supplier C

Current density (mA/cm^2):	30.14
Plating time (min):	35
Est. cathode efficiency (%):	Very low: 30-40
Coating thickness (µm):	11.2
Acid type:	N/A
Acid concentration (wt %):	
Acid residence time (min):	

P38
Electroplating - rack
Zn/Ni - alkaline (non cyanide)

Solvent degrease + acid pickle
Bake 24 h 191 °C (375 °F)

Supplier C

Current density (mA/cm^2):	30.14
Plating time (min):	35
Est. cathode efficiency (%):	Very low: 30-40
Coating thickness (µm):	11.2
Acid type:	Hydrochloric
Acid concentration (wt %):	25
Acid residence time (min):	3

P39
Electroplating - rack
Zn/Ni - alkaline (non cyanide)

Solvent degrease + acid pickle
Not baked

Supplier C

Current density (mA/cm^2):	30.14
Plating time (min):	35
Est. cathode efficiency (%):	Very low: 30-40
Coating thickness (µm):	11.2
Acid type:	Hydrochloric
Acid concentration (wt %):	25
Acid residence time (min):	3

P40
Electroplating - rack
Cadmium - bright - cyanide

No surface cleaning with activation
Bake 4 h 204 °C (400 °F)

Supplier D

Current density (mA/cm^2):	86.11
Plating time (min):	0.75 + 20
Est. cathode efficiency (%):	High: 80-90
Coating thickness (µm):	13.5
Acid type:	N/A
Acid concentration (wt %):	
Acid residence time (min):	

P41
Electroplating - rack
Cadmium - bright - cyanide

No surface cleaning with activation
Not baked

Supplier D

Current density (mA/cm^2):	86.11
Plating time (min):	0.75 + 20
Est. cathode efficiency (%):	High: 80-90
Coating thickness (µm):	13.5
Acid type:	N/A
Acid concentration (wt %):	
Acid residence time (min):	

P42
Electroplating - barrel
Zn/Ni - alkaline (non cyanide)

Full process soak/pickle
Not baked

Supplier B

Current density (mA/cm^2):	5.38
Plating time (min):	120
Est. cathode efficiency (%):	Medium low: 50-60
Coating thickness (µm):	11
Acid type:	Hydrochloric
Acid concentration (wt %):	17
Acid residence time (min):	4

P43
Electroplating - barrel
Zn/Ni - alkaline (non cyanide)

Full process soak/pickle
Not baked

Supplier B

Current density (mA/cm^2):	5.38
Plating time (min):	120
Est. cathode efficiency (%):	Medium low: 50-60
Coating thickness (µm):	8
Acid type:	Hydrochloric
Acid concentration (wt %):	17
Acid residence time (min):	16

P44
Electroplating - barrel
Zn/Ni - alkaline (non cyanide)

No surface cleaning with activation
Not baked

Supplier B

Current density (mA/cm^2):	5.38
Plating time (min):	120
Est. cathode efficiency (%):	Medium low: 50-60
Coating thickness (µm):	6.4
Acid type:	Hydrochloric
Acid concentration (wt %):	17
Acid residence time (min):	0.5

P45
Hot Dip Zinc

Flux only
Not baked

Supplier A

Current density (mA/cm^2):	0.00
Plating time (min):	
Est. cathode efficiency (%):	N/A
Coating thickness (µm):	
Acid type:	N/A
Acid concentration (wt %):	
Acid residence time (min):	

P46
Acid pickle

N/A
Not baked

Supplier M

Current density (mA/cm^2):	0.00
Plating time (min):	
Est. cathode efficiency (%):	N/A
Coating thickness (µm):	
Acid type:	Hydrochloric
Acid concentration (wt %):	9
Acid residence time (min):	30

P47
Acid pickle

N/A
24 h room temperature

Supplier M

Current density (mA/cm^2):	0.00
Plating time (min):	
Est. cathode efficiency (%):	N/A
Coating thickness (µm):	
Acid type:	Hydrochloric
Acid concentration (wt %):	9
Acid residence time (min):	30

P48
Acid pickle

N/A
48 h room temperature + add 30 min HCl

Supplier M

Current density (mA/cm^2):	0.00
Plating time (min):	
Est. cathode efficiency (%):	N/A
Coating thickness (µm):	
Acid type:	Hydrochloric
Acid concentration (wt %):	9
Acid residence time (min):	30

P49
Acid pickle

N/A
72 h room temperature + add 30 min HCl

Supplier M

Current density (mA/cm^2):	0.00
Plating time (min):	
Est. cathode efficiency (%):	N/A
Coating thickness (µm):	
Acid type:	Hydrochloric
Acid concentration (wt %):	9
Acid residence time (min):	30

P50
Acid pickle

N/A
Not baked

Supplier M

Current density (mA/cm^2):	0.00
Plating time (min):	
Est. cathode efficiency (%):	N/A
Coating thickness (µm):	
Acid type:	Hydrochloric
Acid concentration (wt %):	18
Acid residence time (min):	30

P51
Acid pickle

N/A
Not baked

Supplier M

Current density (mA/cm^2):	0.00
Plating time (min):	
Est. cathode efficiency (%):	N/A
Coating thickness (µm):	
Acid type:	Hydrochloric
Acid concentration (wt %):	18
Acid residence time (min):	70

P52
Electroplating - barrel
Zn/Ni - alkaline (non cyanide)

Full process soak/pickle
Not baked

Supplier B

Current density (mA/cm^2):	5.81
Plating time (min):	120
Est. cathode efficiency (%):	Medium low: 50-60
Coating thickness (µm):	5
Acid type:	Hydrochloric
Acid concentration (wt %):	18.2
Acid residence time (min):	4

P53
Electroplating - barrel
Zn/Ni - alkaline (non cyanide)

Full process soak/pickle
Not baked

Supplier B

Current density (mA/cm^2):	6.46
Plating time (min):	120
Est. cathode efficiency (%):	Medium low: 50-60
Coating thickness (µm):	6.6
Acid type:	Hydrochloric
Acid concentration (wt %):	18.2
Acid residence time (min):	15

P54
Electroplating - barrel
Zn clear - acid chloride

Full process soak/pickle
Not baked

Supplier B

Current density (mA/cm^2):	5.06
Plating time (min):	70
Est. cathode efficiency (%):	Very high: 90-99
Coating thickness (µm):	10
Acid type:	Hydrochloric
Acid concentration (wt %):	7.5
Acid residence time (min):	7

P55
Electroplating - barrel
Zn clear - acid chloride

No surface cleaning with activation
Not baked

Supplier B

Current density (mA/cm^2):	5.06
Plating time (min):	70
Est. cathode efficiency (%):	Very high: 90-99
Coating thickness (µm):	10
Acid type:	Hydrochloric
Acid concentration (wt %):	17.1
Acid residence time (min):	0.17

P56
Organic
Dacromet®

Solvent degrease + grit blast
Post cure

Supplier E

Current density (mA/cm^2):	
Plating time (min):	
Est. cathode efficiency (%):	
Coating thickness (µm):	
Acid type:	N/A
Acid concentration (wt %):	
Acid residence time (min):	

P1001
Electroplating - barrel
Zn clear - acid chloride

Full process soak/pickle
Not baked

Supplier G

Current density (mA/cm^2):	
Plating time (min):	
Est. cathode efficiency (%):	Very high: 90-99
Coating thickness (µm):	6.5
Acid type:	Hydrochloric
Acid concentration (wt %):	13
Acid residence time (min):	10

P1002
Electroplating - barrel
Zn clear - acid chloride

Full process soak/pickle
Bake 12 h 204 °C (400 °F)

Supplier G

Current density (mA/cm^2):	
Plating time (min):	
Est. cathode efficiency (%):	Very high: 90-99
Coating thickness (µm):	6.5
Acid type:	Hydrochloric
Acid concentration (wt %):	13
Acid residence time (min):	10

P1003
Electroplating - barrel
Zn clear - acid chloride

Full process soak/pickle
Bake 24 h 204 °C (400 °F)

Supplier G

Current density (mA/cm^2):	
Plating time (min):	
Est. cathode efficiency (%):	Very high: 90-99
Coating thickness (µm):	6.5
Acid type:	Hydrochloric
Acid concentration (wt %):	13
Acid residence time (min):	10

P1004
Mechanical Zinc

Full process soak/pickle

Supplier G

Current density (mA/cm^2):	0.00
Plating time (min):	
Est. cathode efficiency (%):	N/A
Coating thickness (µm):	
Acid type:	Sulphuric at 42 °C
Acid concentration (wt %):	
Acid residence time (min):	

P1005
Mechanical Zinc

Full process soak/pickle

Supplier J

Current density (mA/cm^2):	0.00
Plating time (min):	
Est. cathode efficiency (%):	N/A
Coating thickness (µm):	85
Acid type:	Sulphuric at 42 °C
Acid concentration (wt %):	
Acid residence time (min):	

P1006
Mechanical Zinc

Full process soak/pickle

Supplier H

Current density (mA/cm^2):	0.00
Plating time (min):	
Est. cathode efficiency (%):	N/A
Coating thickness (µm):	66
Acid type:	Sulphuric at 42 °C
Acid concentration (wt %):	
Acid residence time (min):	

P1007
Organic
Dacromet®

Solvent degrease + grit blast
Post cure

Supplier I

Current density (mA/cm^2):	0.00
Plating time (min):	
Est. cathode efficiency (%):	N/A
Coating thickness (µm):	9.28
Acid type:	N/A
Acid concentration (wt %):	
Acid residence time (min):	

P1008
Hot Dip Zinc

Full process - soak/pickle/flux
Not baked

Supplier A

Current density (mA/cm^2):	0.00
Plating time (min):	
Est. cathode efficiency (%):	N/A
Coating thickness (µm):	
Acid type:	Hydrochloric
Acid concentration (wt %):	10
Acid residence time (min):	16

P1009
Hot Dip Zinc

Flux only
Not baked

Supplier A

Current density (mA/cm^2):	0.00
Plating time (min):	
Est. cathode efficiency (%):	N/A
Coating thickness (µm):	
Acid type:	N/A
Acid concentration (wt %):	
Acid residence time (min):	

P1010
Hot Dip Zinc

No surface prep - direct to kettle
Not baked

Supplier A

Current density (mA/cm^2):	0.00
Plating time (min):	
Est. cathode efficiency (%):	N/A
Coating thickness (µm):	
Acid type:	N/A
Acid concentration (wt %):	
Acid residence time (min):	

P1011
Hot Dip Zinc
Bare - not coated

N/A
Heat exposure (furnace 10min @ 455 °C)

Supplier M

Current density (mA/cm^2): 0.00
Plating time (min):
Est. cathode efficiency (%): N/A
Coating thickness (µm):
Acid type: N/A
Acid concentration (wt %):
Acid residence time (min):